

ANALYSIS AND MITIGATION OF EFFECTS OF  
ELECTRIC ARC FURNACE OPERATION ON  
SHAFT OF SYNCHRONOUS GENERATOR

BY

**FAZAL ILLAHI**

A Thesis Presented to the  
DEANSHIP OF GRADUATE STUDIES

**KING FAHD UNIVERSITY OF PETROLEUM & MINERALS**

DHAHRAN, SAUDI ARABIA

In Partial Fulfillment of the  
Requirements for the Degree of

**MASTER OF SCIENCE**

In

**ELECTRICAL ENGINEERING**

**December 2014**

**ANALYSIS AND MITIGATION OF EFFECTS OF  
ELECTRIC ARC FURNACE OPERATION ON SHAFT OF  
SYNCHRONOUS GENERATOR**

**FAZAL ILLAHI**

**ELECTRICAL ENGINEERING**

**DECEMBER 2014**

KING FAHD UNIVERSITY OF PETROLEUM & MINERALS

DHAHRAN- 31261, SAUDI ARABIA

**DEANSHIP OF GRADUATE STUDIES**

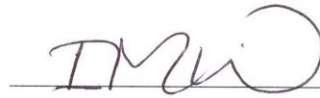
This thesis, written by **FAZAL ILLAHI** under the direction his thesis advisor and approved by his thesis committee, has been presented and accepted by the Dean of Graduate Studies, in partial fulfillment of the requirements for the degree of **MASTER OF SCIENCE IN ELECTRICAL ENGINEERING**.



Dr. Ali Ahmad Al-Shaikhi  
Department Chairman



Dr. Salam A. Zummo  
Dean of Graduate Studies



Dr. Ibrahim M. El-Amin  
(Advisor)



Dr. Mohammed Ali Y. Abido  
(Member)



Dr. Ali Al-Awami  
(Member)

3/5/15  
Date

© FAZAL ILLAHI

2014

## DEDICATION

I would like to dedicate this work to my Mother and Father and my Aunt, without whose prayers, motivation and support I might not have been able to complete my MS successfully

To my Wife who really supported me throughout my studies. Without her co-operation, it would have been really difficult for me to complete my MS studies in time and successfully

To my Uncle Faheem Illahi Memon and Brother Fozeb Illahi Memon for their continuous encouragement and support

To my Teachers for their guidance and tutelage

To my beloved country 'Pakistan'

## ACKNOWLEDGMENTS

*“In the name of Allah, The Most Gracious and The Most Merciful”*

All praise belongs to Allah (S.W.T.) for bestowing me with courage and perseverance to carry out this work sincerely. I thank Almighty Allah for providing me opportunity to do my M.S. successfully at King Fahd University of Petroleum and Minerals, Dhahran.

I would like to express my deepest gratitude to King Fahd University of Petroleum and Minerals for providing me good academic platform and financial support during my M.S.

My deepest gratitude and appreciation goes to my thesis advisor and mentor Dr. Ibrahim M. El-Amin for his continuous guidance, motivation and support during the course of my studies. His valuable suggestions broadened my horizon in the field of power engineering and made this work interesting and challenging for me. Without his invaluable support and help, it would not have been possible for me to complete this work successfully. I wish to express my deep gratitude and appreciation to Dr. Mohammed Ali Y. Abido for his technical help and reviews in the successful completion of this work. The references that he suggested to me to understand sub-synchronous resonance (SSR), were of great help to me. I am also very much grateful to Dr. Ali Al-Awami for his reviews and efforts serving on my thesis committee.

I am very grateful to Research Institute, KFUPM for providing me valuable data and software support for this study. I would like to thank Mr. Arif for his efforts and support

regarding PSCAD and required data for this study and Mr. Firoz for his efforts in data collection.

I would also like to express my deep gratitude to my mother and my whole family for their prayers, encouragement and support during my study at KFUPM.

I am very thankful to Emad Fuad Areed, Fahad Zia, Haroon Ashraf, Muhammad Waqar Ahmed, Anum Ali, Ali Qureshi, Asjad Amin, Muhammad Mujahid Amin, Muhammad Usman Mukhtiar and Yasir Abdullah Siddiqui for their help and encouragement during my Masters. Also special thanks to Muhammad Umer Khan, Ahmer Ali Buzdar and Syed Essamuddin Ahmed for their camaraderie and good spirits. I would also like to acknowledge all the Electrical Engineering department faculty members with whom I took courses during my M.S., who helped me a lot during my coursework. I also owe thanks to all the students and faculty with whom I interacted during my Master's program.

# TABLE OF CONTENTS

ACKNOWLEDGMENTS.....	V
TABLE OF CONTENTS.....	VII
LIST OF TABLES.....	X
LIST OF FIGURES.....	XI
LIST OF ABBREVIATIONS.....	XIV
ABSTRACT.....	XVI
ملخص الرسالة.....	XVIII
CHAPTER 1 INTRODUCTION.....	1
1.1 POWER QUALITY ISSUES CAUSED BY THE ELECTRIC ARC FURNACE .....	1
1.2 POSSIBLE EFFECTS OF EAF ON THE SHAFT AND ROTARY PARTS OF TURBINE-GENERATOR SYSTEM	2
1.3 THESIS MOTIVATION.....	3
1.4 THESIS OBJECTIVES .....	4
1.5 THESIS METHODOLOGY .....	5
1.6 THESIS CONTRIBUTIONS.....	5
1.7 THESIS ORGANIZATION .....	6
CHAPTER 2 LITERATURE REVIEW .....	7
2.1 Mathematical Modeling of the EAF.....	7
2.2 Modeling of the EAF by Using Field Measurements .....	14
2.3 Effects of the EAF on Synchronous Generator .....	19



2.4	Mitigation Techniques Used for Alleviating the EAF Impact on the Grid/Generator .....	20
-----	---	----

**CHAPTER 3 MODELING OF 27TH ORDER FIRST BENCH MARK MODEL OF IEEE..... 22**

3.1	SUB-SYNCHRONOUS RESONANCE (SSR) .....	22
3.1.1	SELF-EXCITATION.....	22
3.1.2	INDUCTION GENERATOR EFFECT .....	23
3.1.3	TORSIONAL INTERACTION .....	23
3.1.4	TRANSIENT TORQUES.....	23
3.2	FIRST BENCH MARK MODEL FOR SSR STUDIES .....	24
3.3	EQUATIONS OF TURBINE-GENERATOR SYSTEM .....	24
3.4	EQUATIONS OF TURBINE TORQUE & GOVERNOR SYSTEM .....	26
3.5	CAPACITOR-COMPENSATED TRANSMISSION LINE EQUATIONS.....	28
3.6	EQUATIONS OF SYNCHRONOUS GENERATOR .....	28
3.7	EQUATIONS OF EXCITATION SYSTEM .....	30
3.8	COMPLETE STATE-SPACE MODEL FOR SSR EIGEN VALUE ANALYSIS .....	30
3.9	SYSTEM DATA FOR THE FIRST BENCH MARK MODEL OF IEEE [57] .....	31
3.10	EIGEN VALUES OF THE 27TH ORDER SYSTEM .....	32
3.11	TORSIONAL OSCILLATION MODES .....	34

**CHAPTER 4 MODELING OF ELECTRIC ARC FURNACE..... 35**

4.1	REAL TIME DATA ACQUISITION AND ANALYSIS .....	37
4.2	MODELING OF INITIAL (FIRST) STAGE of EAF OPERATION .....	38
4.3	MODELING SECOND STAGE of EAF OPERATION .....	42

**CHAPTER 5 SIMULATION RESULTS..... 44**

5.1	Actual EAF Waveforms.....	44
5.2	IEEE FIRST BENCH MARK MODEL SIMULATION RESULTS .....	48
5.3	Comparison of the Real and Simulated Values .....	55

5.4	Simulation Results during first stage of EAF operation:.....	63
5.5	Simulation results during second stage of the EAF operation.....	77
5.6	Analysis of Effects of the EAF Operation on the Shaft of Synchronous Generator .....	82
<b>CHAPTER 6 RECOMMENDED MITIGATION TECHNIQUE .....</b>		<b>83</b>
<b>CHAPTER 7 CONCLUSION AND FUTURE WORK .....</b>		<b>86</b>
<b>REFERENCES.....</b>		<b>89</b>
<b>APPENDIX .....</b>		<b>95</b>
<b>VITAE .....</b>		<b>97</b>

## LIST OF TABLES

Table 3.1 Description of variables used in equations of synchronous generator.....	29
Table 3.2 Eigen values of the 27th order IEEE first bench mark SMIB power system for $X_C = 0.2 * X_L$ .....	32
Table 3.3 Eigen values of the 27th order IEEE first bench mark SMIB power system for $X_C = 0.3 * X_L$ .....	33
Table 3.4 Modal frequencies of six torsional modes of the six-mass-spring system .....	34
Table 4.1 Parameters of the model for the first stage of the EAF operation .....	41
Table 4.2 Parameters of the model for the second stage of the EAF operation.....	43
Table 5.1 FFT of measured and simulated waveforms (sub-synchronous components)..	60
Table 5.2 Comparison of measured and simulated values.....	62

# LIST OF FIGURES

Figure 2.1 Actual and piece-wise linear approximation of V-I characteristics of an EAF load [6] .....	8
Figure 2.2 V-I characteristics of current-controlled non-linear resistance model [8].....	11
Figure 2.3 V-I characteristics of non-linear time-varying resistance model [10].....	12
Figure 3.1 The First Bench Mark Model of IEEE [57].....	24
Figure 3.2 A linear six-mass-spring turbine-generator system [57] .....	25
Figure 3.3 A two-time-constant governor [57] .....	26
Figure 3.4 Transfer functions of steam turbines [57] .....	27
Figure 3.5 A two-time-constant excitation system [57].....	30
Figure 4.1 Single machine infinite bus with EAF as load .....	36
Figure 4.2 Block diagram of the actual power system containing the EAF .....	38
Figure 5.1 Current Recorded at the LV side of the 230/34.5 kV transformer for EAF....	44
Figure 5.2 FFT of current waveform in Figure 5.1 .....	45
Figure 5.3 Voltage Recorded at the LV side of the 230/34.5 kV transformer for EAF ...	45
Figure 5.4 FFT of voltage waveform in Figure 5.3 .....	46
Figure 5.5 PSCAD SSR MODEL.....	48
Figure 5.6 Active power of synchronous generator in steady-state.....	49
Figure 5.7 Reactive power of synchronous generator in steady-state .....	50
Figure 5.8 Rotor angle of synchronous generator in steady-state.....	50
Figure 5.9 Mechanical torque of synchronous generator in steady-state.....	51
Figure 5.10 THI torque of shaft of synchronous generator in steady-state .....	51
Figure 5.11 TIA torque of shaft of synchronous generator in steady-state .....	52

Figure 5.12 TAB torque of shaft of synchronous generator in steady-state .....	52
Figure 5.13 TBG torque of shaft of synchronous generator in steady-state .....	53
Figure 5.14 TGEX torque of shaft of synchronous generator in steady-state .....	53
Figure 5.15 PSCAD MODEL OF THE EAF .....	55
Figure 5.16 EAF measured and simulated current values for comparison .....	56
Figure 5.17 EAF measured and simulated voltage values .....	56
Figure 5.18 V-I characteristics for EAF1 .....	57
Figure 5.19 V-I characteristics for PSCAD based EAF model .....	57
Figure 5.20 Arc length variation for PSCAD model .....	58
Figure 5.21 FFT of EAF1 current .....	59
Figure 5.22 FFT of PSCAD MODELED EAF current .....	59
Figure 5.23 FFT of EAF1 voltage.....	61
Figure 5.24 FFT of PSCAD MODELED EAF voltage .....	61
Figure 5.25 PSCAD SSR and EAF Complete Model.....	63
Figure 5.26 Turbine torque THI during first stage of EAF operation .....	64
Figure 5.27 Initial variations of turbine torque THI during first stage of EAF operation	64
Figure 5.28 FFT of turbine torque THI during initial stage of EAF operation.....	65
Figure 5.29 Turbine torque TIA during first stage of EAF operation .....	66
Figure 5.30 Initial variations of turbine torque TIA during first stage of EAF operation	66
Figure 5.31 FFT of turbine torque TIA during initial stage of EAF operation.....	67
Figure 5.32 Turbine torque TAB during first stage of EAF operation .....	68
Figure 5.33 Initial variations of turbine torque TAB during first stage of EAF operation.....	68

Figure 5.34 FFT of turbine torque TAB during initial stage of EAF operation .....	69
Figure 5.35 Turbine torque TBG during first stage of EAF operation .....	70
Figure 5.36 Initial variations of turbine torque TBG during first stage of EAF operation .....	70
Figure 5.37 FFT of turbine torque TBG during initial stage of EAF operation .....	71
Figure 5.38 Turbine torque TGEX during first stage of EAF operation .....	72
Figure 5.39 Initial variations of turbine torque TGEX (few cycles) during first stage of EAF operation .....	72
Figure 5.40 FFT of turbine torque TGEX during initial stage of EAF operation.....	73
Figure 5.41 SSR Model EAF current during initial stage of EAF operation.....	74
Figure 5.42 SSR Model EAF voltage during initial stage of EAF operation .....	74
Figure 5.43 EAF current FFT .....	75
Figure 5.44 EAF voltage FFT .....	75
Figure 5.45 SSR model EAF VI characteristics during initial stage of EAF operation ...	76
Figure 5.46 THI during second stage of EAF operation.....	77
Figure 5.47 TIA during second stage of EAF operation.....	77
Figure 5.48 TAB during second stage of EAF operation .....	78
Figure 5.49 TBG during second stage of EAF operation .....	79
Figure 5.50 TGEX during second stage of EAF operation.....	79
Figure 5.51 EAF current during second stage of its operation .....	80
Figure 5.52 EAF voltage during second stage of its operation.....	80
Figure 5.53 VI characteristics during second stage of EAF operation .....	81

## LIST OF ABBREVIATIONS

EAF	Electric Arc Furnace
CSIM	Cubic Spline Interpolation Method
HCIM	Harmonic Current Injection Model
HVSM	Harmonic Voltage Source Model
ANN	Artificial Neural Network
LUT	Look-up Table
RBFNN	Radial Basis Function Neural Network
BPN	Back-Propagation Network
THD	Total Harmonic Distortion
DWT	Discrete Wavelet Transform
DE	Differential Evolution
GA	Genetic Algorithm
ANFIS	Adaptive Neuro-Fuzzy Inference Systems
SES	Sequential Event Simulator
SVC	Static Var Compensator
DRI	Direct Reduced Iron
ESS	Energy Storage Systems
FACTS	Flexible Alternating Current Transmission Systems
STATCOM	Static Synchronous Compensator
DSTATCOM	Distribution Static Synchronous Compensator
SES	Static Excitation System
HP	High Pressure turbine
IP	Intermediate Pressure turbine

LPA	Low Pressure turbine A
LPB	Low Pressure turbine B
GEN	Generator (Synchronous Generator)
EX	Exciter
PQ	Power Quality
FFT	Fast Fourier Transform
DFT	Discrete Fourier Transform
HV	High Voltage
LV	Low Voltage
MV	Medium Voltage
SSR	Sub-synchronous Resonance
PCC	Point of Common Coupling
SMIB	Single Machine Infinite Bus
THI	Torque between HP and IP on shaft of synchronous generator
TIA	Torque between IP and LPA on shaft of synchronous generator
TAB	Torque between LPA and LPB on shaft of synchronous generator
TBG	Torque between LPB and GEN on shaft of synchronous generator
TGEX	Torque between GEN and EX on shaft of synchronous generator



## **ABSTRACT**

Full Name : Fazal Illahi

Thesis Title : Analysis and mitigation of effects of electric arc furnace operation on shaft of synchronous generator

Major Field : Electrical Engineering

Date of Degree : December 2014

The purpose of this thesis is to assess the impacts of steel industrial electric arc furnaces on the shaft of the synchronous generator. Actual electric arc furnace current and voltage measurements are taken through Power Quality (PQ) meter. An appropriate analytical modeling technique to build the Electric Arc Furnace (EAF) model is used. The modeling technique utilizes the stochastic variation of arc length to incorporate the dynamic characteristics of the electric arc furnace. The model is built in PSCAD. Parameters of the model are estimated on the basis of values of ignition and extinction voltages of the dataset taken from the measured data. The modeled current and voltage waveforms are compared with the measured data on the basis of Total Harmonic Distortion (THD) and Fast Fourier Transform (FFT) in order to validate the model. To assess the effects of the EAF operation on the shaft of the generator, IEEE First Bench Mark Power System is modeled into PSCAD and the EAF is connected to the generator bus. The operation of the EAF is divided into two major stages as happens in real electric arc furnaces. The first stage represents the initial melting stage in which scrap is melted and arc length changes very rapidly. This stage is represented by a non-linear time varying resistance model with the arc length varying stochastically. The second stage represents the later melting stage also called quiet melting stage in which most of the scrap has been melted and there are

very less arc length variations. This stage has been modeled by a simple non-linear current-controlled resistance model with a constant arc length. It is found that the EAF causes torsional oscillations during the first stage of its operation. Second, third, fourth and fifth torsional modes of the shaft of the turbine-generator system are found to be susceptible. The EAF does not cause Sub-Synchronous Resonance (SSR) during the first stage of its operation because the sub-synchronous frequencies appearing in the turbine torques are not equal to the oscillating frequencies of torsional modes of the turbine-generator system. Since the EAF does not cause the SSR, no mitigation technique is applied. However, based on the critical analysis of literature, a mitigation technique is recommended to improve the power quality and alleviate the torsional oscillations caused by the EAF. During the second stage, the EAF does not cause any torsional oscillations.

## ملخص الرسالة

الاسم الكامل: فضل الهي

عنوان الرسالة: تحليل وتخفيف لاثار تشغيل أفران القوس الكهربائي على عامود المولد المتزامن

التخصص: الهندسة الكهربائية

تاريخ الدرجة العلمية: ديسمبر-2014

الهدف من هذه الرسالة البحثية هو تقييم تأثير أفران القوس الكهربائية الصناعية المستخدمة للفولاذ على عمود المولد المتزامن. تم أخذ القراءات الفعلية سواء كانت للفولتية أو التيار لأفران القوس باستخدام عدادات الطاقة النوعية (PQ). بالإضافة الى ذلك، تم استعمال تقنية النمذجة التحليلية الصحيحة لبناء نموذج فرن القوس الكهربائي (EAF). النموذج المستخدم في ذلك يستعمل التغيير العشوائي لطول القوس لدمج الخصائص الديناميكية لهذا الفرن. تم بناء هذا النموذج باستخدام برنامج PSCAD. تم تخمين معاملات النموذج بناء على قيم اشتعال وخمود الفولتية المنبثقة من مجموعة البيانات المستقاة من قيم البيانات المقاسة. بالإضافة الى ذلك، تم مقارنة قيم الفولتية والتيار بالقيم المقاسة بناء على التشوه التوافقي الكلي (THD) وأيضاً تحويله فوربيير السريعة (FFT) للتأكد من صحة هذا النموذج.

ولتقييم تأثيرات تشغيل أفران القوس الكهربائية على عامود المولد، تم بناء نظام الطاقة (IEEE First Bench Mark Power System) على برنامج (PSCAD) وأيضاً توصيل فرن القوس الكهربائي على نقطة ربط المولد. يمر تشغيل الفرن الكهربائي بمرحلتين أساسيتين كما الواقع العملي لأفران القوس الكهربائي. فأما المرحلة الأولى فتتمثل المرحلة المبدئية حيث يتم صهر الخرودة مع تغيير سريع لطول القوس الكهربائي حيث أن هذه المرحلة تمثل نموذج المقاومة المعتمدة على المعادلات الزمنية المتغيرة غير الخطية مع تغيير عشوائي لطول القوس. أما المرحلة الثانية فهي تمثل مرحلة الصهر الأخيرة أو ما يدعى بمرحلة الصهر التام حيث أنه في هذه المرحلة يكون تغيير طول القوس أقل بكثير من المرحلة السابقة. هذه المرحلة يتم تمثيلها ونمذجتها باستخدام نموذج المقاومة ذات التيار المتحكم به بالمعادلات غير الخطية البسيطة مع المحافظة على طول ثابت لطول القوس الكهربائي.

مما سبق تبين أن أفران القوس الكهربائي (EAF) تسبب التواءات تذبذبية خلال المرحلة الأولى من تشغيلها و أن القيم الذاتية الالتوائية الثانية والثالثة والرابعة والخامسة لعامود توربين المولد حساسة. لا تسبب هذه الأفران الكهربائية أيا من الرنين المتزامن الفرعي (SSR) خلال المرحلة الأولى من التشغيل لأن الترددات المتزامنة الفرعية لعزم التوربين لا تساوي تلك الترددات المتذبذبة للقيم الذاتية الالتوائية لنظام توربين المولد. وحيث أن أفران القوس الكهربائي لا تسبب هذا الرنين المتزامن الفرعي فلم يطبق أيا من تقنيات التخفيف. على أية حال، بناء على التحليل الحرج في أدبيات الموضوع فإنه تم التوصية بتقنية التخفيف لتحسين نوعية الطاقة والتقليل من التذبذبات الالتوائية الناتجة من أفران القوس الكهربائي. وأما المرحلة الثانية فإن هذه الأفران الكهربائية لا تسبب أيا من تلك التذبذبات الالتوائية.

# CHAPTER 1

## INTRODUCTION

### 1.1 POWER QUALITY ISSUES CAUSED BY THE ELECTRIC ARC FURNACE

Steel-making industries widely employ electric arc furnaces (EAFs) in the process of recycling of scrap. The EAF makes use of low voltage and high current electric arc existing between the electrodes and the melting material to produce high temperatures. Since the melting process of an EAF is a non-stationary stochastic process, the EAF causes significant flickers, harmonics and inter-harmonics in the supply network especially at the point of common coupling. EAF is a major energy consumer in the steel plant and can cause flickering and harmonic effects back to the network utility. An electric arc furnace is a highly non-linear load due to the chaotic nature of arc impedance [1] as the factors of temperature and pressure determine its conductivity [2]. So, the modeling and control of EAF have become an important subject of the current research. In order to mitigate the severe effects of EAF on the power systems, utilities and industrial users are going for different viable solutions, some of which include the use of D-STATCOMS, series reactors and SVCs.

EAF can be supplied either by AC or DC power. Power quality problems are caused due to the non-linear nature of the operation of an AC EAF. It is difficult to predict the flicker caused due to AC EAF accurately. DC EAF operation is more stable as compared to that

of AC EAF because of firing and extinction of the arc at zero crossings of the waveform and DC arc furnace technology causes reduction in flicker as compared to AC arc furnace. However, the use of power electronic converter in the DC EAF gives rise to harmonic pollution. But the characteristics of the DC EAF are more predictable because most of the harmonics are caused due to the converter and the harmonic content of a converter can be easily calculated [3].

## **1.2 POSSIBLE EFFECTS OF EAF ON THE SHAFT AND ROTARY PARTS OF TURBINE-GENERATOR SYSTEM**

Due to pulsating nature of the arc, the EAF can be considered as a non-linear and pulsating load for the network or generator supplying it [4]. Non-linear and pulsating loads may cause sub-synchronous resonance and enforce large transient torques on turbine-generator shaft. This problem becomes more critical when a generator is closely coupled to an EAF load and if the generation power is approximately equal to the consumed power of the EAF. There exists the possibility of immediate damage and loss of fatigue life of the interconnecting shafts and associated rotating parts.

One of the most remarkable cases where the EAFs caused generator problems is that of the Comanche power station, situated in Pueblo, Colorado, USA. The plant includes two generators: Unit 1, 450 MVA, commissioned in 1973 and Unit 2, 440MVA, commissioned in 1975 [5]. A steel mill equipped with two 60 MVA arc furnaces and one SVC is located at a distance of approximately 5 km away from the Comanche power station. Unit 2 generator suffered a cracked generator shaft near the turbine end coupling

in 1987. Metallurgical investigations divulged that torsional stresses, combined with a shaft configuration that concentrated the forces, initiated the crack. Further tests revealed that sub-synchronous natural frequencies did not cause any considerable amount of torsional stress. However, it was noticed that the sixth mode natural frequency coincided with 120 Hz (122.5 Hz for Unit 1) which had caused a dangerous resonant coupling between the generator and the power system. The shaft was repaired and the sixth natural torsional frequency of both the units was shifted away from 120 Hz. Again two faults occurred on the brushless exciter of unit 2 due to torsional effects on generator shaft in 1993. The retaining ring on the generator of Unit 2 failed in 1994 and a metallurgical examination of the failed ring showed that the torsional stress again caused the failure. Further tests showed that an inter-harmonic component in the current spectrum whose frequency ranged from 114 Hz to 118 Hz and whose magnitude was about 1% of the fundamental current. The source of this inter-harmonic current component was found to be a control loop within the SVC unit at the steel mill. Under certain operating conditions, this control loop was becoming unstable. This control loop within the SVC unit at the steel mill was retuned to lower the speed of response and after that it was found to be stable.

### **1.3 THESIS MOTIVATION**

The EAF causes severe harmonics and flicker problems to the neighboring power systems and can also affect the grid or a synchronous generator to which it is closely coupled because of its non-linear and stochastic characteristics. Many research articles have addressed the modeling and analysis of the harmonics and flicker caused by the

EAF load. The EAF can also cause severe damage to the shaft of the generator. Due to increasing use of the EAF in the steel industry, it is very much indispensable to study the effects of the EAF on the shaft of the synchronous generator. Limited research articles are written on this topic. Thus, there is a strong need to explore the effects of the EAF in the vicinity of a power plant.

## **1.4 THESIS OBJECTIVES**

This thesis attempts to address the following objectives:

1. Modeling of the EAF. The model is to be used in conjunction with the IEEE First Bench Mark model used for the sub-synchronous resonance (SSR) studies.
2. Modeling of the First Bench Mark IEEE Single Machine Infinite Bus power system.
3. The main objective of this thesis is to analyze the effects of the electric arc furnace operation on the shaft of the synchronous generator.
4. Proposing mitigation techniques, if warranted.



## **1.5 THESIS METHODOLOGY**

The IEEE First Bench Mark power system is modeled in PSCAD. Eigen value analysis is performed in MATLAB by writing a program. The state equations for the generator are derived. Finally, the EAF is modeled in PSCAD. This is done to study the effects of the EAF on a nearby synchronous generator.

Two separate stages of EAF operation are considered to model the EAF and to study its effect on the shaft of the generator. The first stage is when EAF has started operating and it is melting Direct Reduced Iron (DRI) and the scrap. During this stage the EAF is modeled as a non-linear time varying resistance whose arc length varied along with time. The second stage begins when whole of scrap has been melted and the disturbances have been reduced. This stage is quiet melting stage. A simple non-linear current-controlled resistance model has been used to model the EAF during this stage.

## **1.6 THESIS CONTRIBUTIONS**

There are mainly two contributions.

1. Integration of the approach of stochastic variation of arc length into the non-linear resistance model for the modeling of the EAF.
2. Analyzing the effects of the EAF operation on the shaft of the synchronous generator by including an EAF model which is verified with the actual EAF data.

## **1.7 THESIS ORGANIZATION**

This thesis report is organized as follows:

Chapter 2 presents Literature Survey. The literature survey includes the research articles which have mainly focused on mathematical modeling of the EAF, modeling of the EAF based on field measurements, effects of the EAF operation on the shaft of the synchronous generator and mitigation techniques proposed to alleviate the effects of the EAF operation on the power system.

Chapter 3 explains the modeling of IEEE First Bench Mark Power System. Eigen values and torsional modes for the power system are derived.

Chapter 4 presents the modeling of the electric arc furnace based on field measurements. Two different types of models are used to represent the two stages of the EAF operation. Stochastic variation of arc length is used to model the initial stage of the EAF operation.

Chapter 5 presents simulation results and the analysis of the effects of the EAF operation on the shaft of the synchronous generator.

Chapter 6 presents the recommendation of a mitigation technique on the basis of critical analysis of the literature.

Chapter 7 concludes the thesis report and recommendations for future work are also presented in it.

## CHAPTER 2

### LITERATURE REVIEW

#### 2.1 Mathematical Modeling of the EAF

A time domain based current controlled voltage source model is developed in [6] and simulation is performed using Electro Magnetic Transients Program (EMTP). Piecewise linear approximation of the V-I characteristics of the EAF load is presented on the basis of which the developed model is derived. Both static and dynamic models are presented. The dynamic variation of the EAF load is taken into account by considering sinusoidal and band limited white noise variation of the arc resistance in the V-I characteristics of EAF load. Figure 2.1 shows the actual V-I characteristics and piece-wise linear V-I characteristics of an EAF. The piecewise linear model is given as:

$$V = \begin{cases} R_1 i & -i_1 \leq i < i_1 \\ R_2 i + V_{ig} \left(1 - \frac{R_2}{R_1}\right) & i_1 < i \leq i_2 \\ R_2 i - V_{ig} \left(1 - \frac{R_2}{R_1}\right) & -i_2 \leq i < -i_1 \end{cases} \quad (2.1)$$

$$i_1 = \frac{V_{ig}}{R_1} \quad (2.2)$$

$$i_2 = \frac{V_{ex}}{R_2} - V_{ig} \left(\frac{1}{R_2} - \frac{1}{R_1}\right) \quad (2.3)$$

Where  $R_1$  and  $R_2$  are the slopes of the low and high current sections of the V-I characteristics of the EAF load respectively,  $V_{ig}$  is the arc ignition voltage,  $V_{ex}$  is the arc

extinction voltage and  $i_1$  and  $i_2$  are currents corresponding to the arc ignition and arc extinction voltages respectively.

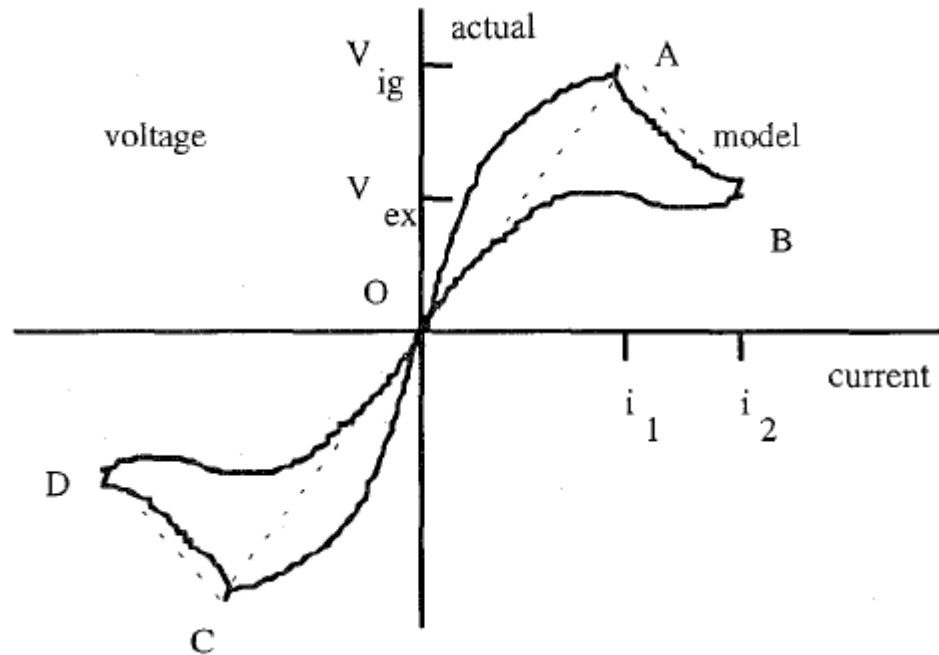


Figure 2.1 Actual and piece-wise linear approximation of V-I characteristics of an EAF load [6]

A non-linear approximation model of EAF is given in [7]. This model divides the arc melting process into three sections. In the first section, the EAF behaves like a resistance and the arc goes from extinction to re-ignition. The second section refers to the beginning of the EAF melting process. The third section shows the normal arc melting process. The non-linear approximation model is given as:

$$V = \left\{ \begin{array}{ll} R_1 i & (-i_3 \leq i < i_1, \text{inc}) \text{ or} \\ & (-i_1 \leq i < i_3, \text{dec}) \\ V_{st} + (V_{ig} - V_{st}) e^{\frac{i_1-i}{i_T}} & (i_1 \leq i < i_2, \text{inc}) \\ V_{st} + (i - i_2) R_2 & (i \geq i_2, \text{inc}) \\ V_{ex} + (i - i_3) R_3 & (i \geq i_3, \text{dec}) \\ -V_{st} + (V_{st} - V_{ig}) e^{\frac{i_1+i}{i_T}} & (-i_2 \leq i < -i_1, \text{dec}) \\ -V_{st} + (i + i_2) R_2 & (i < -i_2, \text{dec}) \\ -V_{ex} + (i + i_3) R_3 & (i < -i_3, \text{inc}) \end{array} \right\} \quad (2.4)$$

$$i_1 = \frac{V_{ig}}{R_1}, \quad i_T = 1.5i_1, \quad i_2 = 3i_1, \quad i_3 = \frac{V_{ex}}{R_1} \quad (2.5)$$

Where,  $R_1$ ,  $R_2$  and  $R_3$  are the corresponding slopes of each section and ‘inc’ and ‘dec’ represent the increasing and decreasing trend of the EAF current respectively.

The electric arc furnace load is modeled as a current controlled non-linear resistance in [8] and [9]. In an electric arc furnace, the electrical energy is converted into the thermal energy. The melting material is moved randomly due to which no two cycles of the arc current and voltage waveforms are identical. During the refining period, less number of fluctuations occur. After observing the V-I characteristics of the EAF, the melting process of EAF is divided into three periods. The first period represents the re-ignition of the arc. During the second period, the arc is established while in the third period the arc commences to extinguish. The non-linear resistance of the EAF load depends on the arc length which can be determined by the position of the electrodes. The model is given as:

$$R_a = \left\{ \begin{array}{l} R_g \\ \left[ \frac{V_d + (V_{ig} - V_d)e^{-\frac{|i| - i_{ig}}{\tau_1}}}{|i|} \right] \\ \left[ \frac{V_t + (V_{ig} - V_t)e^{-\frac{|i|}{\tau_2}}}{|i| + i_{ig}} \right] \end{array} \right. \left. \begin{array}{l} 0 \leq |i| < i_{ig}, \frac{d|i(t)|}{dt} > 0 \\ |i| \geq i_{ig}, \frac{d|i(t)|}{dt} > 0 \\ \frac{d|i(t)|}{dt} < 0 \end{array} \right\} \quad (2.6)$$

Where:

$$V_{ig} \approx 1.15V_d, i_{ig} = \frac{V_{ig}}{R_g}, V_t = \left[ \frac{I_{max} + i_{ig}}{I_{max}} \right] V_d \quad (2.7)$$

‘ $R_g$ ’ is the arc resistance during the first period of EAF operating cycle, ‘ $V_{ig}$ ’ is the ignition voltage, ‘ $i_{ig}$ ’ is the ignition current, ‘ $\tau_1$ ’ and ‘ $\tau_2$ ’ are time constants and ‘ $V_t$ ’ is the extinction voltage. When the arc is established during the second period of the EAF operation, the voltage drops from the ignition voltage to a certain value and ‘ $V_d$ ’ represents this value of the voltage.

The average arc voltage ‘ $V_d$ ’ depends on average arc length ‘ $l$ ’ and is given as:

$$V_d = A + B.l \quad (2.8)$$

Where, ‘ $A$ ’ and ‘ $B$ ’ are constants. Therefore, the non-linear resistance is dependent on the arc length. The V-I characteristics for this model are shown in Figure 2.2.

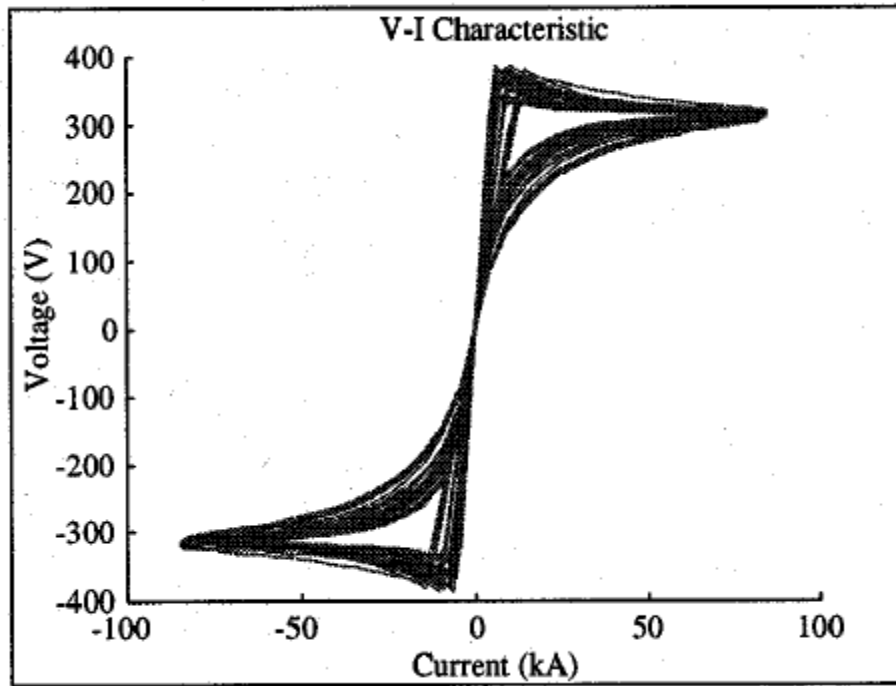


Figure 2.2 V-I characteristics of current-controlled non-linear resistance model [8]

The electric arc furnace is modeled as a non-linear time varying resistance in [10] and this model was reviewed in [7]. According to [7], this model ignores the voltage rising time. The positive half-cycle of the V-I characteristics is expressed as:

$$V = \text{sig}(i) \cdot \left[ V_{\text{at}} + \frac{C}{D+|i|} \right] \quad (2.9)$$

Let ' $l$ ' be the arc length, 'A' and 'B' are the coefficients from experimental formula, then

$$V_{\text{at}} = A + B \cdot l \quad (2.10)$$

Where ' $V_{\text{at}}$ ' is the threshold value to which voltage tends when current increases, C and D are constants whose values determine the difference between the increasing and

decreasing-current parts of the V-I characteristics. The V-I characteristics for this model (Figure 2.3) are given as:

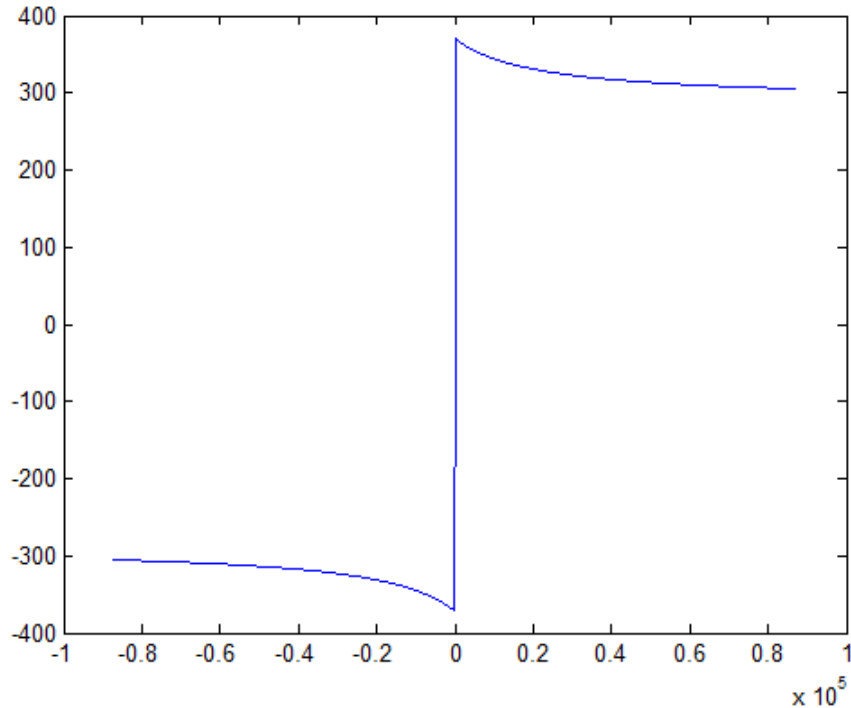


Figure 2.3 V-I characteristics of non-linear time-varying resistance model [10]

Four EAF models including piecewise linear model, non-linear approximation model, current controlled non-linear resistance model and non-linear time varying resistance model are reviewed in [11] and through simulation it is concluded that non-linear approximation model and the current controlled non-linear resistance prove to be more accurate. Finally, a new technique for developing the dynamic model of the EAF is proposed in [11]. According to the new dynamic model, the slope of the high current section of the V-I characteristics of the EAF load is chosen as the modulation index whereas in all the previous models reviewed the slope of the low current section of the V-



I characteristics of the EAF load was taken as modulation index. Using a MATLAB simulation, it is concluded that the proposed new dynamic model generates more flicker which is expected.

The simplest method to model an EAF load is by using an inductor in series with a resistor [12]. EAF has been modeled as a time-varying voltage source in [13] [14] by defining the arc voltage as a non-linear function of the arc length. Non-linear differential equation based classic models are presented in [15] [16] for EAF modeling. Mayr's and Cassie's equations are solved to get the non-linear conductance of the EAF.

Because of the pulsating nature of the arc, the EAF is considered as a non-linear and pulsating load for the network or generator supplying it [4]. Non-linear and pulsating loads cause sub-synchronous resonance and enforce huge transient torque on turbine-generator shaft. There exists the potential for immediate damage and fatigue life of the interconnecting shafts and associated rotating parts can be reduced.

An EAF model based on frequency-domain analysis method is proposed in [17]. The arc current and voltage are represented by their harmonic components. Assumption which is made in this model is that the EAF draws maximum power at its fundamental frequency, which is not always true [18]. The stochastic nature of the arc cannot be represented by this model [19].

Six different EAF models (time-domain and frequency-domain) presented in the literature are simulated in [20] and are analyzed and compared on the basis of harmonics and voltage distortion. Sinusoidal variation or band-limited white noise variation around a reference value can be used to represent the actual arc resistance [21].

A flicker severity analysis module has been developed in [22] to determine the voltage flicker at the point of common coupling (PCC) for a network containing multiple EAFs fed from one substation. EAFs are modeled by piece-wise linear model described in [6]. To introduce flicker into the model, arc resistance is varied by sinusoidal modulation and stochastic variation. Short-term flicker severity index has been calculated for both the cases (sinusoidal and stochastic). It is found that short-term flicker severity index for model based on sinusoidal modulation is higher than the one based on stochastic variation of arc resistance. A MATLAB program is used to implement International Electro-technical Commission (IEC) flicker meter which is used to calculate the flicker at the point of common coupling. The main contribution is that the proposed flicker severity analysis module can be used to estimate the flicker caused by multiple EAFs at PCC. Assumption is made that the EAFs are fed from same substation.

## **2.2 Modeling of the EAF by Using Field Measurements**

Field measurements of the voltage and current can describe the non-linear behavior of an EAF represented by V-I characteristics in an effective manner. Sufficient measured information can be utilized to characterize specific sources of harmonics, to determine the background harmonics level in a power system and to develop the appropriate non-linear V-I characteristics. Based on the measured electric arc furnace (EAF) voltages and currents, a dynamic EAF conductance model developed by using a curve-fitting based method called cubic spline interpolation method (CSIM) is proposed in [23]. This model can be used to represent the V-I characteristics of an EAF in steady state. Two other classic models including harmonic current injection model (HCIM) and harmonic voltage source model (HVSM) are also reviewed in this paper to compare their performance with

that of the proposed model. The results are compared by analyzing the harmonic contents of EAF current and voltage waveforms and by calculating the average relative error compared to the measured data.

In recent years, artificial neural network (ANN) has emerged as a powerful scheme for function learning and modeling non-linear loads. Nevertheless, a direct application of ANN for modeling time-varying loads can lead to inaccuracies. An efficient approach which combines radial basis function neural network (RBFNN) and look-up table (LUT) method is presented in [24] to model the highly non-linear v-i characteristics of an EAF accurately. Though RBFNN is more computationally efficient than back propagation network (BPN) and is known to be very apt to solve the non-linear curve-fitting problems, the traditional problem of wrong mapping exists in RBFNN also. Stationary input-output relationship is the cause of wrong mapping problem occurring in RBFNN and other neural networks. This drawback of functional mapping inaccuracy is overcome by incorporating LUT method into the proposed RBFNN based model. The proposed model based results are compared with the results obtained by two traditional neural network models which are Back-Propagation Network (BPN) and Radial Basis Function Neural Network (RBFNN) models and the actual measured data. The results show better performance for the proposed model. The comparison is drawn on the basis of total voltage harmonic distortion ( $THD_V$ ), real power, reactive power, apparent power, RMS voltage and short-term flicker severity of EAF voltage during the refining period.

An EAF model based on the combination of discrete wavelet transform (DWT), RBFNN and enhanced look-up tables is proposed in [25] and the results are compared with the

measured data. The results are compared on the basis of relative RMS voltage value error, harmonic voltage distortions and short-term flicker severity.

An EAF model is presented in [26]. The model is derived by linear approximation of the V-I characteristics of the EAF. Parameters of the model are tuned with field data using Monte-Carlo method. Probability distribution function for the third-order harmonic is calculated for the measured values, proposed model and Cassie conductance model of the EAF on the basis of which results are compared.

Extended Kalman filter is used in [27] to identify the parameters of the EAF current after which the differential equation describing the V-I characteristics of the EAF load is solved and the results are compared with the measured data by comparing power quality indices and co-relation indices. The differential equation is:

$$k_1 r^n + k_2 r \frac{dr}{dt} = \frac{k_3}{r^{m+2}} i^2 \quad (2.11)$$

Where: 'r' is the arc radius, 'i' is the arc current,  $k_1$ ,  $k_2$ ,  $k_3$ , m and n are constants.

A model of EAF based on the parameters of voltage taps, scrap and distance between the electrodes is presented in [28]. The model considers a new parameter of the EAF called capacitance of the EAF. The results are compared with the measured data by analyzing arc impedance and computing the error between the values.

Differential Evolution (DE) algorithm is used in [29] to estimate the parameters of differential equation describing the characteristics of the EAF. The results are compared with the measured data. The differential equation is:

$$(2.12)$$

$$\frac{dg}{dt} = \frac{k_2}{L} i^2 - k_1 k_2 g^{-\lambda}$$

$$\lambda = \beta - 1 \quad (2.13)$$

Where 'g' is the arc conductance, 'L' is the arc length, 'k1', 'k2' and 'β' are constants.

The EAF is modeled by a non-linear model in [30]. The non-linear model is:

$$V_a = V_{at}(l) + \frac{C}{D+I_a} \quad (2.14)$$

$$V_{at}(l) = A + B.l \quad (2.15)$$

Where: 'V<sub>a</sub>' and 'I<sub>a</sub>' are the arc voltage and current respectively; 'l' is the arc length; 'A', 'B', 'C' and 'D' are constants.

The values of parameters 'A', 'B', 'C' and 'D' are estimated by using a two-step genetic algorithm (GA) based algorithm and 'l' is described by a uniformly distributed random variable. Current waveforms and flicker severity index are used to compare the results of proposed model with the data obtained from a real EAF plant.

An adaptive neuro-fuzzy inference systems (ANFIS) based method is used in [31] for the modeling and simulation of EAF electrode positioning system called electrode regulator loop. Individual components of the EAF regulator loop are modeled using ANFIS and are assembled by using a discrete-sequential event simulator (SES). The effectiveness of the proposed technique is shown by comparing the simulator output results with those of an actual plant data. The uniqueness of this research lies in the fact that instead of modeling the whole EAF electrode regulator loop, individual components of the regulator loop are modeled and are then assembled. Tunable parameters required for ANFIS are much less

as compared with traditional neural networks. Therefore, ANFIS is much faster and more accurate than pure neural network based methods [32].

A novel EAF model based on the Hidden Markov Model theory is proposed in [33]. The results are compared with the measured data to verify the accuracy of the model. An adaptive neuro-fuzzy model is presented in [34] to model the non-linear V-I characteristics of the EAF.

A new time-varying, dynamic (differential) and non-linear model is presented in [35]. Proposed relationship between the EAF voltage and current is differential, non-linear and uses time-varying parameters. The dynamic characteristics of the EAF are modeled by a linear differential equation of the order of four (4). The order of the differential equation is set by comparing the calculated voltage values with the real EAF voltage values measured from a steel plant. Non-linearity is introduced into the model by modeling the error signal of the dynamic model as a third order polynomial function of the EAF current. All the coefficients related to the non-linear and dynamic parts in the model are modeled by time series to incorporate the time-varying nature of the EAF characteristics into the model. Second order autoregressive moving average (ARMA) models are used to represent all the coefficients of the model.

A stochastic time-domain model of the EAF based on a normalized inter-harmonic frequency spectrum of a real EAF measured current waveform is presented in [36].

### **2.3 Effects of the EAF on Synchronous Generator**

Torsional interactions caused by EAF load in the turbine-generator set are presented in [37]. Two different stages of EAF operation are considered. At the first stage when EAF is melting Direct Reduced Iron (DRI) and scrap, a pulsing load model is used for EAF. During the quiet melting stage which is the second stage of EAF operation, all the scraps have changed to melted material and distortion in EAF quantities is reduced. In this stage, EAF enforces less torque as compared to the first stage. A non-linear model is used to describe EAF behavior in this stage. Generator shafts interconnection experiences excessive torque imposed by EAFs especially when all the EAFs have been in scrap melting stage simultaneously. These torques can cause immediate or impending damage in turbine-generator shaft.

A power system containing EAF as load is considered in [38] and the effect of EAF on generator torque is analyzed. The EAF is modeled as a pulsing load. EAFs draw power in the form of pulses at around 5-6 Hz. This pulsing load is usually modeled as step-load-step-unload where the step is a complete load and complete unload. This step in power causes a step in the electrical torque of the generator supplying electricity to the EAF. A torsional interaction is produced due to this step in torque which can potentially cause damage to the interconnecting shafts and other parts of the generator rotor.

Effects of EAF operation on the shaft of the local power system generator are analyzed in [39]. Three types of models including pulsing load model, probability sampling based non-linear model with low power factor and hyperbolic exponential model (non-linear model with high power factor) are used to model the different stages of EAF operation and the resulting effects on the interconnecting shafts of the turbo-generator are analyzed.

It is found that the EAF exerts excessively high torques on the shaft of the generator located near it as compared to the steady-state value of the torque. The torque exerted by the EAF on the shaft of the local generator touches the highest peak during the stage when EAF is melting scrap and sponge iron charge (pulsing load model).

## **2.4 Mitigation Techniques Used for Alleviating the EAF Impact on the Grid/Generator**

The advantages of energy storage systems (ESS) are discussed in [40] to alleviate the effects of the EAF load. It is emphasized that ESS must be used along with Flexible Alternating Current Transmission System (FACTS) devices and using conventional compensation techniques (such as STATCOM) only will not be sufficient.

A non-linear multi-level STATCOM control scheme is used in [41] to mitigate the voltage flicker caused by the EAF.

Either a static VAR compensator (SVC) or a static synchronous compensator (STATCOM) is added to a power system containing the EAF for reactive power compensation in [42] [43] [44]. Multilevel-converter based STATCOMs are proposed and utilized in [45] and [46] to mitigate the arc furnace flicker. A non-linear control technique developed for STATCOM to achieve fast load regulation in the EAF applications is presented in [47]. An offline design online synthesis model predictive control algorithm is presented in [48] to regulate the electrode regulator system of the EAF. Lyapunov method is used to check the closed-loop system stability. Control algorithms for distribution static synchronous compensator (DSTATCOM) are developed



in [49] to alleviate the voltage flicker caused by the EAF. A novel electronic compensator is designed in [50] to compensate the reactive power consumed by the arc furnace.

Static excitation systems (SESs) of the generators located near arc furnaces are well tuned in [51] to improve the performance of generators during the period when the arc furnaces are operating. The parameters of SESs are identified and retuned in [52] to improve the dynamic performance of synchronous generators feeding the EAF loads.

A rolling Grey model and a Grey-Markov model based prediction method is used in [53] to forecast the reactive power consumption of the EAF for a half-cycle ahead. This method improves the performance of the SVC considerably. The results show that when the proposed prediction method is used to update the SVC for the reactive power compensation, SVC reduces the flicker caused by the EAF substantially higher than the case when no prediction method is used. It is also found that the rolling Grey model and the Grey-Markov model based prediction method for reactive power compensation reduces more flicker as compared to the ARMA models based prediction method.

An integrated hybrid approach combining Grey model and an improved radial basis function neural network (IRBFNN) is presented in [54] to forecast the flicker severity caused by electric arc furnaces. The proposed method can be very useful for the mitigation of voltage fluctuations caused by the EAFs because it can predict the flicker.

A first order and one variable Grey Model is employed in [55] to predict the reactive power consumption of the EAF at the SVC bus.

A phase-loop locked (PLL) based control technique for 6-pulse D-STATCOM is utilized in [56] to compensate voltage flicker due to the EAF load.

## **CHAPTER 3**

### **MODELING OF 27TH ORDER FIRST BENCH MARK**

#### **MODEL OF IEEE**

##### **3.1 SUB-SYNCHRONOUS RESONANCE (SSR)**

Sub-synchronous Resonance (SSR) phenomenon is defined as:

“Sub-synchronous resonance is an electric power system condition where the electric network exchanges energy with a turbine generator at one or more of the natural frequencies of the combined system below the synchronous frequency of the system.”

SSR problem can be caused in the following two aspects:

1. Self-excitation (steady-state SSR)
2. Transient torques (transient SSR)

##### **3.1.1 SELF-EXCITATION**

Low frequency (sub-synchronous) currents entering the generator terminals become the cause of producing sub-synchronous frequency voltage components across generator terminals. These voltage components may sustain the currents to produce an effect that is called self-excitation. Self-excitation can be further divided into two types which are induction generator effect and torsional interaction.

### **3.1.2 INDUCTION GENERATOR EFFECT**

Mechanical dynamics of rotor are not considered in the induction generator effect and only the rotor electrical dynamics are involved. Sub-synchronous frequency armature currents produce the rotating magneto-motive force (MMF). Speed of this rotating MMF is less than the speed of the rotor. Therefore, resistance of the rotor at the sub-synchronous frequency (viewed from the armature terminals) is negative due to the negative slip of the machine. If the magnitude of this negative resistance exceeds the sum of the network and armature resistances, self-excitation will be caused.

### **3.1.3 TORSIONAL INTERACTION**

Torsional interaction involves both electrical and mechanical dynamics of the rotor of the machine. When the sub-synchronous frequency component coincides or is very close to an electrical resonant frequency, the electrical resonance and the torsional oscillation will be mutually excited resulting in SSR. This interaction between mechanical and electrical modes is termed as torsional interaction. In such a case, torsional oscillation acts as a negative resistance to the electrical resonance and the electrical resonance behaves like a negative damping to the torsional oscillation. Torsional interaction effect is a much more significant problem as compared to the induction generator effect. It can cause shaft damage also.

### **3.1.4 TRANSIENT TORQUES**

Oscillatory torques on the generator rotor can be excited by system disturbances resulting from switching in the network. The transient electrical torque has many components which include unidirectional, exponentially decaying and oscillatory torques from sub-

synchronous and multiples of synchronous frequency components. Due to SSR phenomenon, the sub-synchronous frequency components of torque can have large amplitudes immediately following the disturbance, although they may decay eventually. Occurrence of these high amplitude transient torques can result in loss of shaft life due to shaft fatigue.

### 3.2 FIRST BENCH MARK MODEL FOR SSR STUDIES

To study the effects of the operation of the EAF on the shaft of synchronous generator, the 27<sup>th</sup> order IEEE first bench mark power system is modeled in PSCAD. Differential equations of the 27<sup>th</sup> order system are described below. Also, eigen value analysis of the system is performed in MATLAB. Before the MATLAB programming, the state equations for the synchronous generator are derived [57]. First Bench Mark Model of IEEE is shown in Figure 3.1.

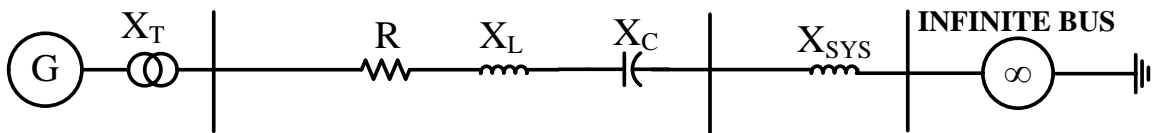


Figure 3.1 The First Bench Mark Model of IEEE [57]

### 3.3 EQUATIONS OF TURBINE-GENERATOR SYSTEM

Figure 3.2 shows a schematic diagram of the mass-spring system for tandem-compound and single-reheat steam turbines, generator and exciter set. Six rotating masses, High-Pressure turbine (HP), Intermediate Pressure turbine (IP), two Low-Pressure turbines (LPA & LPB), Generator (GEN) and Exciter (EX) all on one shaft, are shown in the figure.

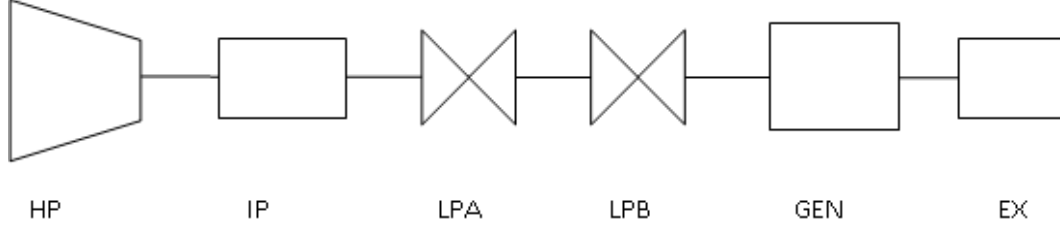


Figure 3.2 A linear six-mass-spring turbine-generator system [57]

The state equations of the linear six-mass-spring system are given as:

$$\Delta \dot{\omega}_H = \frac{1}{M_H} [\Delta T_H - D_H \Delta \omega_H - K_{HI} (\Delta \theta_H - \Delta \theta_I)] \quad (3.1)$$

$$\Delta \dot{\theta}_H = \omega_b \Delta \omega_H \quad (3.2)$$

$$\Delta \dot{\omega}_I = \frac{1}{M_I} [\Delta T_I - D_I \Delta \omega_I + K_{HI} (\Delta \theta_H - \Delta \theta_I) - K_{IA} (\Delta \theta_I - \Delta \theta_A)] \quad (3.3)$$

$$\Delta \dot{\theta}_I = \omega_b \Delta \omega_I \quad (3.4)$$

$$\Delta \dot{\omega}_A = \frac{1}{M_A} [\Delta T_A - D_A \Delta \omega_A + K_{IA} (\Delta \theta_I - \Delta \theta_A) - K_{AB} (\Delta \theta_A - \Delta \theta_B)] \quad (3.5)$$

$$\Delta \dot{\theta}_A = \omega_b \Delta \omega_A \quad (3.6)$$

$$\Delta \dot{\omega}_B = \frac{1}{M_B} [\Delta T_B - D_B \Delta \omega_B + K_{AB} (\Delta \theta_A - \Delta \theta_B) - K_{BG} (\Delta \theta_B - \Delta \delta)] \quad (3.7)$$

$$\Delta \dot{\theta}_B = \omega_b \Delta \omega_B \quad (3.8)$$

$$\Delta \dot{\omega} = \frac{1}{M_G} [-\Delta T_e - D_G \Delta \omega + K_{BG} (\Delta \theta_B - \Delta \delta) - K_{GX} (\Delta \delta - \Delta \theta_X)] \quad (3.9)$$

$$\Delta \dot{\delta} = \omega_b \Delta \omega \quad (3.10)$$

$$\Delta \dot{\omega}_X = \frac{1}{M_X} [-\Delta T_{ex} - D_X \Delta \omega_X + K_{GX} (\Delta \delta - \Delta \theta_X)] \quad (3.11)$$

$$\Delta \dot{\theta}_X = \omega_b \Delta \omega_X \quad (3.12)$$

Where:

The subscripts H, I, A, B, G and X are used for the HP, IP, LPA and LPB turbines, generator and exciter. The variables  $\omega_H$ ,  $\omega_I$ ,  $\omega_A$ ,  $\omega_B$ ,  $\omega$  and  $\omega_X$  are the rotor speeds of HP, IP, LPA and LPB turbines, synchronous generator and exciter in per unit.  $M_H$ ,  $M_I$ ,  $M_A$ ,

$M_B$ ,  $M_G$  and  $M_X$  are the inertia constants.  $K_{HI}$ ,  $K_{IA}$ ,  $K_{AB}$ ,  $K_{BG}$  and  $K_{GX}$  are stiffness constants. The variables  $\theta_H$ ,  $\theta_I$ ,  $\theta_A$ ,  $\theta_B$  and  $\theta_X$  are the mechanical rotor angles of the HP, IP, LPA and LPB turbines and exciter in mechanical radians and  $\delta$  is the electrical rotor angle in electrical radians.  $\omega_b$  is the base speed i.e 377 radians/second.  $T_e$  is the generator torque and  $T_{ex}$  is the exciter torque.  $D_H$ ,  $D_I$ ,  $D_A$ ,  $D_B$ ,  $D_G$  and  $D_X$  are self-damping factors. The variables  $T_H$ ,  $T_I$ ,  $T_A$ ,  $T_B$  and  $T_e$  denote HP-IP torque on the shaft (THI), IP-LPA torque on the shaft (TIA), LPA-LPB torque on the shaft (TAB), LPB-GEN torque on the shaft (TBG) and GEX-EX torque on the shaft (TGEX) respectively.

### 3.4 EQUATIONS OF TURBINE TORQUE & GOVERNOR SYSTEM

Figure 3.3 shows a block diagram of a two-time-constant governor where ‘a’ denotes speed relay position and ‘g’ represents the governor opening.

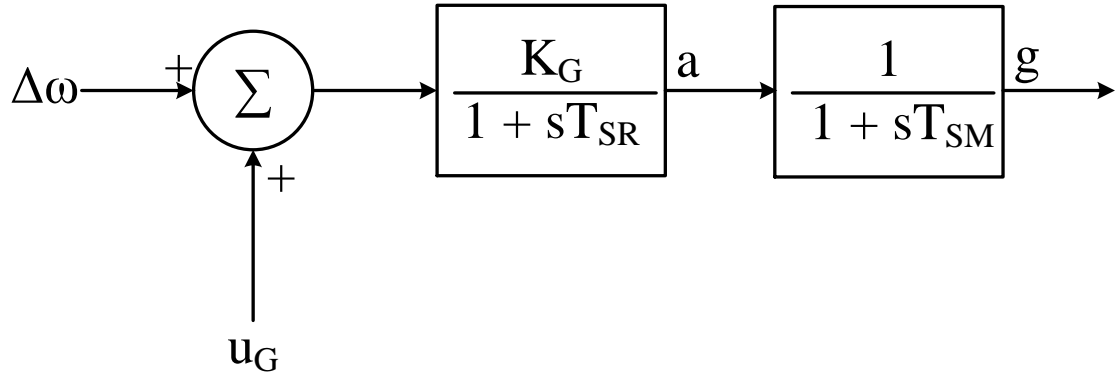


Figure 3.3 A two-time-constant governor [57]

Two differential equations for the governor are:

$$(1 + sT_{SR})a = K_G(\Delta\omega + u_G) \quad (3.13)$$

$$(1 + sT_{SM})g = a \quad (3.14)$$

$K_G$  is the governor gain.  $T_{SR}$  is the time constant of the speed relay and  $T_{SM}$  is the time constant of servomotor. A supplementary input  $u_G$  is provided to the governor that can be used for governor control.

Figure 3.4 shows transfer functions of steam turbines. The output of the governor is fed to the HP turbine. Four turbine torques sum up to be equal to  $\Delta T_m$ . All turbine torques are proportional, with each turbine contributing a fraction, and the sum of the fractions is equal to one.

$$\Delta T_H + \Delta T_I + \Delta T_A + \Delta T_B = \Delta T_m \quad (3.15)$$

$$F_H + F_I + F_A + F_B = 1 \quad (3.16)$$

Where  $F_H$ ,  $F_I$ ,  $F_A$  and  $F_B$  are turbine torque shares.

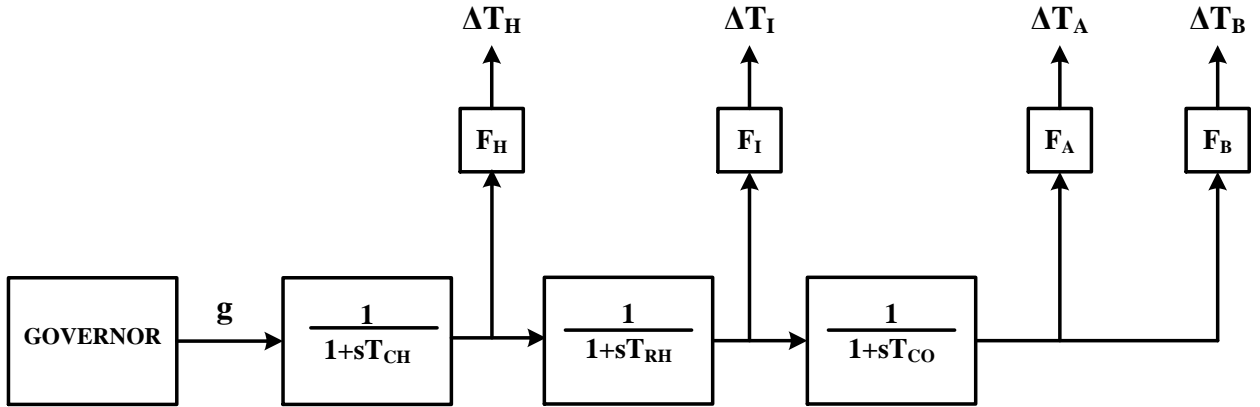


Figure 3.4 Transfer functions of steam turbines [57]

Three differential equations for turbine torques are given as:

$$(1 + sT_{CH})\Delta T_H = F_H g \quad (3.17)$$

$$(1 + sT_{RH})\Delta T_I = (F_I/F_H)\Delta T_H \quad (3.18)$$

$$(1 + sT_{CO})\Delta T_A = (F_A/F_I)\Delta T_I \quad (3.19)$$

$$\Delta T_B = (F_B/F_A)\Delta T_A \quad (3.20)$$

$T_{CH}$  represents time constant due to steam flow in the chamber in front of the HP turbine.

$T_{RH}$  denotes the time constant due to steam flow in the reheater between the HP and IP turbines.  $T_{CO}$  represents the time constant due to steam flow in the crossover connection between the IP and Low Pressure turbines.

### 3.5 CAPACITOR-COMPENSATED TRANSMISSION LINE EQUATIONS

Four state variables are expressed in terms of transmission line parameters. The four state variables are d-axis current ( $\Delta i_d$ ), q-axis current ( $\Delta i_q$ ), d-axis voltage across capacitor in transmission line ( $\Delta e_{cd}$ ), q-axis voltage across capacitor in transmission line ( $\Delta e_{cq}$ ). Resistance (R), inductive reactance (X) and capacitive reactance ( $X_c$ ) of the transmission line are constants. Components (d-q) of terminal voltage ( $\Delta V_t$ ) of the synchronous generator are  $\Delta V_d$  and  $\Delta V_q$  and initial values of these d-q components are  $\Delta V_{0d}$  and  $\Delta V_{0q}$ .

$$\Delta i_d = \frac{1}{\omega_b X_c} \Delta \dot{e}_{cd} - \frac{1}{X_c} \Delta e_{cq} \quad (3.21)$$

$$\Delta i_q = \frac{1}{\omega_b X_c} \Delta \dot{e}_{cq} + \frac{1}{X_c} \Delta e_{cd} \quad (3.22)$$

$$\Delta V_d = R\Delta i_d - X\Delta i_q + \frac{X}{\omega_b} \Delta \dot{i}_d + \Delta e_{cd} + \Delta V_{0d} \quad (3.23)$$

$$\Delta V_q = X\Delta i_d + R\Delta i_q + \frac{X}{\omega_b} \Delta \dot{i}_q + \Delta e_{cq} + \Delta V_{0q} \quad (3.24)$$

### 3.6 EQUATIONS OF SYNCHRONOUS GENERATOR

A second damper winding 'S' is assumed on q-axis. There are now two rotor windings per axis: D and F on the d-axis and Q and S on the q-axis. The synchronous generator voltage equations in linear form can be written as:



$$\frac{1}{\omega_b}(-x_d\Delta\dot{i}_d + x_{md}\Delta\dot{i}_F + x_{md}\Delta\dot{i}_D) = (-x_q\Delta\dot{i}_q + x_{mq}\Delta\dot{i}_Q + x_{mq}\Delta\dot{i}_S) + \varphi_{q0}\Delta\omega + r_a\Delta i_d + \Delta V_d \quad (3.25)$$

$$\frac{1}{\omega_b}(-x_{md}\Delta\dot{i}_d + x_F\Delta\dot{i}_F + x_{md}\Delta\dot{i}_D) = -r_F\Delta i_F + \Delta V_F \quad (3.26)$$

$$\frac{1}{\omega_b}(-x_{md}\Delta\dot{i}_d + x_{md}\Delta\dot{i}_F + x_D\Delta\dot{i}_D) = -r_D\Delta i_D \quad (3.27)$$

$$\frac{1}{\omega_b}(-x_q\Delta\dot{i}_q + x_{mq}\Delta\dot{i}_Q + x_{mq}\Delta\dot{i}_S) = -(-x_d\Delta i_d + x_{md}\Delta i_F + x_{md}\Delta i_D) - \varphi_{d0}\Delta\omega + r_a\Delta i_q + \Delta V_q \quad (3.28)$$

$$\frac{1}{\omega_b}(-x_{mq}\Delta\dot{i}_q + x_Q\Delta\dot{i}_Q + x_{mq}\Delta\dot{i}_S) = -r_Q\Delta i_Q \quad (3.29)$$

$$\frac{1}{\omega_b}(-x_{mq}\Delta\dot{i}_q + x_{mq}\Delta\dot{i}_Q + x_S\Delta\dot{i}_S) = -r_S\Delta i_S \quad (3.30)$$

The variables used in the above equations are defined in Table 3.1.

**Table 3.1 Description of variables used in equations of synchronous generator**

Variable Used	Variable Name
$x_d$	d-axis synchronous reactance
$x_q$	q-axis synchronous reactance
$x_{md}$	d-axis mutual reactance
$x_{mq}$	q-axis mutual reactance
$r_a$	Armature resistance
$\Psi_{d0}$	d-axis initial operating flux
$\Psi_{q0}$	q-axis initial operating flux
$x_F$	Field winding leakage reactance
$r_F$	Field winding resistance
$x_D$	d-axis damper winding leakage reactance
$r_D$	d-axis damper winding resistance
$x_Q$	q-axis damper winding No. 1 leakage reactance
$r_Q$	q-axis damper winding No. 1 resistance
$x_S$	q-axis damper winding No. 2 leakage reactance
$r_S$	q-axis damper winding No. 2 resistance

### 3.7 EQUATIONS OF EXCITATION SYSTEM

The excitation system is described by two differential equations. First block in Figure 3.5 represents transfer function of a voltage regulator having a gain ' $K_A$ ' and a time constant ' $T_A$ '. Output voltage of the voltage regulator is ' $\Delta V_R$ '. Second block represents the transfer function of the exciter. Constant ' $T_E$ ' is the exciter time constant and ' $\Delta E_{FD}$ ' is the output voltage of the exciter.

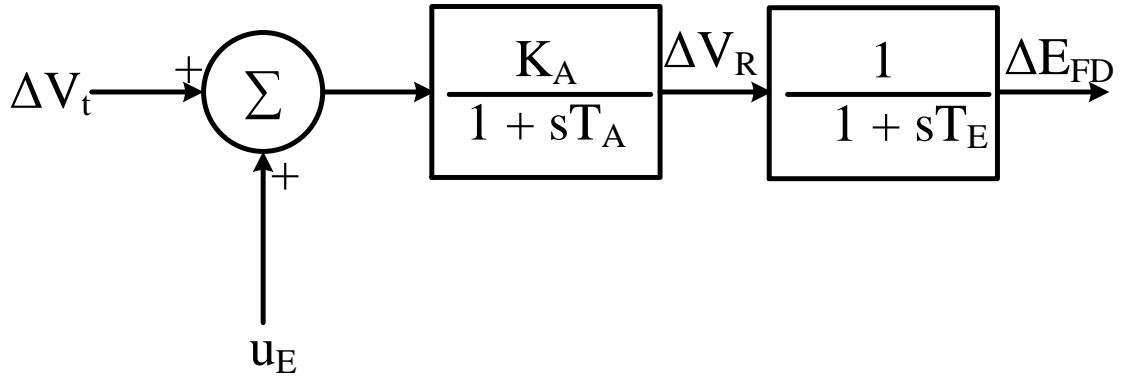


Figure 3.5 A two-time-constant excitation system [57]

The excitation system equations are:

$$(1 + sT_A)\Delta V_R = K_A(\Delta V_t + u_E) \quad (3.31)$$

$$(1 + sT_E)\Delta E_{FD} = \Delta V_R \quad (3.32)$$

### 3.8 COMPLETE STATE-SPACE MODEL FOR SSR EIGEN VALUE ANALYSIS

$$[\dot{x}] = [A][x] + [B][u] \quad (3.33)$$

Where:

$$[x] = [\Delta\omega_H, \Delta\theta_H, \Delta\omega_I, \Delta\theta_I, \Delta\omega_A, \Delta\theta_A, \Delta\omega_B, \Delta\theta_B, \Delta\omega, \Delta\delta, \Delta\omega_X, \Delta\theta_X, \Delta T_H, \Delta T_I, \Delta T_A, a, g,$$

$$\Delta e_{cd}, \Delta e_{cq}, \Delta i_d, \Delta i_q, \Delta i_F, \Delta i_D, \Delta i_Q, \Delta i_S, \Delta V_R, \Delta E_{FD}]^T$$

The system contains 17 mechanical states and 10 electrical states. The complete mechanical and electrical model of a single-machine infinite bus power system is a 27<sup>th</sup> order system.

### **3.9 SYSTEM DATA FOR THE FIRST BENCH MARK MODEL OF IEEE [57]**

System data for the First Bench Mark Model of IEEE is given in Appendix.

### 3.10 EIGEN VALUES OF THE 27TH ORDER SYSTEM

The twenty seven eigen values for IEEE First Bench Mark Model are tabulated in Table 3.2 for  $X_C = 0.2 * X_L$ . ' $\lambda_{GOVR}$ ' represents the zeroth torsional mode. ' $\lambda_H$ ', ' $\lambda_I$ ', ' $\lambda_A$ ', ' $\lambda_B$ ', ' $\lambda_G$ ' and ' $\lambda_X$ ' represent the sub-synchronous torsional mode eigen values.

Table 3.2 Eigen values of the 27th order IEEE first bench mark SMIB power system for  $X_C = 0.2 * X_L$

$X_C = 0.2 * X_L$		
State	Eigen Value	
	Yu Book Values [57]	Derived values
$\lambda_H$	$-0.18 \pm j298.18$	$-0.18 \pm j298.18$
$\lambda_I$	$-0.21 \pm j203.20$	$-0.22 \pm j 203.42$
$\lambda_A$	$-0.22 \pm j160.66$	$-0.24 \pm j 160.77$
$\lambda_X$	$-0.67 \pm j127.03$	$-0.68 \pm j 127.04$
$\lambda_B$	$-0.26 \pm j99.13$	$-0.32 \pm j 99.31$
$\lambda_G$	$+0.0415 \pm j8.0234$	$-0.034 \pm j 8.12$
$\lambda_C$	$-6.07 \pm j241.01$	$-6.11 \pm j 241.38$
$\lambda_{d,q}$	$-6.98 \pm j512.30$	$-6.98 \pm j 512.14$
$\lambda_D$	-2.020	-1.97
$\lambda_Q$	-25.40	-24.78
$\lambda_S$	-32.58	-32.72
$\lambda_F$	-8.568	-8.40
$\lambda_{VR}$	-102	-101.68
$\lambda_{Efd}$	-500	-500
$\lambda_{CH}$	-2.9	-2.87
$\lambda_{RH}$	-0.1416	-0.14
$\lambda_{CO}$	-4.668	-4.66
$\lambda_{GOVR}$	$-4.704 \pm j0.7567$	$-4.69 \pm j 0.74$

**Table 3.3 Eigen values of the 27th order IEEE first bench mark SMIB power system for  $X_C = 0.3 * X_L$**

$X_C=0.3 * X_L$		
State	Eigen Value	
	Yu Book Values [57]	Derived values
$\lambda_H$	$-0.18 \pm j298.18$	$-0.18 \pm j298.18$
$\lambda_I$	$+0.15 \pm j204.35$	$+0.15 \pm j 202.91$
$\lambda_A$	$-0.25 \pm j160.72$	$-0.25 \pm j 160.89$
$\lambda_X$	$-0.67 \pm j127.03$	$-0.68 \pm j 127.08$
$\lambda_B$	$-0.28 \pm j99.21$	$-0.33 \pm j 99.47$
$\lambda_G$	$-0.048 \pm j8.4801$	$-0.062 \pm j 8.74$
$\lambda_C$	$-6.2 \pm j209.20$	$-6.23 \pm j 209.44$
$\lambda_{d,q}$	$-7.02 \pm j542.80$	$-7.02 \pm j 542.62$
$\lambda_D$	-1.983	-1.96
$\lambda_Q$	-25.41	-24.80
$\lambda_S$	-31.92	-32.04
$\lambda_F$	-8.44	-8.37
$\lambda_{VR}$	-101.9	-101.63
$\lambda_{Efd}$	-500	-500
$\lambda_{CH}$	-3.034	-2.96
$\lambda_{RH}$	-0.1417	-0.14
$\lambda_{CO}$	-4.616	-4.61
$\lambda_{GOVR}$	$-4.673 \pm j0.6269$	$-4.66 \pm j 0.60$

It is observed from Table 3.3 that with increase in compensation, more eigen values shift towards the right half plane and the system becomes more unstable.

### 3.11 TORSIONAL OSCILLATION MODES

There are six torsional oscillation modes corresponding to six-mass-spring system. The modal frequencies are determined by dividing the imaginary part of the eigen values by  $2\pi$ . The modal frequencies of the six torsional oscillation modes are given in Table 3.4.

**Table 3.4 Modal frequencies of six torsional modes of the six-mass-spring system**

Component	GEN	LPA	EX	LPB	IP	HP
Frequency (rad/s)	8.12	160.77	127.04	99.31	203.42	298.18
Frequency (Hz)	1.29	25.58	20.219	15.805	32.37	47.45

Therefore, modal frequencies for the shaft of the generator are: 1.29 Hz, 15.805 Hz, 20.219 Hz, 25.58 Hz, 32.37 Hz and 47.45 Hz. So, the eigen value analysis confirms the presence of six sub-synchronous modes for the shaft of the synchronous generator.

The voltage and current waveforms of the EAF may contain the low-frequency components which may resonate with the low frequency torsional modes of the turbine-generator shaft. This may cause severe sub-synchronous resonance (SSR) and may also damage the mechanical shaft of the synchronous generator.

## **CHAPTER 4**

### **MODELING OF ELECTRIC ARC FURNACE**

Complexity of the modern power system is increasing day by day. Utilities are planning to install more power plants which will probably be more nearer to the industrial zones where the steel mills are located. Due to the increasing use of the EAFs by the steel industry because of high production rate in minimum time duration, this subject has attained huge attention in the area of research. Most of the research has been contributed to areas of power quality issues caused by the EAF in a power system and the modeling of the EAF characteristics. But, very few research articles have focused on the analysis of effects of the EAF operation on the shaft of the synchronous generator, though; it is a very important issue. Even the research articles which have concentrated on this important issue, have not validated their EAF model with real-time data and have mostly relied on the pulsing load model which does not fully represent the dynamics of the EAF. Therefore, it is necessary to explore this important area of research with a more evidential, distinct and detailed approach.

The main objective of this research is to analyze the effects of electric arc furnace on the shaft of the synchronous generator. As the EAF voltage and current waveforms contain low frequency (sub-synchronous) components (also verified by real-time data), it is very essential to analyze the effects of the EAF operation on the shaft of the generator. For this purpose, the EAF is modeled by using a novel method of integrating the stochastic variation of arc length into a non-linear resistance model. The synchronous generator, its

shaft, exciter, transmission line and the infinite bus are modeled according to the IEEE First Bench Model explained earlier in the chapter 3.

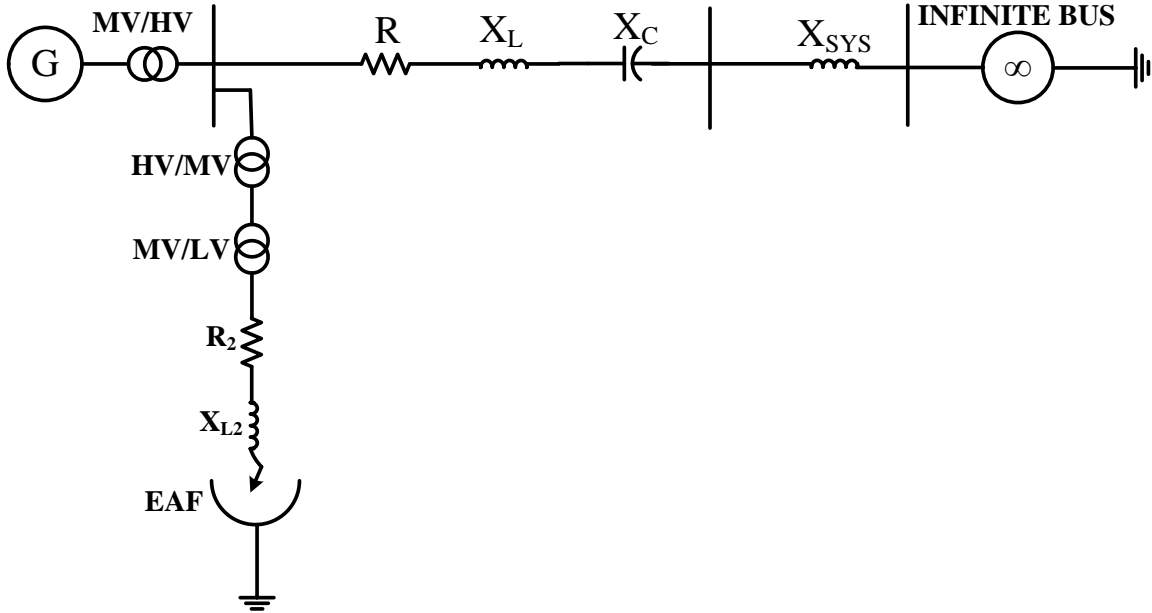


Figure 4.1 Single machine infinite bus with EAF as load

Single-machine infinite bus power system containing the EAF as a load is shown in the Figure 4.1. The generating capacity of the synchronous generator is 170 MVA (active power of 153 MW and reactive power of 74.1 MVar). The synchronous generator is generating power with a lagging power factor of 0.9. The MVA rating of the EAF is approximately 85 MVA.

The modeling of EAF is divided into two stages. During the first stage when EAF is melting scrap and Direct Reduced Iron (DRI), EAF is modeled as a non-linear resistance with variable arc length. The second stage is when scrap and DRI have been melted and disturbances have decreased. During this stage, EAF is modeled as a simple non-linear resistance. The parameters of the model are estimated manually on the basis of ignition



and extinction voltages of the dataset taken from the measured data. The simulated waveforms are compared with the measured waveforms. The voltage and current of a real EAF in a steel mill are measured at the EAF bus by power quality (PQ) meter. Analysis of the real time data is performed through Dran-View power quality tool. The comparison of the measured and the simulated values is done on the basis of Total Harmonic Distortion (THD) and Fast Fourier Transform (FFT).

Fast Fourier Transform (FFT) tool is used to calculate the EAF voltage and current harmonics. FFT is basically a high-speed algorithm that implements Discrete Fourier Transform (DFT). Equation (2) is a formula for transforming a sequence  $\{x(n)\}$  of length  $L \leq N$  into a sequence of frequency samples  $\{X(k)\}$  of length  $N$ . Since the frequency samples are obtained by evaluating the Fourier Transform  $X(\omega)$  at a set of  $N$  (equally spaced) discrete frequencies, equation (2) is called the Discrete Fourier Transform (DFT) of  $x(n)$  [58].

$$X(k) \equiv X\left(\frac{2\pi k}{N}\right) = \sum_{n=0}^{L-1} x(n)e^{-\frac{j2\pi kn}{N}} \quad (4.1)$$

$$X(k) = \sum_{n=0}^{N-1} x(n)e^{-\frac{j2\pi kn}{N}} \quad k = 0, 1, 2, \dots, N-1$$

#### 4.1 REAL TIME DATA ACQUISITION AND ANALYSIS

The real time data of current and voltage for three different arc furnaces, located at Hadeed Sabic Steel Plant in Al-Jubail, is collected. Power Quality (PQ) meter is used to measure the voltage and current. First, the data is collected at 34.5kV side of the transformer. Secondly, the data is collected at the 600V side of the transformer (EAF bus). Thirdly, the measurements are taken at the 230 kV side of the transformer.

The data is read and converted to excel format through Dran-View tool. DranView makes it possible for power grid specialists to easily and quickly view and analyze monitored data from the mains.

The data is analyzed and taken into consideration to model the EAF parameters. Figure 4.2 shows the power system block diagram to which the real EAF is connected.

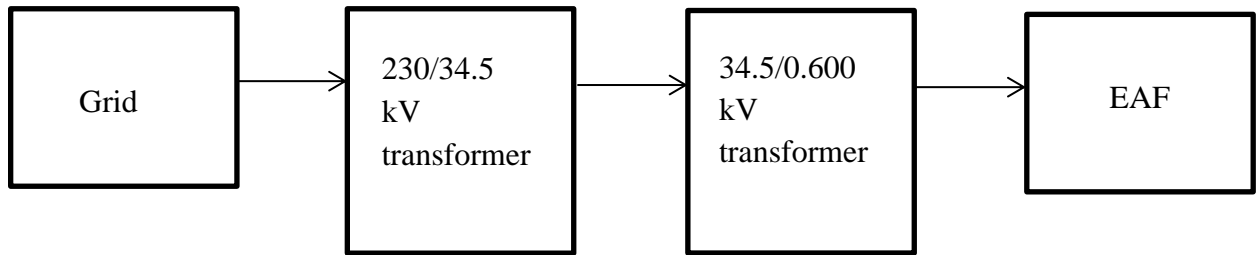


Figure 4.2 Block diagram of the actual power system containing the EAF

## 4.2 MODELING OF INITIAL (FIRST) STAGE of EAF OPERATION

The EAF during its initial stage of operation is modeled by a non-linear time-variant resistance model which is described by the following equations.

$$R_a = \left\{ \begin{array}{l} R_g \\ \frac{V_d + (V_{ig} - V_d)e^{-\frac{|i| - i_{ig}}{\tau_1}}}{|i|} \\ \frac{[V_t + (V_{ig} - V_t)e^{-\frac{|i|}{\tau_2}}]}{|i| + i_{ig}} \end{array} \right. \left. \begin{array}{l} 0 \leq |i| < i_{ig}, \frac{d|i(t)|}{dt} > 0 \\ |i| \geq i_{ig}, \frac{d|i(t)|}{dt} > 0 \\ \frac{d|i(t)|}{dt} < 0 \end{array} \right\} \quad (4.2)$$

Where:

$$V_d = A + B \cdot l(t) \quad (4.3)$$

‘A’ is a constant which denotes voltage drop in the cathode and anode electrodes of the EAF and ‘B’ is a constant that represents voltage per unit length across the arc. Units of ‘A’ and ‘B’ are Volt and Volt/cm respectively. ‘l’ is the arc length. The voltages ‘V<sub>d</sub>’ and ‘V<sub>ig</sub>’ represent the extinction and ignition voltages respectively. ‘i<sub>ig</sub>’ is the ignition current. ‘R<sub>g</sub>’ is the constant resistance during the extinction period. Voltage drop from ‘V<sub>ig</sub>’ to ‘V<sub>d</sub>’ is expressed by an exponential function with a time constant  $\tau_1$ . The beginning of the period when the arc extinguishes is also represented by an exponential function with a time constant  $\tau_2$ .

$$V_{ig} \approx 1.15V_d \quad (4.4)$$

$$i_{ig} = \frac{V_{ig}}{R_g} \quad (4.5)$$

$$V_t = \left[ \frac{I_{max} + i_{ig}}{I_{max}} \right] V_d \quad (4.6)$$

There are many methods discussed in the literature to incorporate dynamic behavior of the arc furnace into the respective models. Pulsing load model is used for this purpose by some researchers [37], [38] and [39]. Others have incorporated this dynamic nature of the arc by the sinusoidal variation (amplitude modulation) of the either the arc voltage or the arc resistance [9], [10] and [11]. Another approach is the stochastic variation of one of the arc resistance and arc voltage [6], [30]. The pulsing load model is not suitable for the modeling of the EAF because it only represents a load to which the power is supplied in the form of pulses. It does not represent many dynamics of the EAF during the earlier melting stage. So, to represent the important earlier melting stage, it is not fair to use the

pulsing load model. Its only advantage is that it represents the low frequency components of the EAF voltage and current waveforms in a well manner.

This objective (representation of the low-frequency components) can also be achieved with the traditional models by including either the sinusoidal variation or the stochastic variation of the arc resistance or arc voltage. The arc resistance and the arc voltage depend on the arc length. So, both of the sinusoidal and the stochastic variation approaches can also be applied to the arc length. The sinusoidal change of the arc length follows the deterministic law [30] and band-limited white noise change of the arc length around a reference value follows the stochastic laws [30].

Considering the arc length time variation like a random phenomenon supports the stochastic approach [59]. The stochastic model is more accurate for more realistic calculations [60]. Therefore, the arc length is varied stochastically in this research work. The equation for the arc length is given as:

$$l(t) = l_r - r(t) \quad (4.7)$$

Where:

‘ $l_r$ ’ is the reference arc length and ‘ $r(t)$ ’ is the band-limited white noise signal with a frequency range in which the voltage fluctuations produce flicker (5 to 20 Hz).

The difference between this model and the one discussed in the literature survey [8] is that in this model stochastic variation of the arc length is implemented. Sinusoidal and stochastic variations of the arc length are implemented for the non-linear current controlled voltage source model but not for the non-linear current controlled resistance model. Though, non-linear resistance model has an advantage over the non-linear voltage

source model. The non-linear resistance model models the ignition to extinction period and the extinction to the re-ignition period more accurately as compared to the non-linear voltage source model. The parameters of the proposed model are estimated manually on the basis of the ignition and extinction voltages ( $V_{ig}$  and  $V_{ex}$ ) of the dataset of the measured data. The parameters of the model are estimated in accordance with their ranges given in [30]. The parameters are given in the following Table 4.1.

**Table 4.1 Parameters of the model for the first stage of the EAF operation**

Parameter	Value
$I_{max}$	100kA
$\tau_1$	0.01 seconds
$\tau_2$	0.02 seconds
$R_g$	0.075 ohm
A	71 Volt
B	30 Volt/cm
$l_r$	30 cm
m	25 cm

The band-limited white noise signal ' $r(t)$ ' is varied in the interval [5 15] [30]. According to [30], ' $r(t)$ ' can be varied in the interval [ $l_r - m$   $l_r$ ], where, ' $m$ ' is maximum arc length deviation. The maximum arc length deviation ( $m$ ) is 25 cm and the reference arc length

( $l_r$ ) is 30 cm. So, the interval [5 15] lies within the range of [ $l_r - m$   $l_r$ ]. The reference arc length ( $l_r$ ) and maximum arc length deviation ( $m$ ) are selected on the basis of the single value (average) of constant arc length ( $l$ ).

### 4.3 MODELING SECOND STAGE of EAF OPERATION

During the quiet melting stage of the EAF operation, the EAF is simply modeled as a non-linear resistance [8]. The equations for the model are already given in section 2.1 (Equation No. 2.6, 2.7 and 2.8). For convenience, the equations are written below:

$$R_a = \left\{ \begin{array}{l} R_g \\ \left[ \frac{V_d + (V_{ig} - V_d)e^{-\frac{|i| - i_{ig}}{\tau_1}}}{|i|} \right] \\ \left[ \frac{V_t + (V_{ig} - V_t)e^{-\frac{|i|}{\tau_2}}}{|i| + i_{ig}} \right] \end{array} \quad \left. \begin{array}{l} 0 \leq |i| < i_{ig}, \frac{d|i(t)|}{dt} > 0 \\ |i| \geq i_{ig}, \frac{d|i(t)|}{dt} > 0 \\ \frac{d|i(t)|}{dt} < 0 \end{array} \right\} \quad (4.8)$$

Where:

$$V_d = A + B \cdot l \quad (4.9)$$

$$V_{ig} \approx 1.15V_d \quad (4.10)$$

$$i_{ig} = \frac{V_{ig}}{R_g} \quad (4.11)$$

$$V_t = \left[ \frac{I_{\max} + i_{ig}}{I_{\max}} \right] V_d \quad (4.12)$$

The difference between this model and the one used for the first stage of the EAF operation is that in this model the arc length is fixed and it is not varying. Parameters of the model are given in the following Table 4.2.

**Table 4.2 Parameters of the model for the second stage of the EAF operation**

Parameter	Value
$I_{\max}$	100kA
$\tau_1$	0.01 seconds
$\tau_2$	0.02 seconds
$R_g$	0.075 ohm
A	71 Volt
B	30 Volt/cm
l	15 cm

# CHAPTER 5

## SIMULATION RESULTS

### 5.1 Actual EAF Waveforms

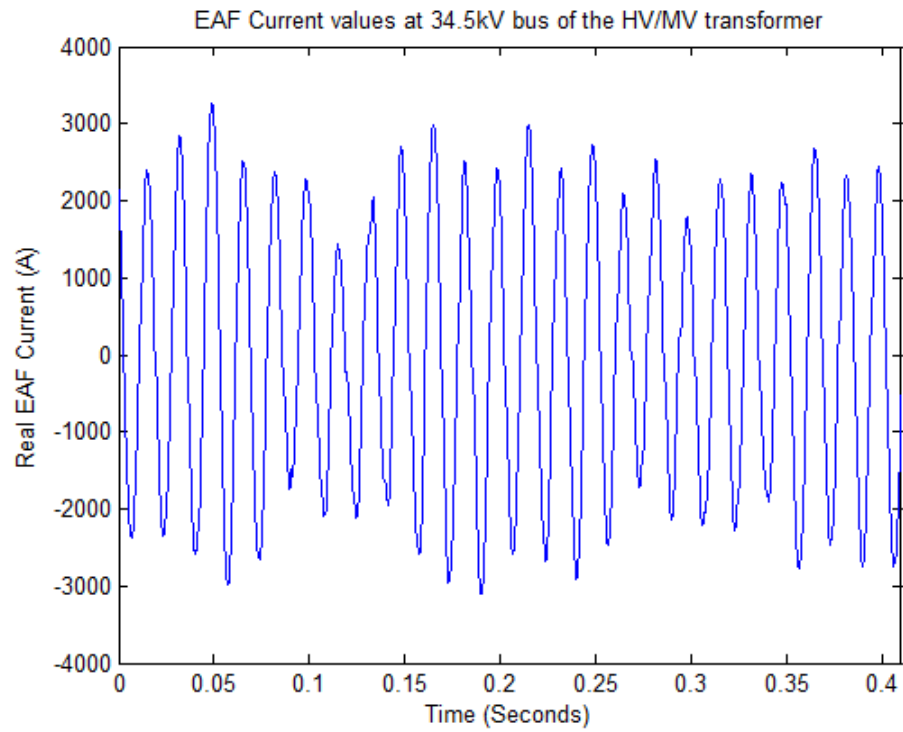


Figure 5.1 Current Recorded at the LV side of the 230/34.5 kV transformer for EAF

Figure 5.1 shows the current waveform of an actual EAF installed in a steel mill. The readings are taken at the 34.5 kV bus of a HV/MV transformer.



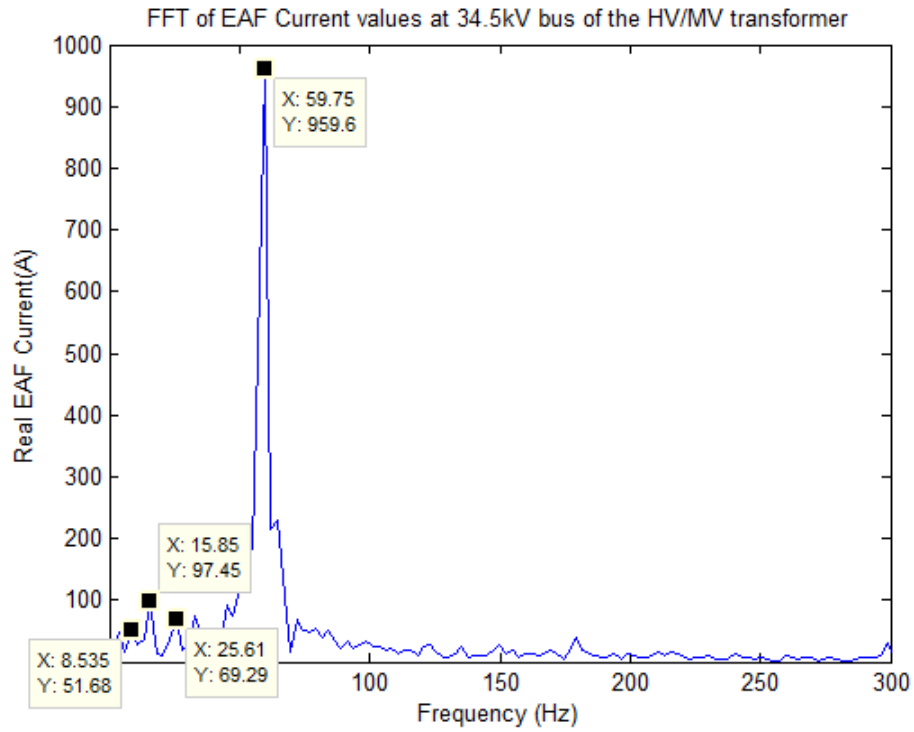


Figure 5.2 FFT of current waveform in Figure 5.1

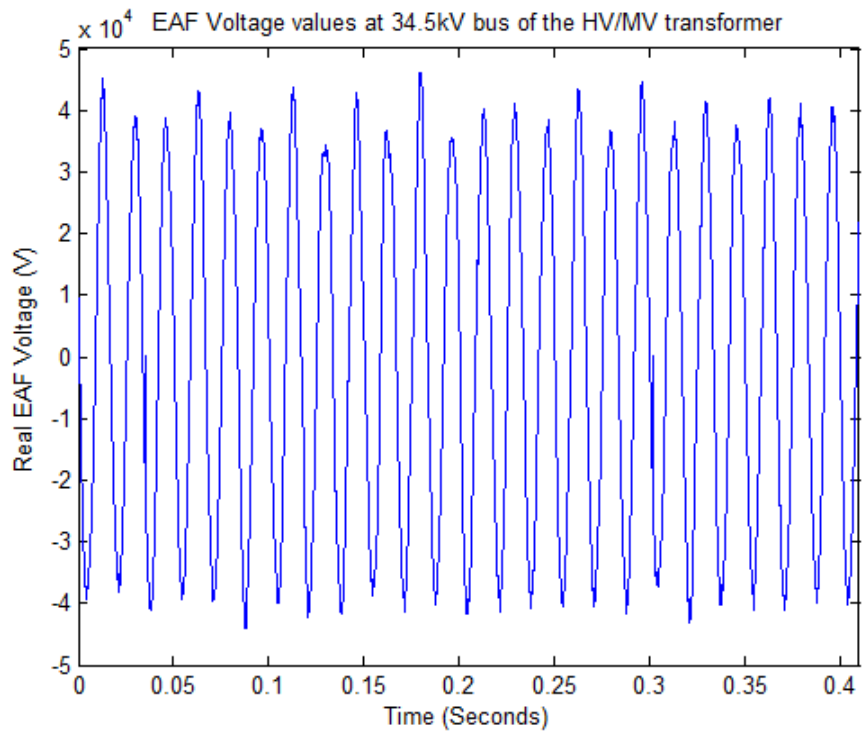


Figure 5.3 Voltage Recorded at the LV side of the 230/34.5 kV transformer for EAF

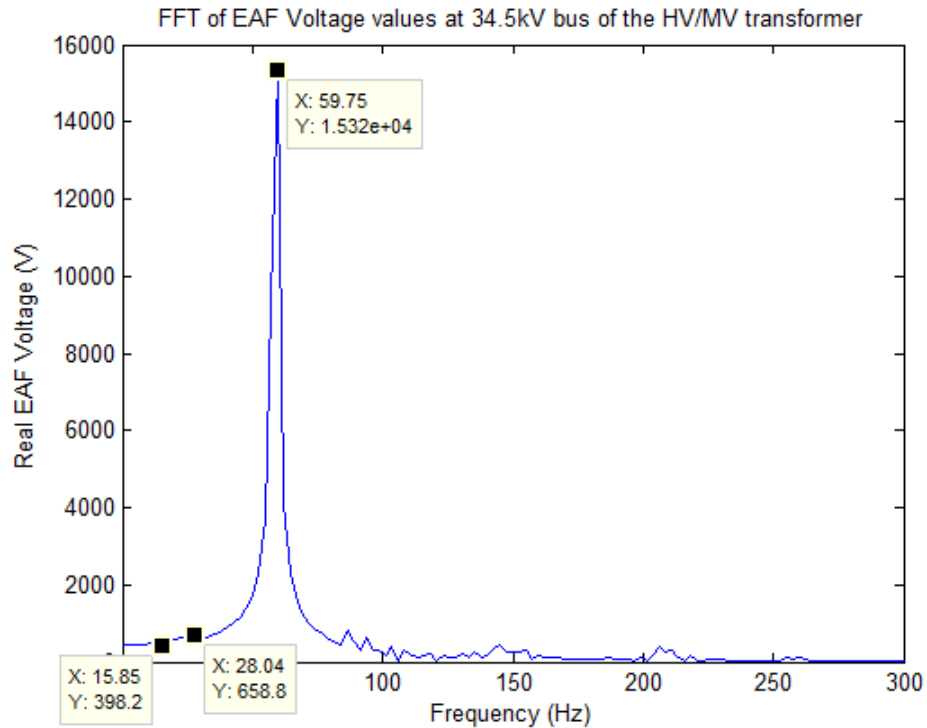


Figure 5.4 FFT of voltage waveform in Figure 5.3

Figure 5.3 shows the voltage waveform of the actual EAF installed in the steel mill. The readings are taken at the 34.5 kV bus of a HV/MV transformer. Figure 5.2 and Figure 5.4 show the frequency components of the actual EAF current and voltage waveforms respectively. Figures 5.2 and 5.4 clearly show that the low frequency components such as (15.85 Hz) are prevalent in the EAF current and voltage waveforms. This frequency of 15.85 Hz is close to the second torsional sub-synchronous mode of the shaft of the synchronous generator which in the case of IEEE First Bench Mark Power System is approximately 15.805 Hz. Though these readings are not directly taken at the EAF bus but even then the sub-synchronous frequency components are quite apparent. Any sudden change in the power system containing the synchronous generator and the EAF close to each other can cause severe damage to the shaft of the synchronous generator because of

the sub-synchronous frequency components. From these results, it is proved that the EAF voltage and current waveforms contain the sub-synchronous frequency components. Now, the question arises whether, these sub-synchronous frequency components can occur in the turbine torques when the EAF is located close to the synchronous generator. This is investigated further.

## 5.2 IEEE FIRST BENCH MARK MODEL SIMULATION RESULTS

Figure 5.5 shows the SSR model (IEEE First Bench Mark Model) built in PSCAD. Multimass (SyncM/c) block models twelve differential equations described in section 3.3. These differential equations represent the mechanical dynamics of the turbine-generator system. Synchronous generator block is based on the sixth order model explained in section 3.6. Equations of turbine torques described in section 3.4 are modeled through the Steam Turbine block. The governor block is modeled by using two differential equations representing the governor in section 3.4. The exciter is modeled by using the two differential equations described in section 3.7. Parameters of the synchronous generator, the transformer and the transmission line used in the PSCAD model are mentioned in Appendix.

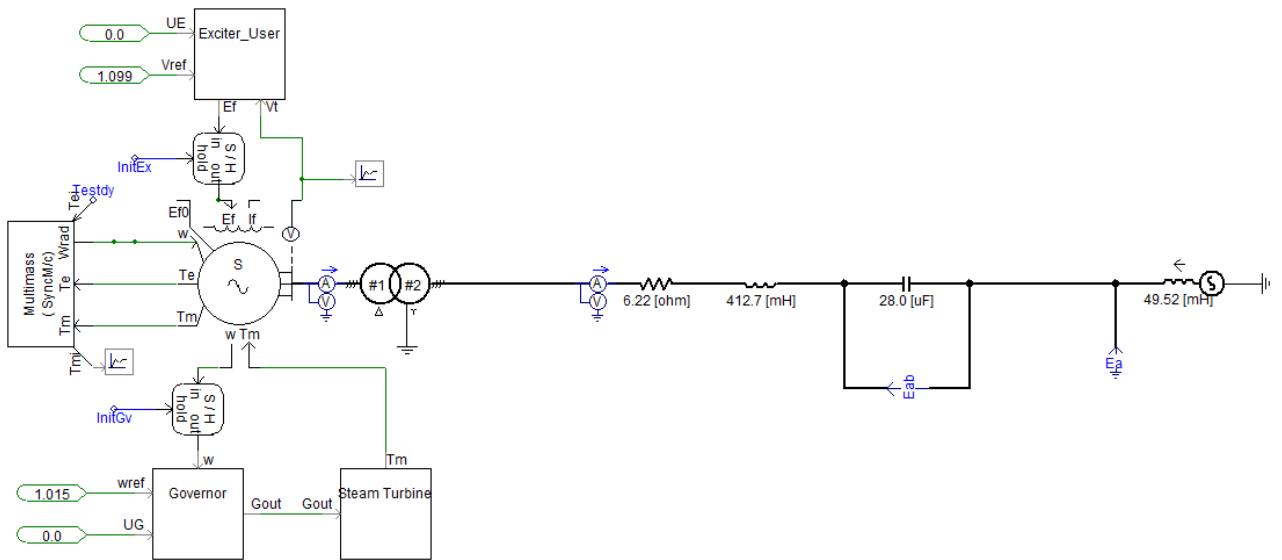
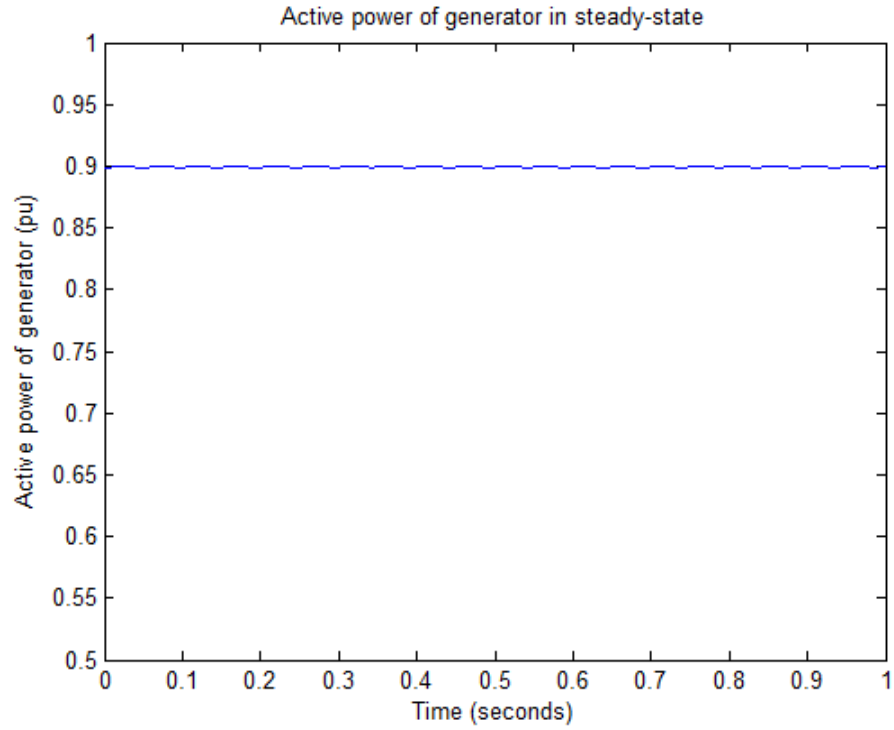
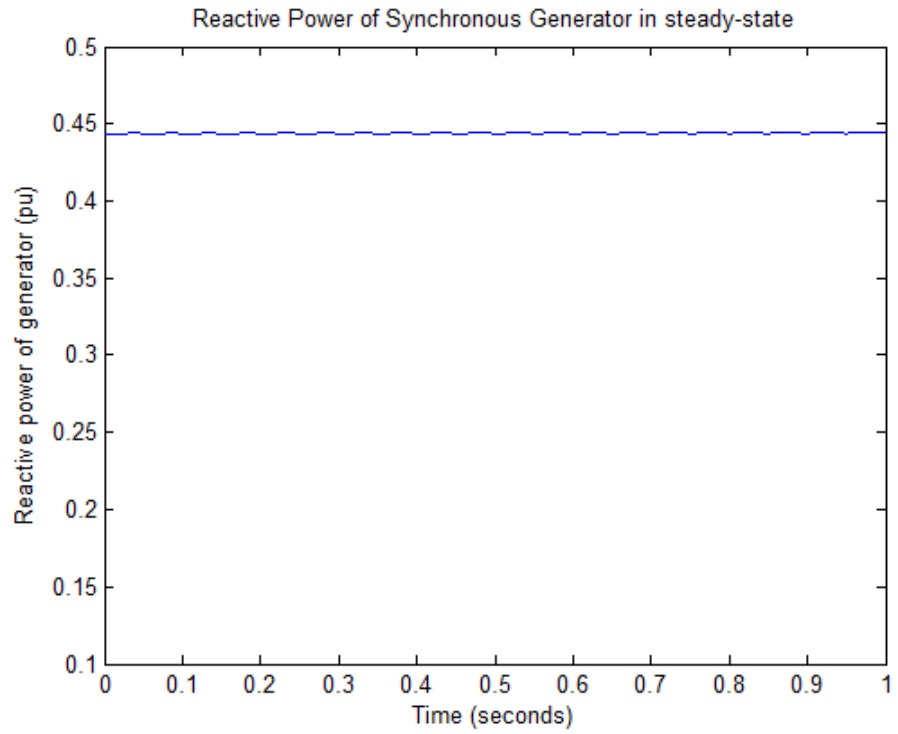


Figure 5.5 PSCAD SSR MODEL



**Figure 5.6 Active power of synchronous generator in steady-state**

Figure 5.6 shows the steady-state active power of synchronous generator. The IEEE First Bench Mark Model is built in PSCAD. The steady-state value of the active power is 0.9 pu. The results are plotted into MATLAB. At first the curves in the PSCAD are converted to excel sheets and the same excel sheet data is plotted in the MATLAB.



**Figure 5.7** Reactive power of synchronous generator in steady-state

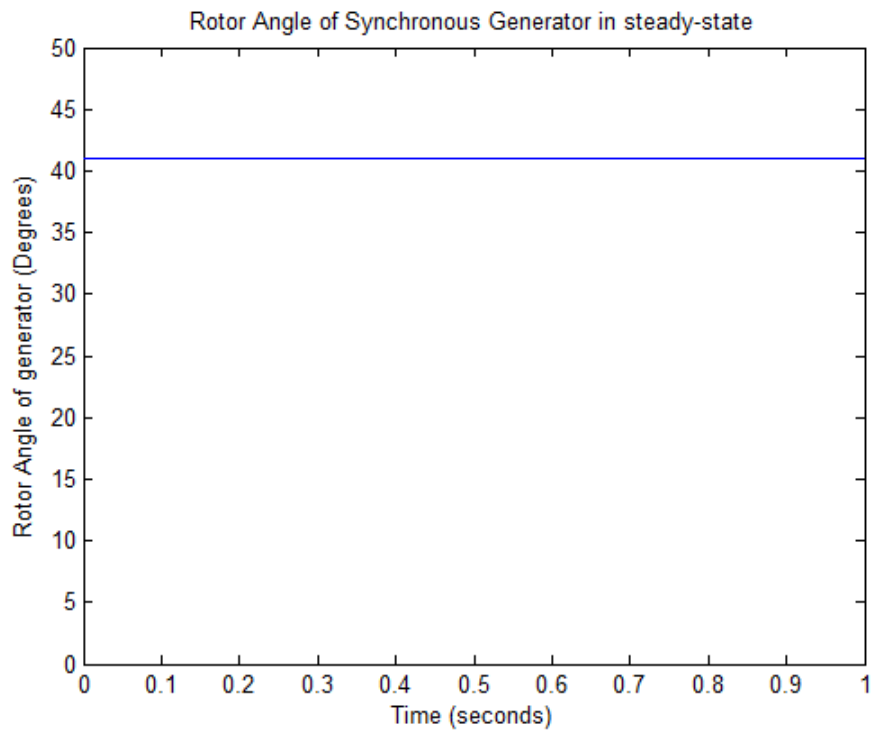


**Figure 5.8** Rotor angle of synchronous generator in steady-state

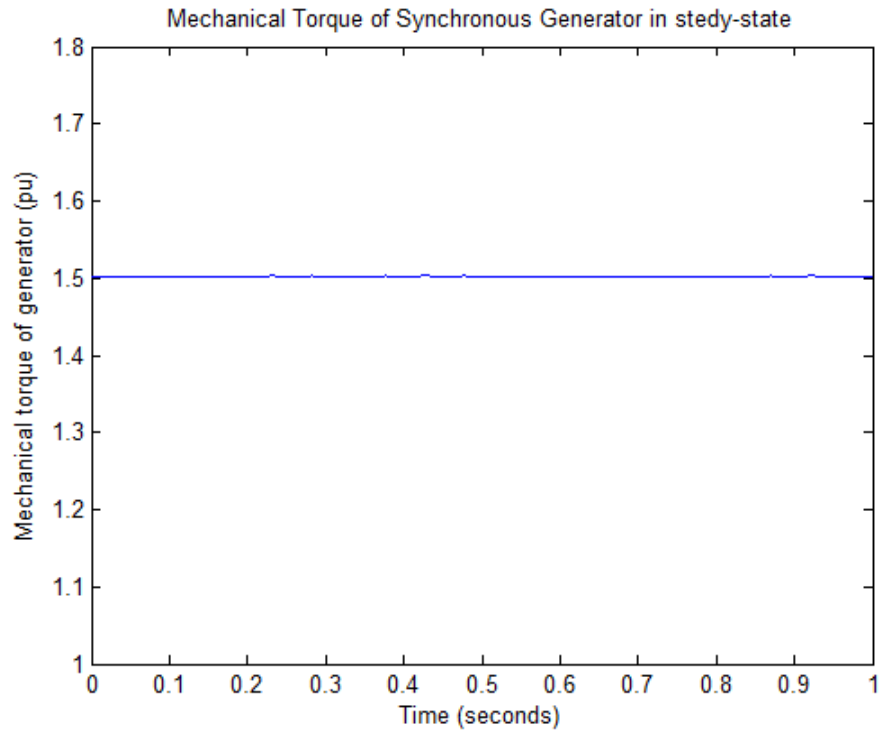


**Figure 5.9 Mechanical torque of synchronous generator in steady-state**

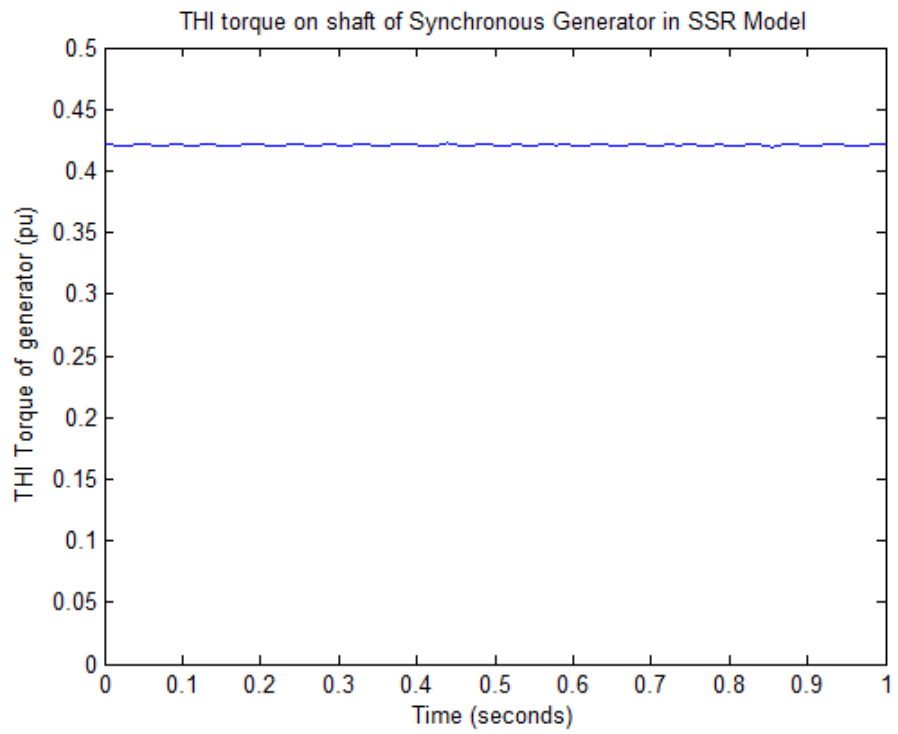


**Figure 5.10 THI torque of shaft of synchronous generator in steady-state**

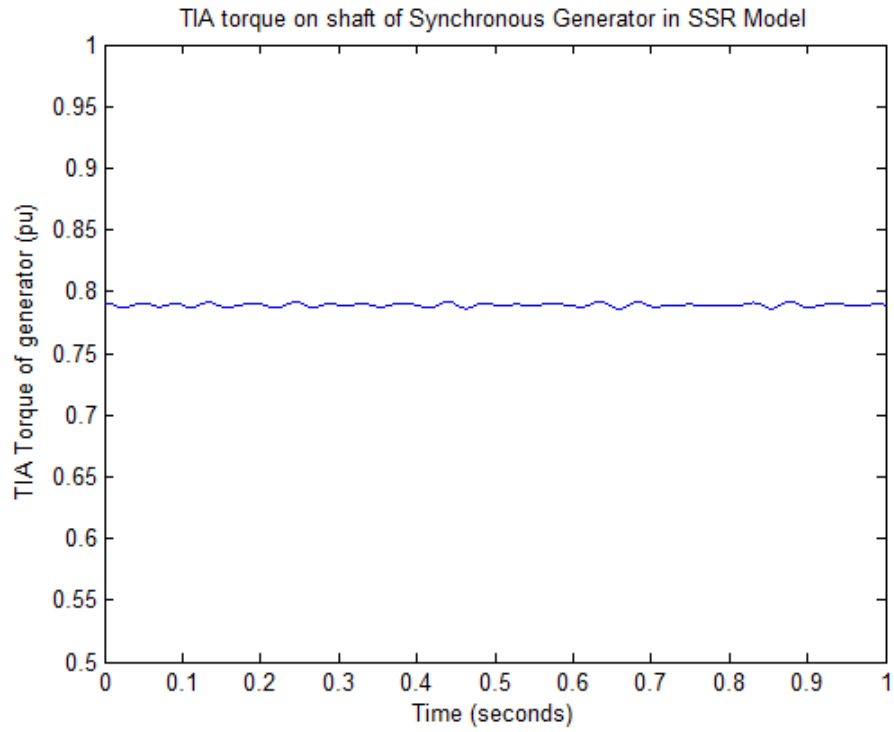


**Figure 5.11 TIA torque of shaft of synchronous generator in steady-state**

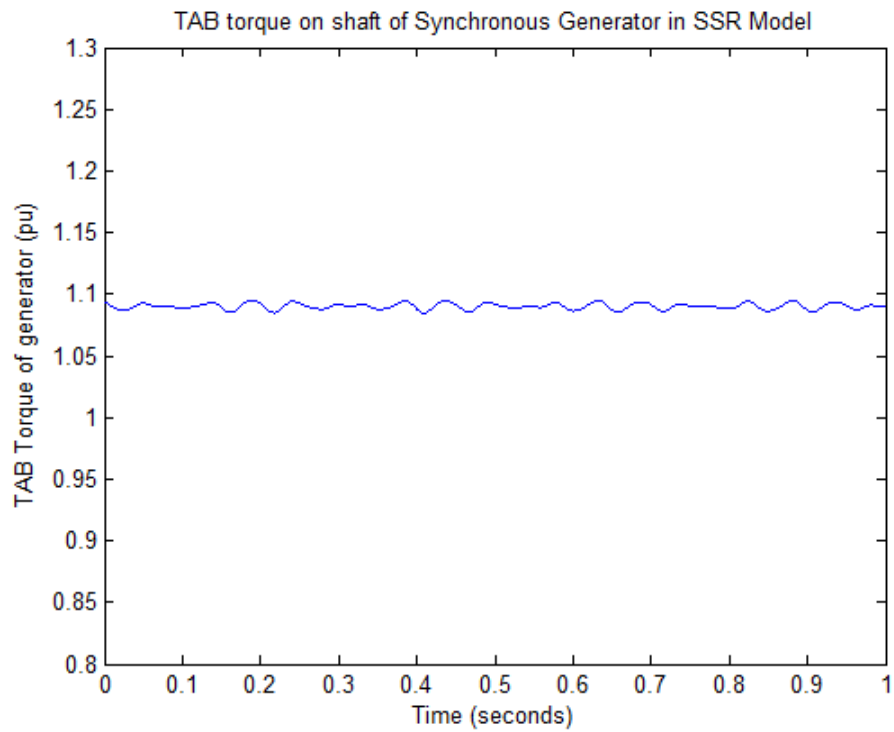


**Figure 5.12 TAB torque of shaft of synchronous generator in steady-state**



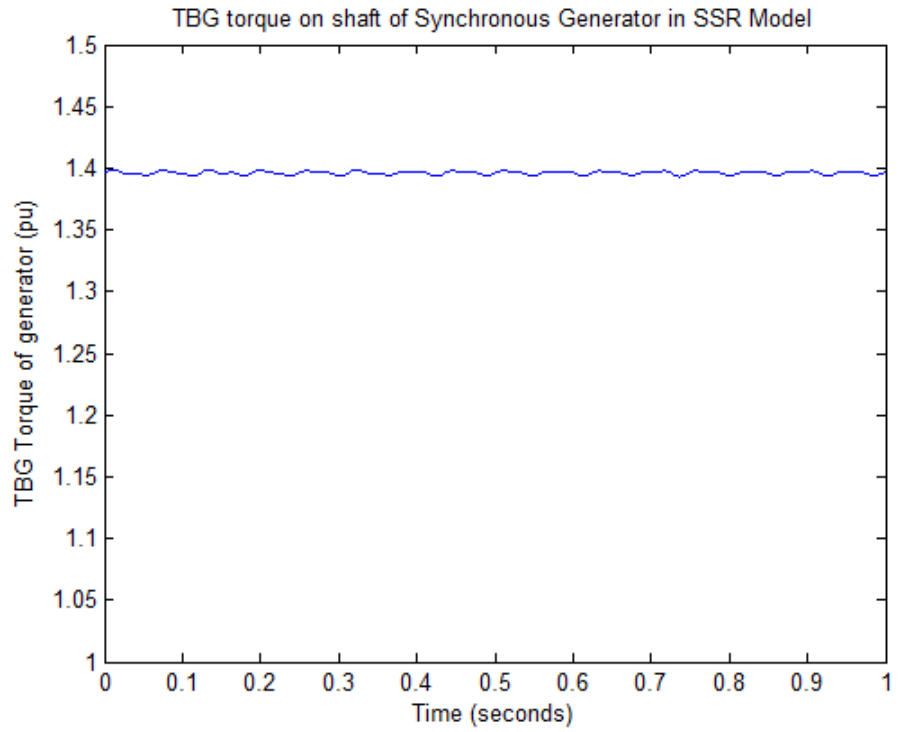


**Figure 5.13 TBG torque of shaft of synchronous generator in steady-state**

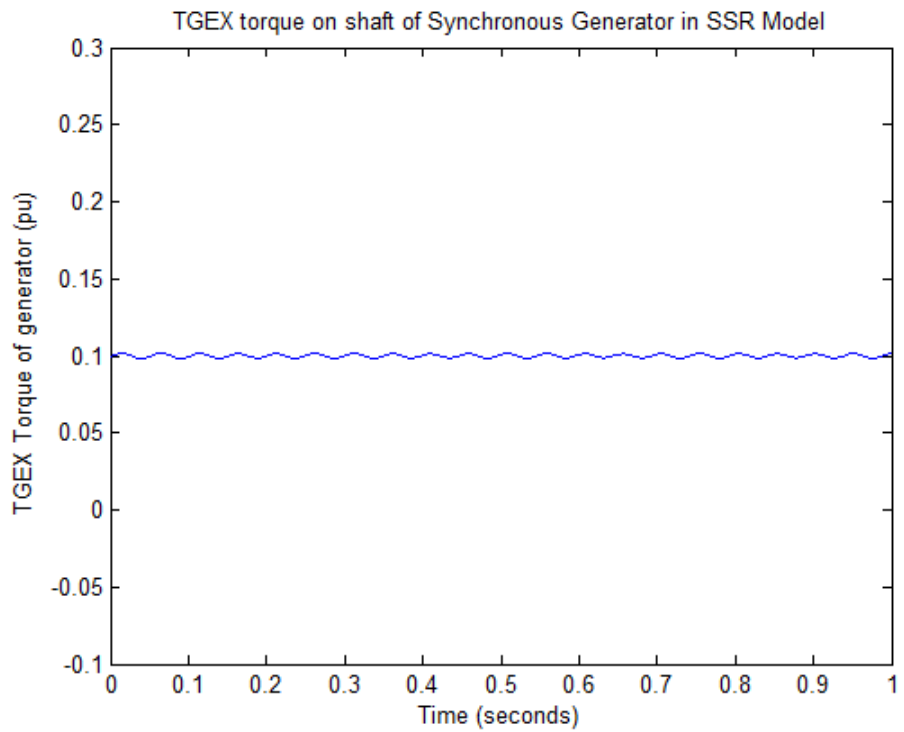


**Figure 5.14 TGEX torque of shaft of synchronous generator in steady-state**

Figures 5.7 – 5.14 represent the reactive power, rotor angle, mechanical torque of synchronous generator, interconnecting torque from high pressure (HP) turbine to low pressure (LP) turbine, interconnecting torque from intermediate pressure (HP) turbine to low pressure A (LPA) turbine, interconnecting torque from low pressure A (LPA) turbine to low pressure B (LPB) turbine, interconnecting torque from low pressure B (LPB) turbine to generator (BG) and interconnecting torque from generator to exciter (GEX) in steady-state respectively. The value of reactive power in steady-state is 0.4358 pu approximately. The value of rotor angle is approximately 41 degrees. The values of  $T_{HI}$ ,  $T_{IA}$ ,  $T_{AB}$ ,  $T_{BG}$  and  $T_{GEX}$  are 0.42 pu, 0.364 pu, 0.308 pu and 0.1pu, respectively. These values are validated by the turbine torque shares specified in the IEEE First Benchmark Model data given in chapter 3. The turbine torque shares for HP, IP, LPA and LPB turbines are 0.3, 0.26, 0.22 and 0.22. The mechanical torque of generator is 1.5 pu. It is because the electrical torque is 0.9 pu and every mass exhibits a damping factor of 0.1 pu.

### 5.3 Comparison of the Real and Simulated Values

Figure 5.15 shows model of the EAF built in PSCAD. This model builds an actual power system structure containing the EAF. This model is same as shown in Figure 4.2 of section 4.1. First block represents the 230 kV Grid. The Grid is connected to the 230/34.5kV transformer. The second transformer steps the voltage down from 34.5 kV to 600 V. This second transformer is connected to the EAF. The EAF is modeled by the equations described in sections 4.2 and 4.3 representing both the stages of its operation. The EAF block is simulated through a FORTRAN code written in the PSCAD.

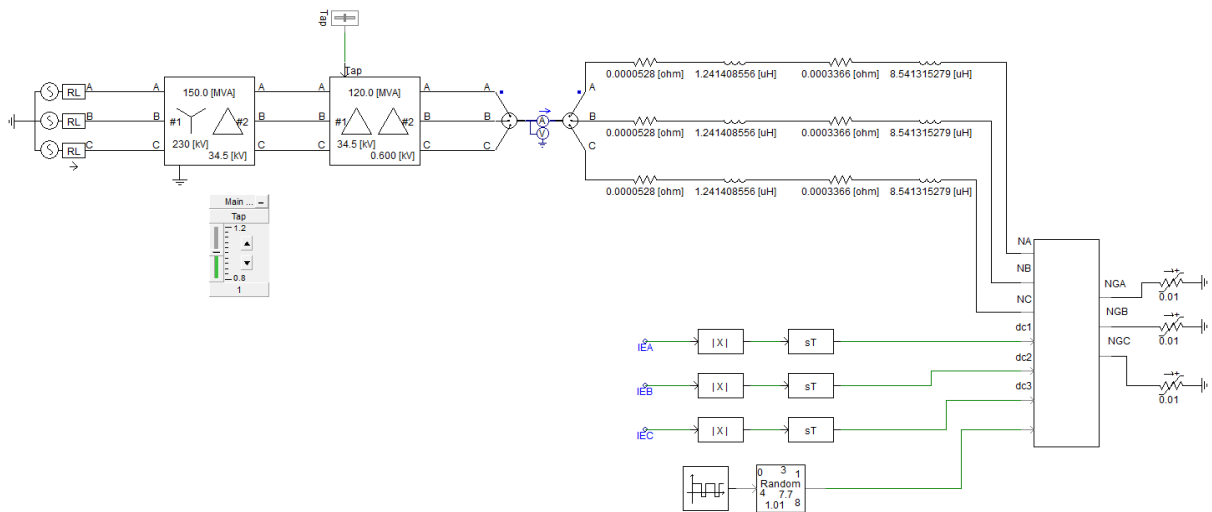


Figure 5.15 PSCAD MODEL OF THE EAF

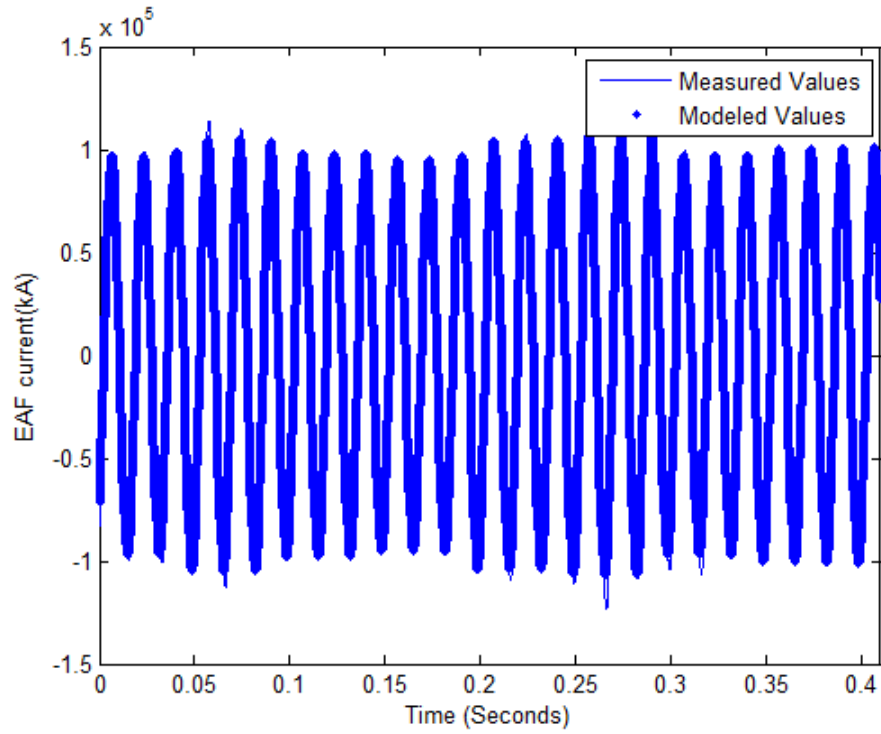


Figure 5.16 EAF measured and simulated current values for comparison

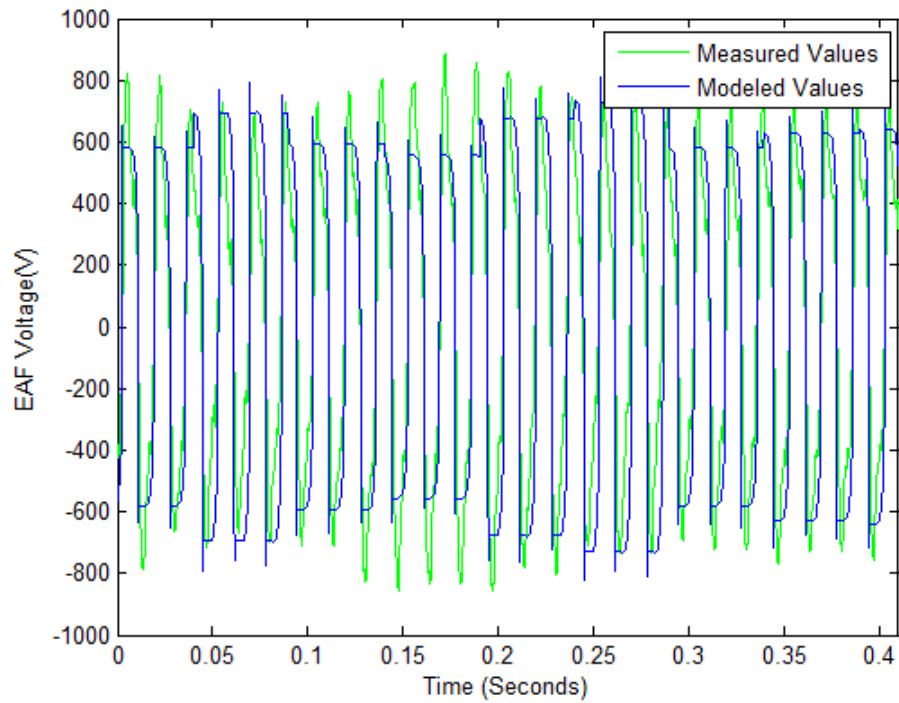


Figure 5.17 EAF measured and simulated voltage values

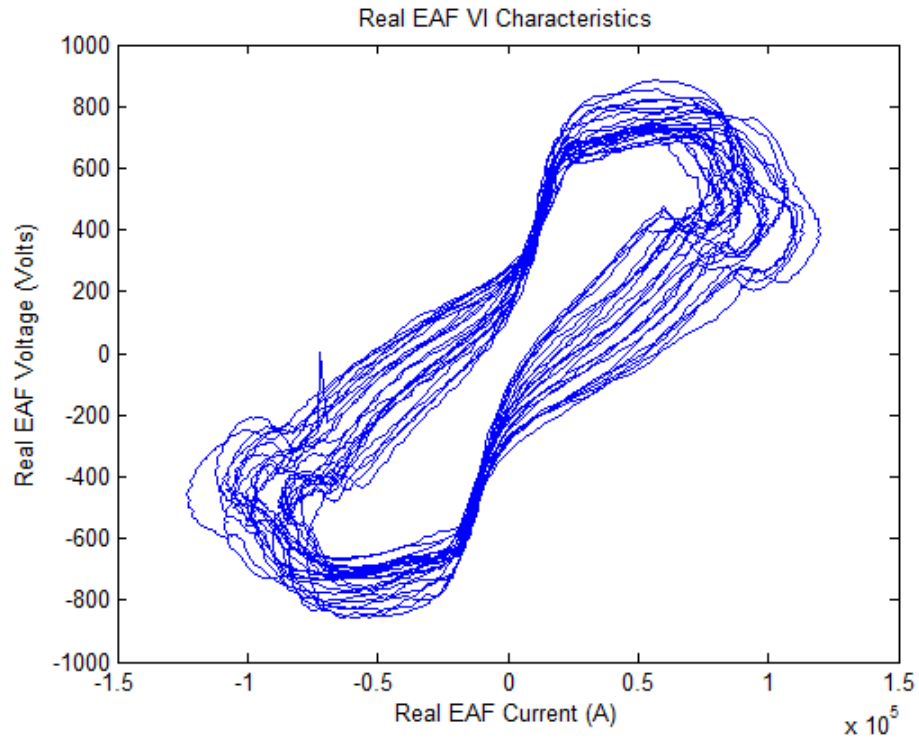


Figure 5.18 V-I characteristics for EAF1

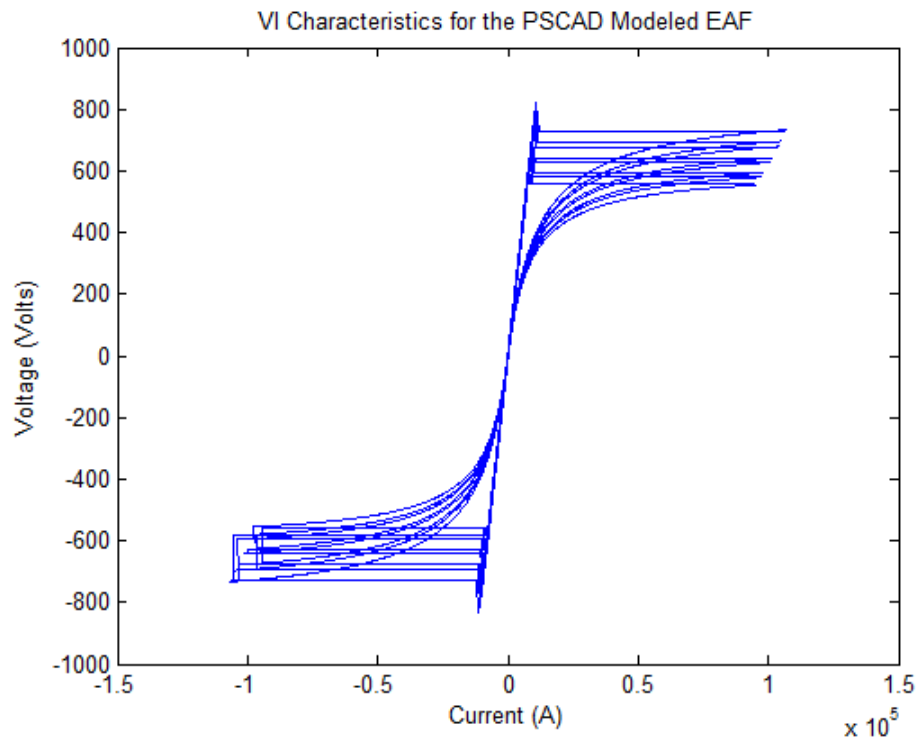
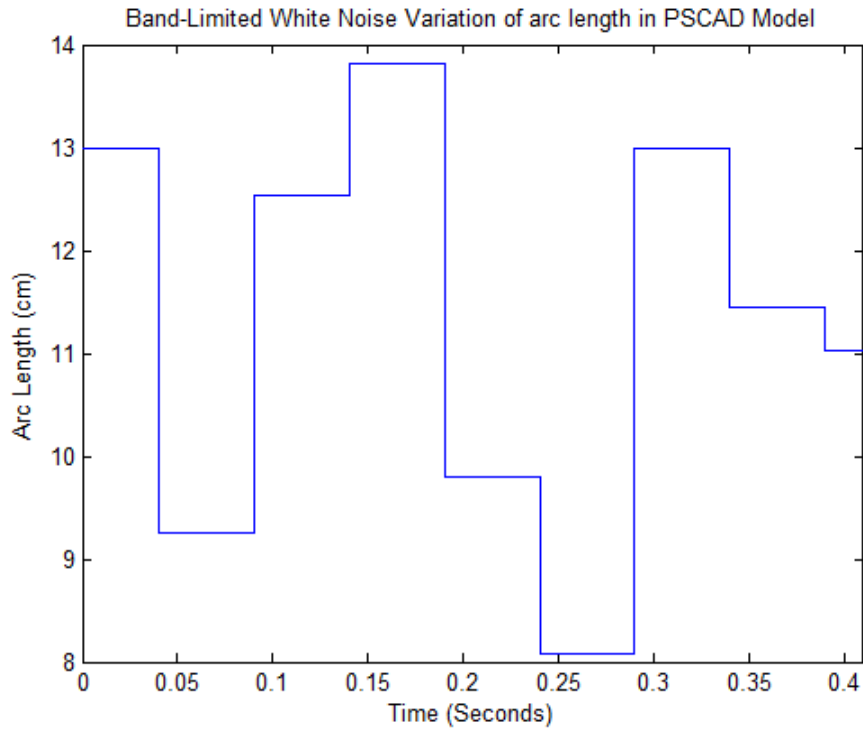


Figure 5.19 V-I characteristics for PSCAD based EAF model



**Figure 5.20 Arc length variation for PSCAD model**

Figure 5.16 shows the current measured at the EAF bus (LV side of the 34.5kV/600V transformer) and the modeled EAF current waveform. Figure 5.17 shows the measured and simulated EAF voltage. Figure 5.18 and Figure 5.19 show the measured and simulated VI-characteristics respectively. Figure 5.20 shows the band-limited white noise variation of the arc length incorporated into the simulated model.

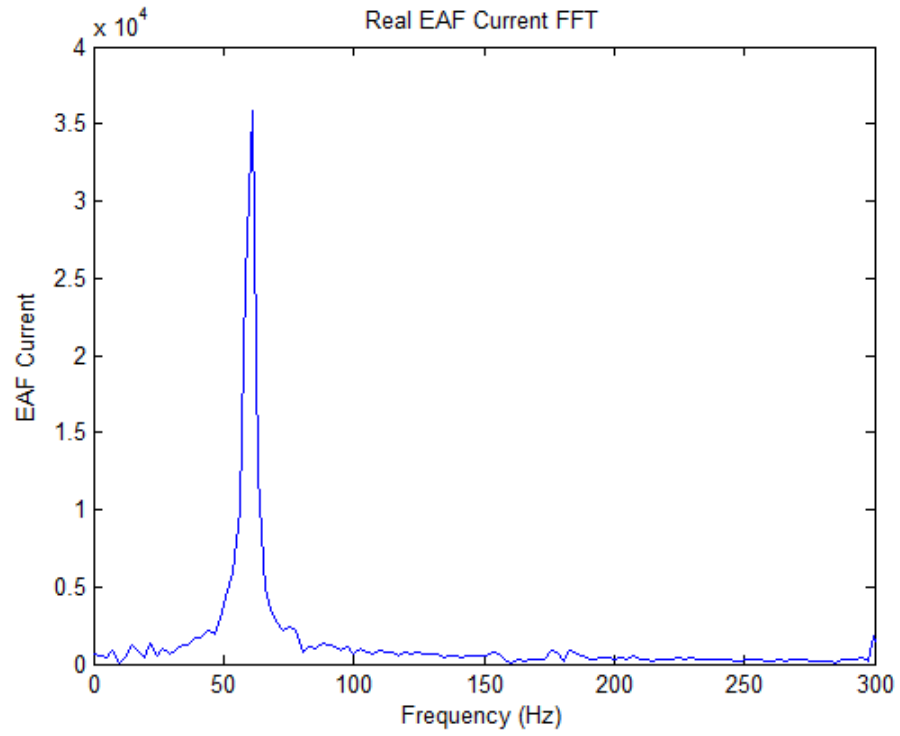


Figure 5.21 FFT of EAF1 current

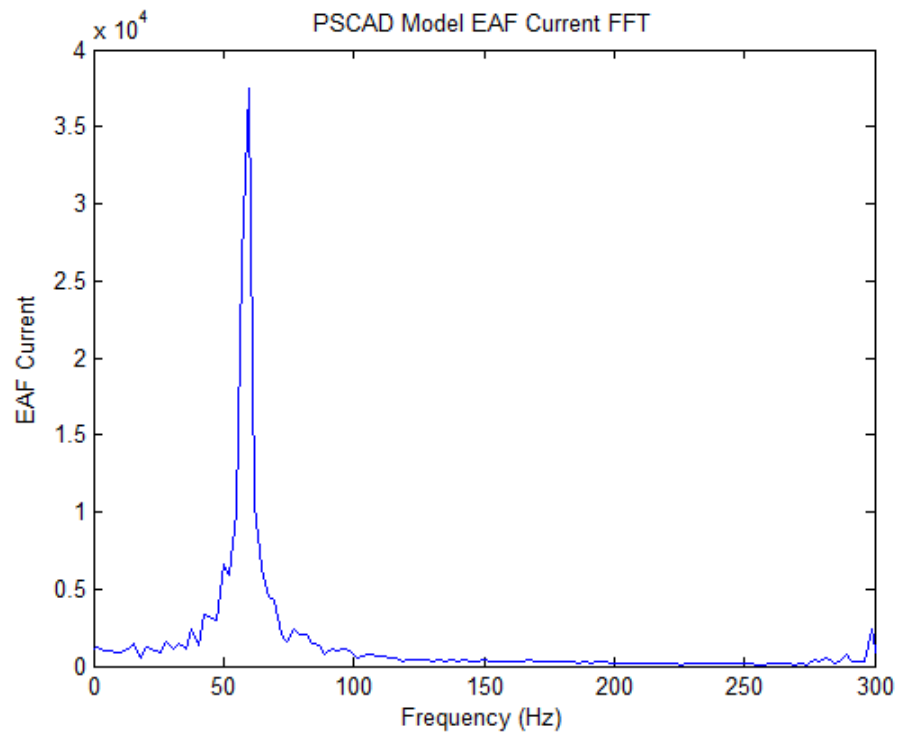


Figure 5.22 FFT of PSCAD MODELED EAF current

**Table 5.1 FFT of measured and simulated waveforms (sub-synchronous components)**

FFT of measured and simulated waveforms (sub-synchronous components)										
Measured (Hz)	2.44	4.87	7.316	9.75	12.19	14.63	17.07	21.95	24.39	26.82
PSCAD Model (Hz)	3.66	6.097	8.536	10.97	13.41	15.85	18.29	20.73	23.17	26.01

Figure 5.21 and Figure 5.22 show the FFT of the measured and simulated EAF currents respectively. The sub-synchronous components are tabulated in Table 5.1. The frequency components of 14.63 Hz (15.85 Hz in case of PSCAD model), 21.95 Hz (20.73 Hz in case of PSCAD model) and 24.39 Hz (23.17 Hz in case of PSCAD model) are close to the second (15.805 Hz), third (20.219 Hz) and fourth (25.58 Hz) torsional oscillation modes of the turbine generator system.



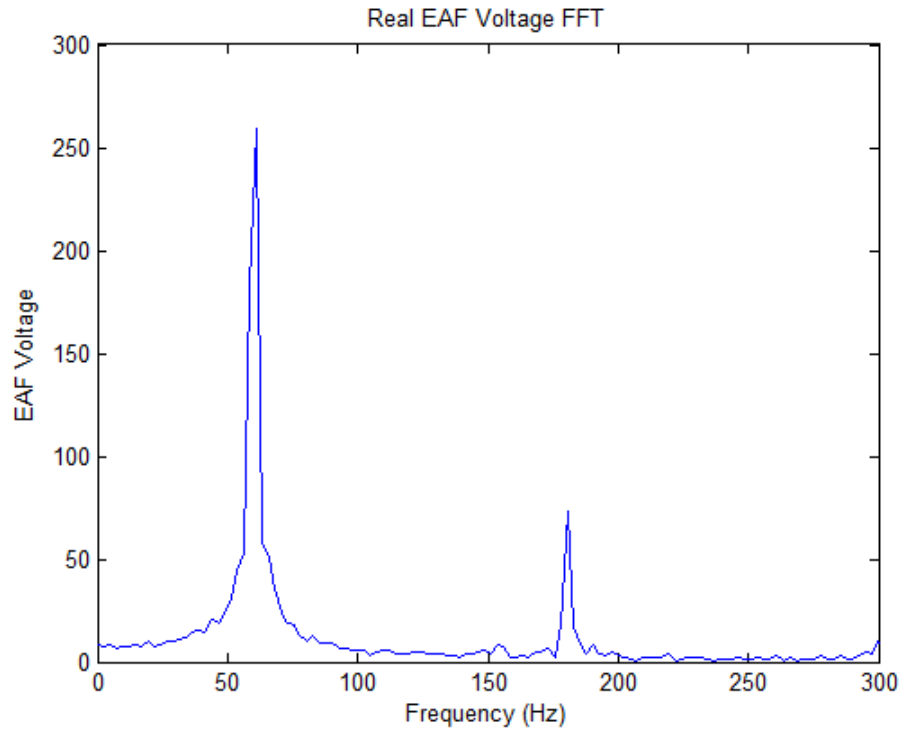


Figure 5.23 FFT of EAF1 voltage

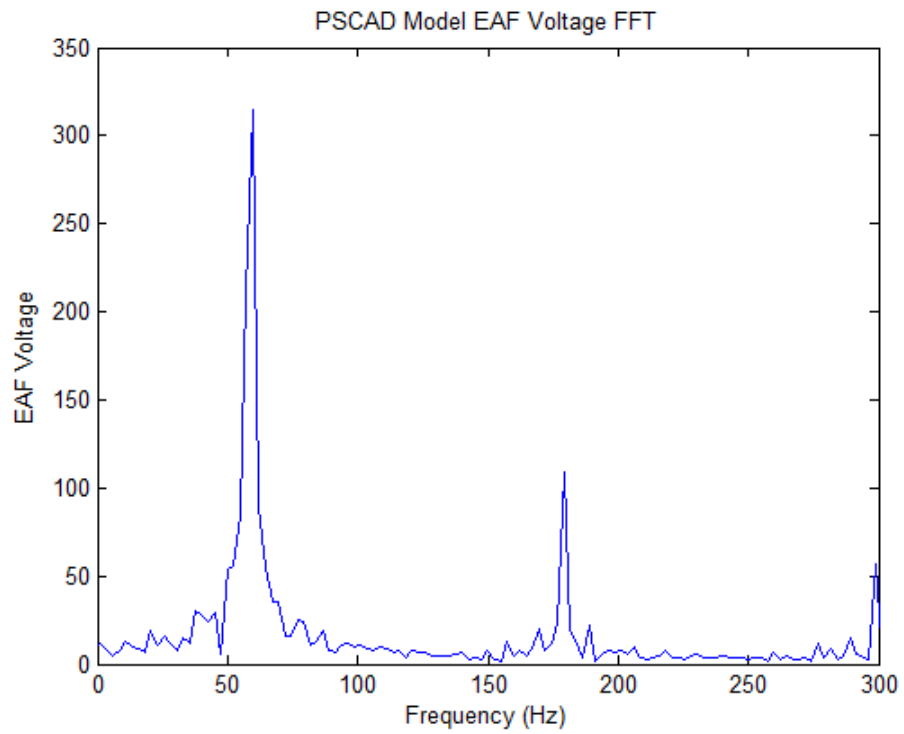


Figure 5.24 FFT of PSCAD MODELED EAF voltage

**Table 5.2 Comparison of measured and simulated values**

Parameter	Real EAF Value	PSCAD Model Value
THD <sub>v</sub>	30.04%	35.12%
THD <sub>i</sub>	10.31%	9.09%

Figure 5.23 and Figure 5.24 show the FFT of EAF voltage for measured and simulated signals respectively. The measured and simulated values are also compared on the basis of total harmonic distortion (THD) and the results are tabulated in Table 5.2. There is some difference among the values of total voltage harmonic distortion (THD<sub>v</sub>). It is because in the real system the SVC and filters are installed at the EAF bus.

## 5.4 Simulation Results during first stage of EAF operation:

Figure 5.25 shows the EAF connected to the SSR model (IEEE First Bench Mark Model) in PSCAD. The SSR model in the PSCAD is already described in section 5.2. The EAF model in the PSCAD is described in section 5.3. Parameters of the SSR model are given in Appendix. While, the parameters of the EAF model are given in sections 4.2 and 4.3. Both the first and second stages of the EAF operation are simulated through this same model as shown in Figure 5.25. Only the parameters for simulating the two stages of the EAF operation are changed in the EAF block properties in the PSCAD.

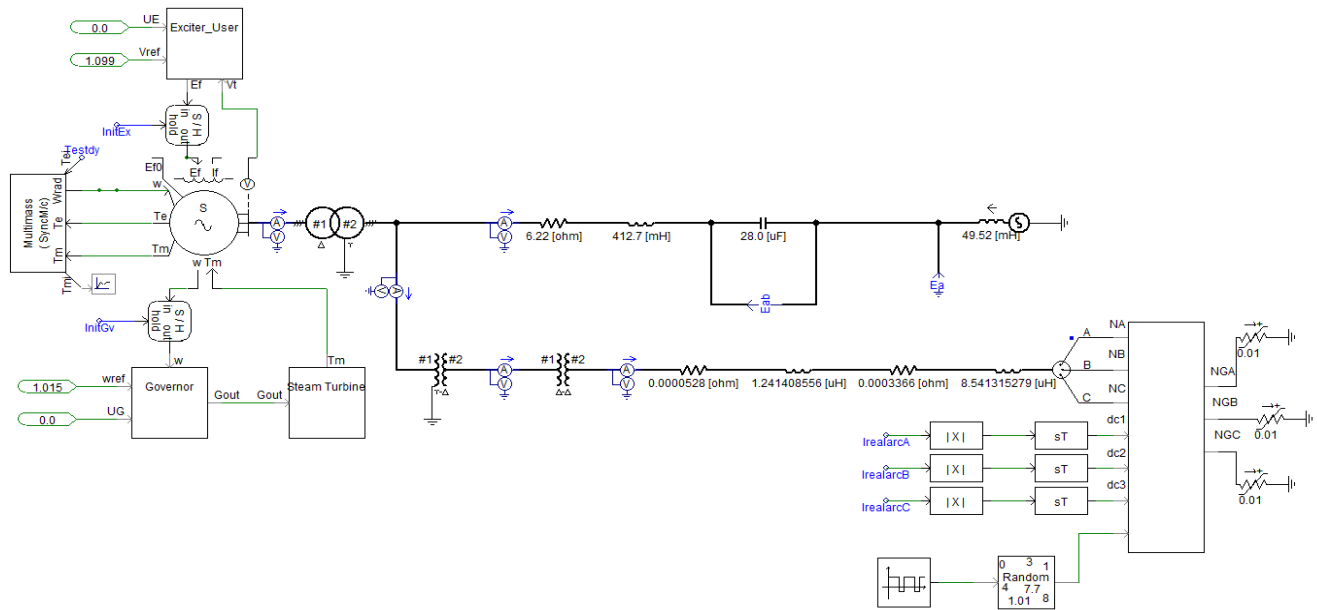


Figure 5.25 PSCAD SSR and EAF Complete Model

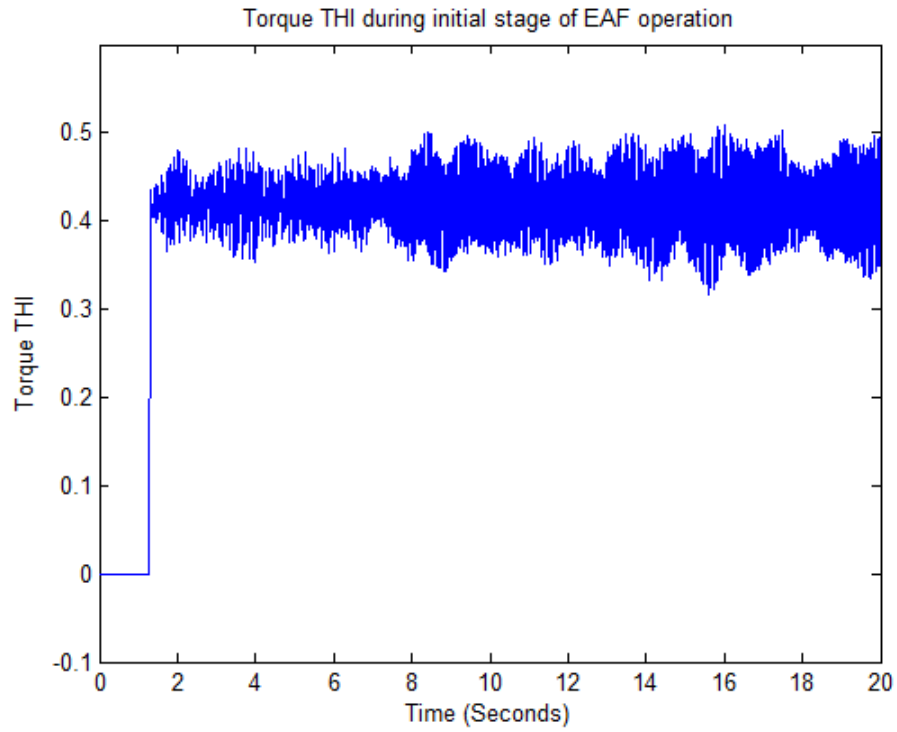


Figure 5.26 Turbine torque THI during first stage of EAF operation

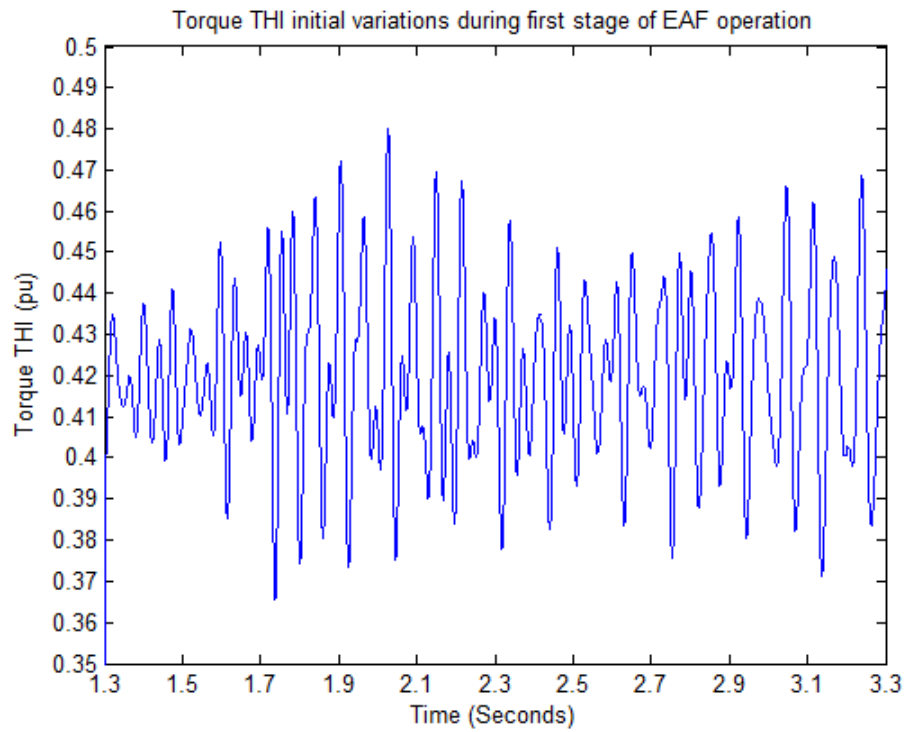
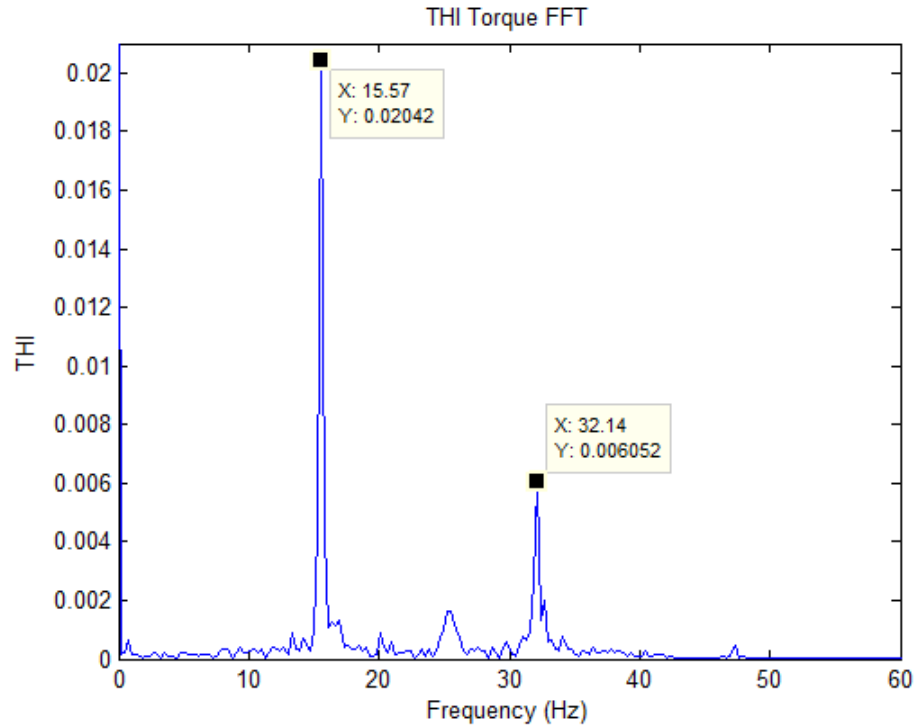


Figure 5.27 Initial variations of turbine torque THI during first stage of EAF operation



**Figure 5.28 FFT of turbine torque THI during initial stage of EAF operation**

Figure 5.26 shows the graph for THI during the first stage of the EAF operation. Figure 5.27 shows the graph for initial variations of THI (for the purpose of a clear view) during the first stage of the EAF operation. Figure 5.28 shows the FFT of the THI. These results are very critical. It is clearly shown in Figure 5.28 that low frequency components of 15.57Hz and 32.14 Hz are occurring in THI. It means that the sub-synchronous components being generated at the EAF side are so powerful that they are also appearing in the turbine torques. Though, the EAF consuming power is less than the generating power of the synchronous generator, even then the low-frequency harmonics caused by the EAF are directly affecting the generator torques.

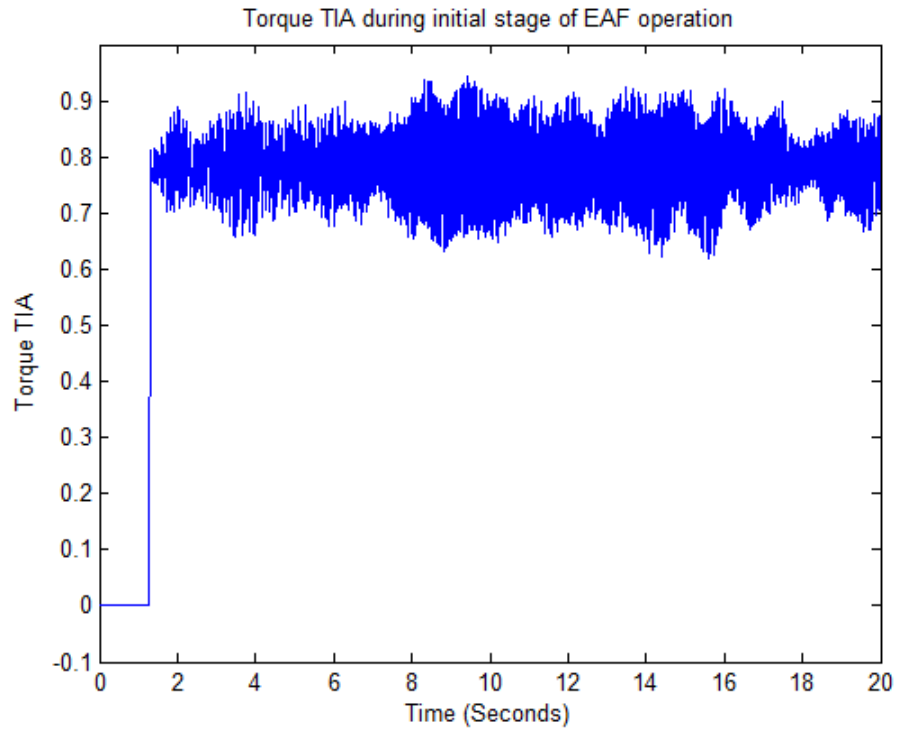


Figure 5.29 Turbine torque TIA during first stage of EAF operation

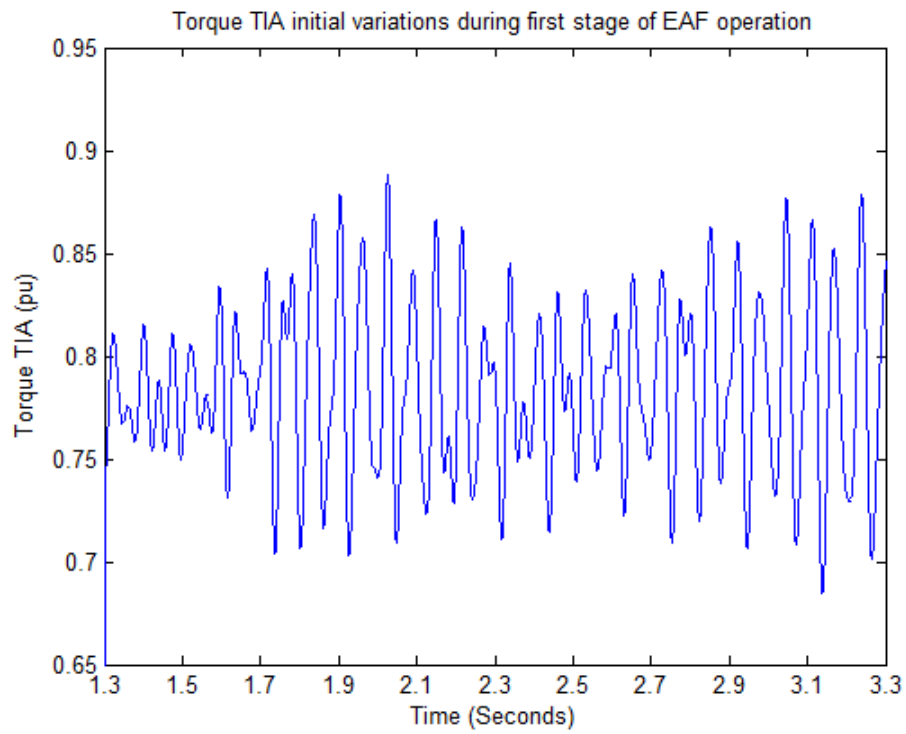
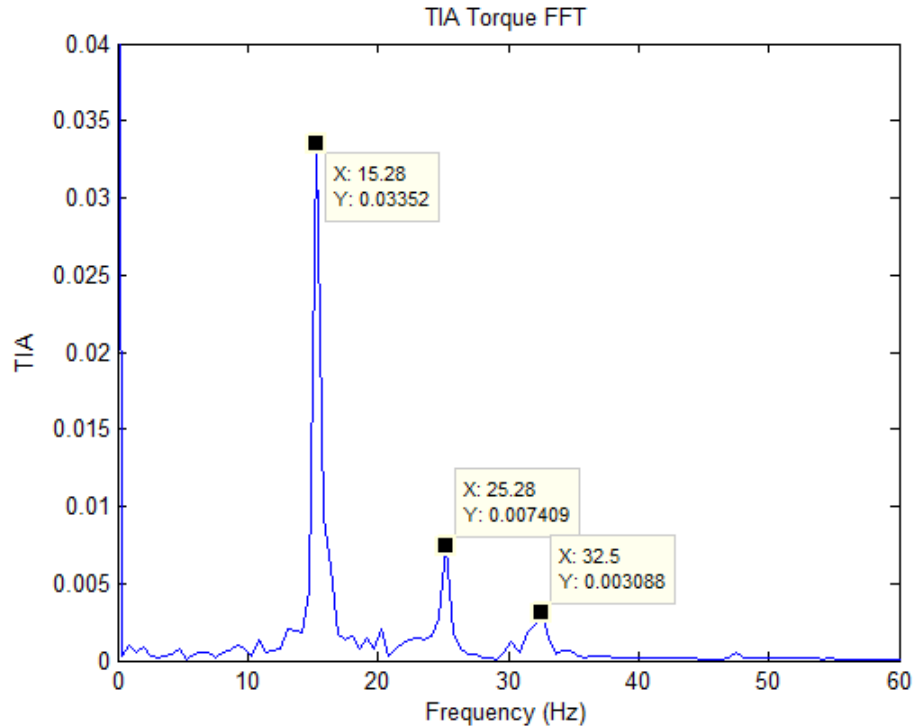


Figure 5.30 Initial variations of turbine torque TIA during first stage of EAF operation



**Figure 5.31 FFT of turbine torque TIA during initial stage of EAF operation**

Figure 5.29 shows the graph for TIA during the first stage of the EAF operation. Figure 5.30 shows the graph for initial variations of TIA (for the purpose of a clear view) during the first stage of the EAF operation. Figure 5.31 shows the FFT of the TIA. These results are very critical. It is clearly shown in Figure 5.31 that low frequency components of 15.28Hz, 25.28 Hz and 32.5 Hz are occurring in TIA torque. It means that the sub-synchronous components being generated at the EAF side are so powerful that they are also appearing in the turbine torques. Though, the EAF consuming power is less than the generating power of the synchronous generator, even then the low-frequency harmonics caused by the EAF are directly affecting the generator torques.

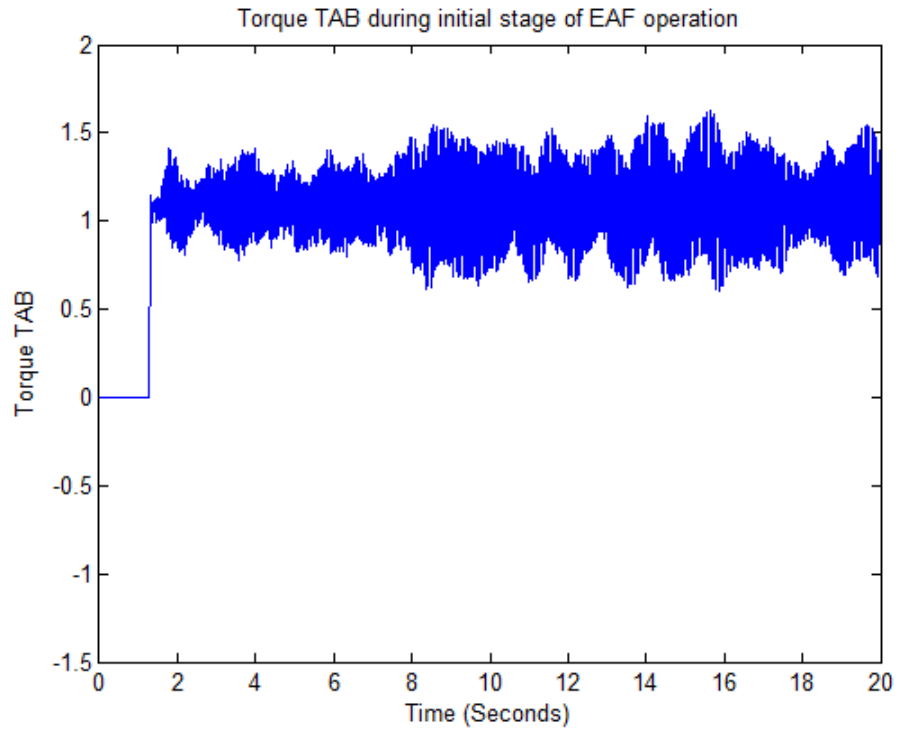


Figure 5.32 Turbine torque TAB during first stage of EAF operation

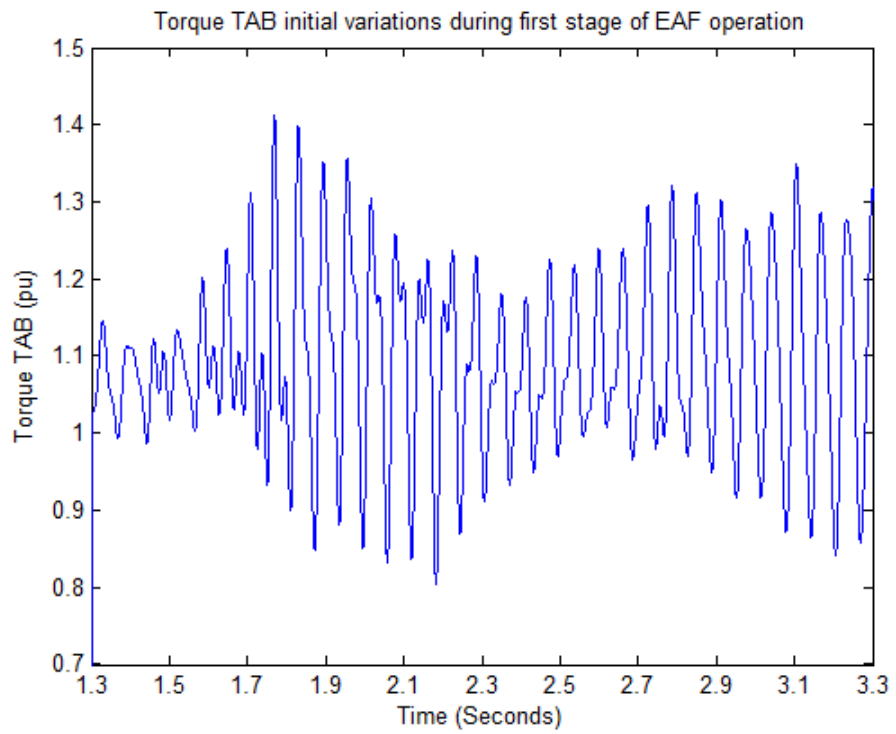
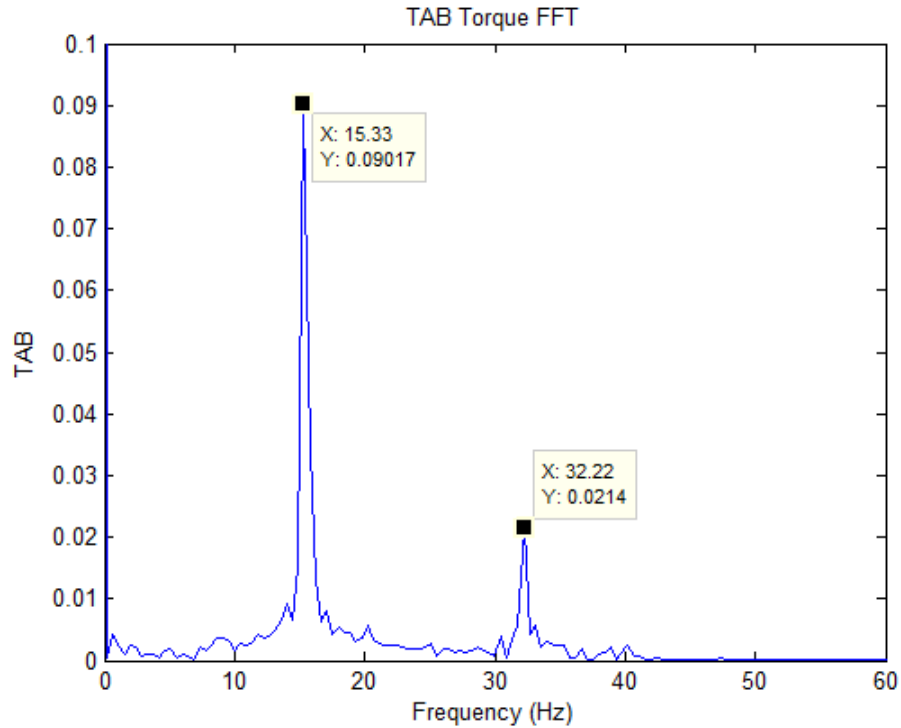


Figure 5.33 Initial variations of turbine torque TAB during first stage of EAF operation





**Figure 5.34 FFT of turbine torque TAB during initial stage of EAF operation**

Figure 5.32 shows the graph for TAB during the first stage of the EAF operation. Figure 5.33 shows the graph for initial variations of TAB (for the purpose of a clear view) during the first stage of the EAF operation. Figure 5.34 shows the FFT of the TAB. These results are very critical. It is clearly shown in Figure 5.34 that low frequency components of 15.33Hz and 32.22 Hz are occurring in TAB. It means that the sub-synchronous components being generated at the EAF side are so powerful that they are also appearing in the turbine torques. Though, the EAF consuming power is less than the generating power of the synchronous generator, even then the low-frequency harmonics caused by the EAF are directly affecting the generator torques.

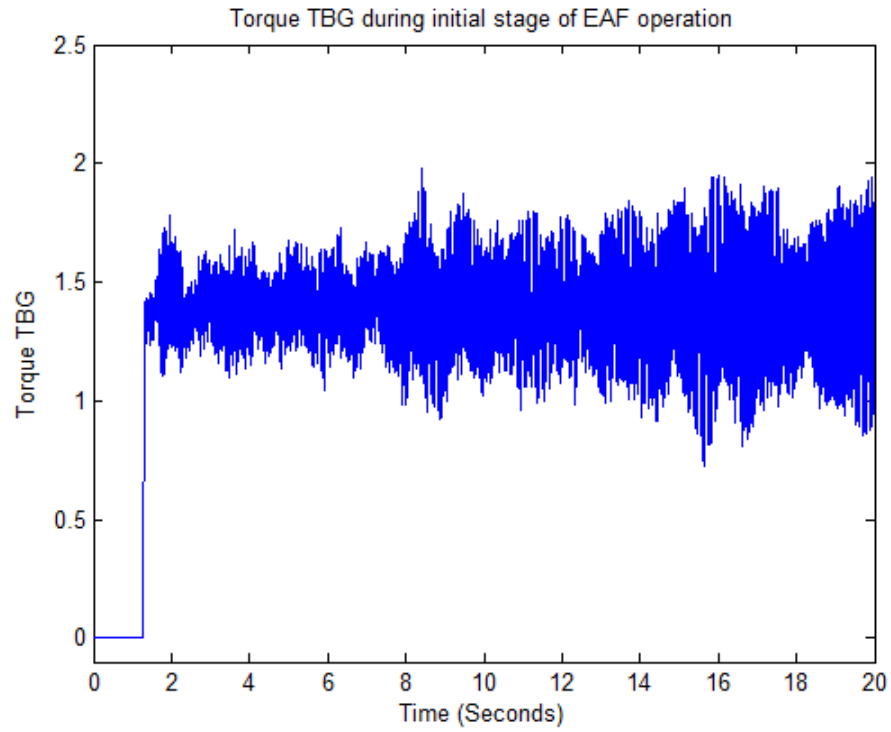


Figure 5.35 Turbine torque TBG during first stage of EAF operation

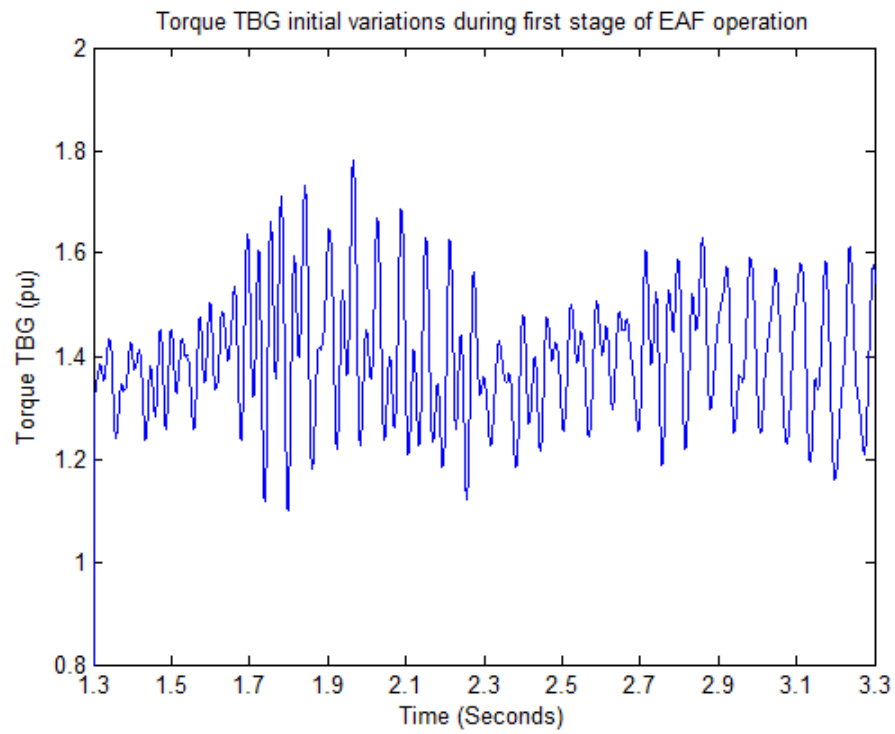
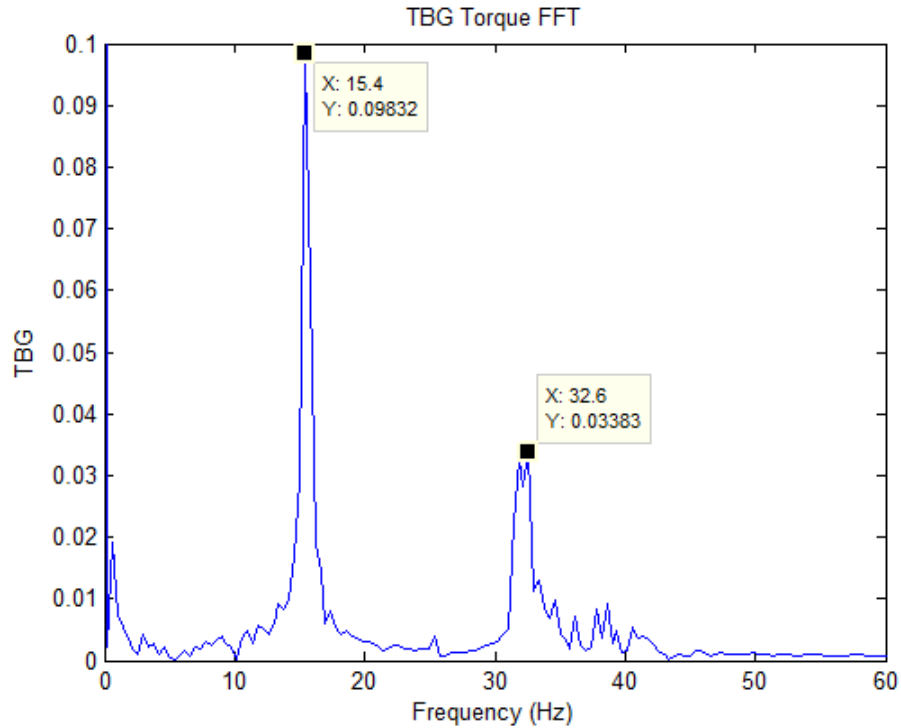


Figure 5.36 Initial variations of turbine torque TBG during first stage of EAF operation



**Figure 5.37 FFT of turbine torque TBG during initial stage of EAF operation**

Figure 5.35 shows the graph for TBG during the first stage of the EAF operation. Figure 5.36 shows the graph for initial variations of TBG (for the purpose of a clear view) during the first stage of the EAF operation. Figure 5.37 shows the FFT of the TBG. These results are very critical. It is clearly shown in Figure 5.37 that low frequency components of 15.4 Hz and 32.6 Hz are occurring in TBG. It means that the sub-synchronous components being generated at the EAF side are so powerful that they are also appearing in the turbine torques. Though, the EAF consuming power is less than the generating power of the synchronous generator, even then the low-frequency harmonics caused by the EAF are directly affecting the generator torques.

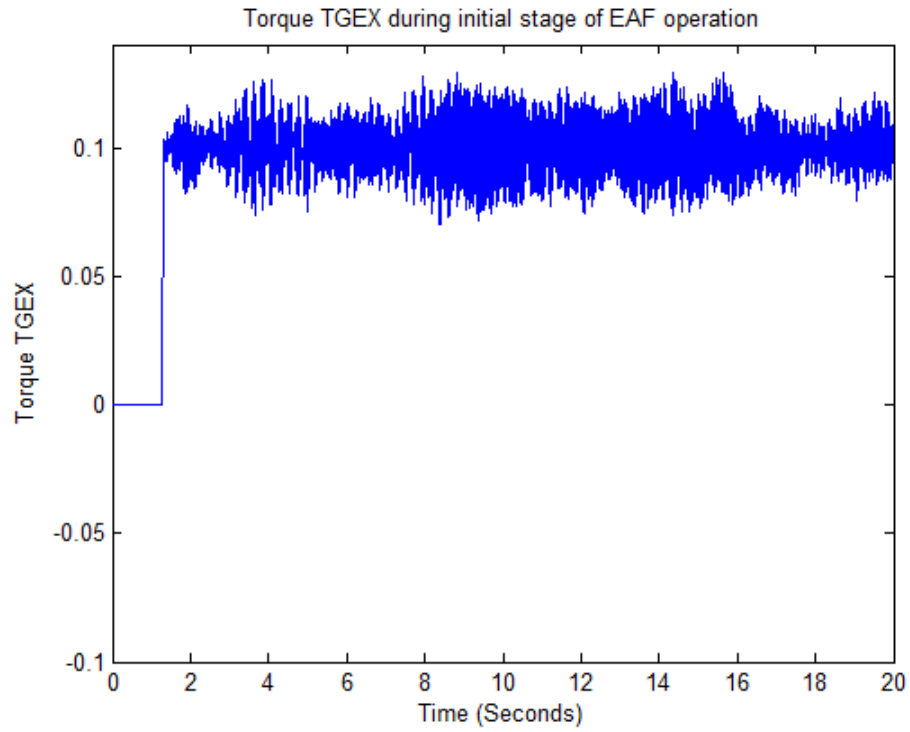


Figure 5.38 Turbine torque TGEX during first stage of EAF operation

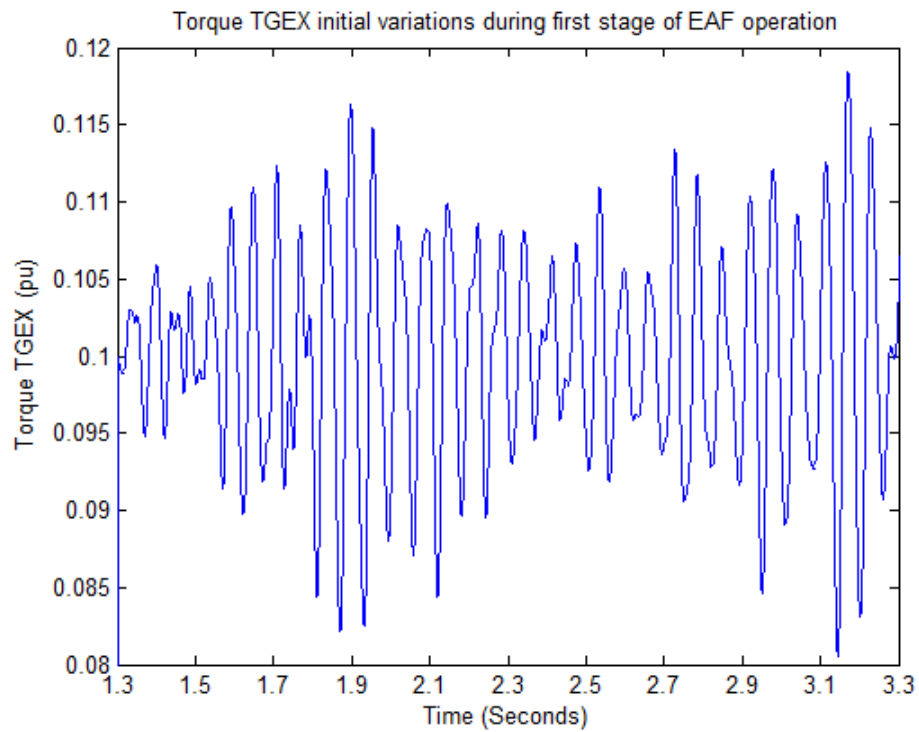
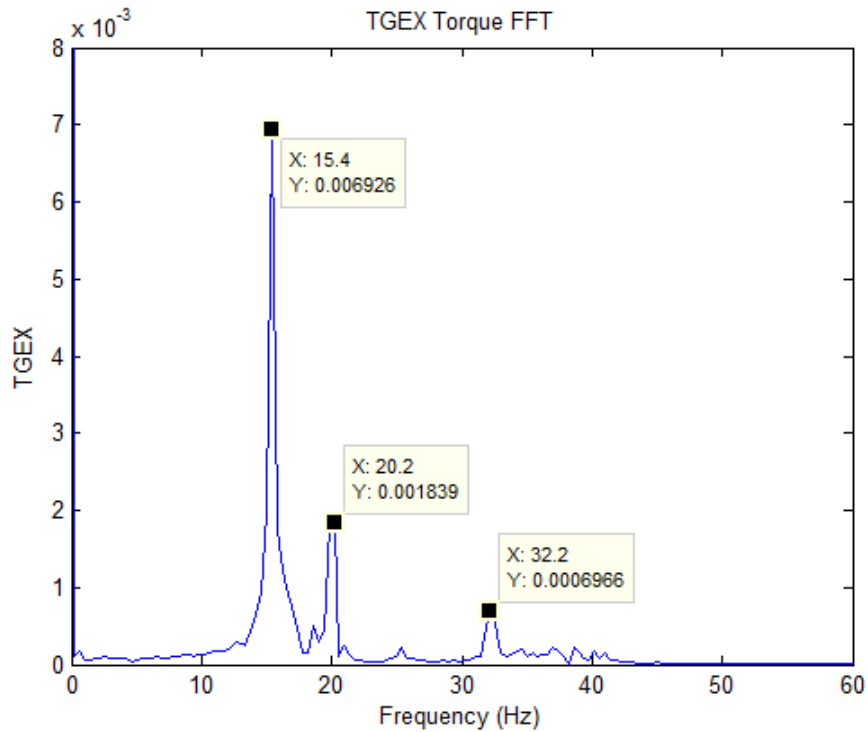
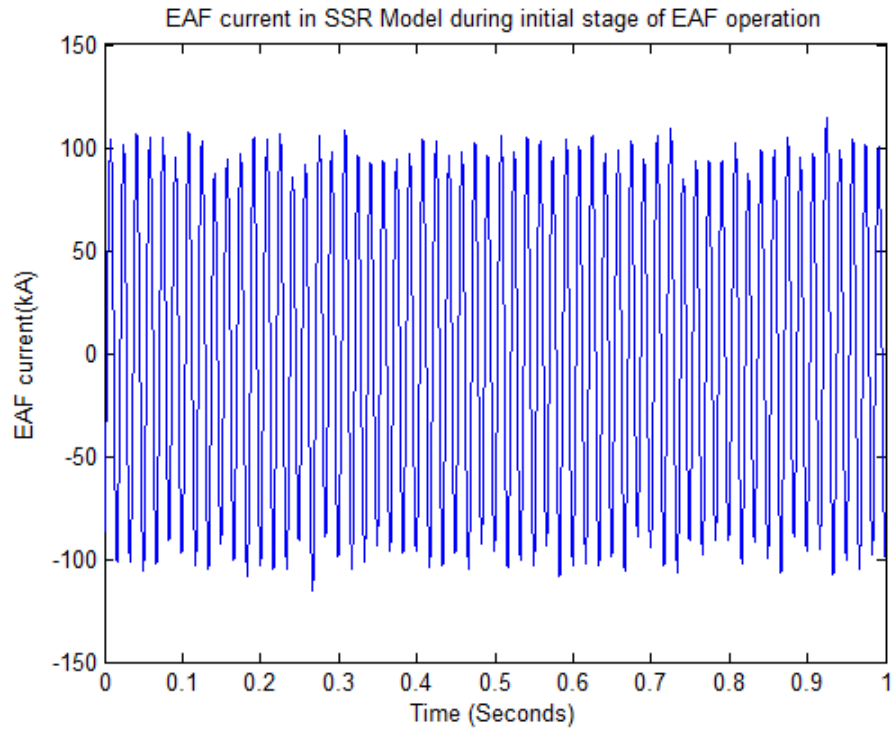


Figure 5.39 Initial variations of turbine torque TGEX (few cycles) during first stage of EAF operation



**Figure 5.40 FFT of turbine torque TGEX during initial stage of EAF operation**

Figure 5.38 shows the graph for TGEX during the first stage of the EAF operation. Figure 5.39 shows the graph for initial variations of TGEX (for the purpose of a clear view) during the first stage of the EAF operation. Figure 5.40 shows the FFT of the TGEX. These results are very critical. It is clearly shown in Figure 5.40 that low frequency components of 15.4 Hz, 20.2 Hz and 32.2 Hz are occurring in TGEX. It means that the sub-synchronous components being generated at the EAF side are so powerful that they are also appearing in the turbine torques. Though, the EAF consuming power is less than the generating power of the synchronous generator, even then the low-frequency harmonics caused by the EAF are directly affecting the generator torques.



**Figure 5.41 SSR Model EAF current during initial stage of EAF operation**

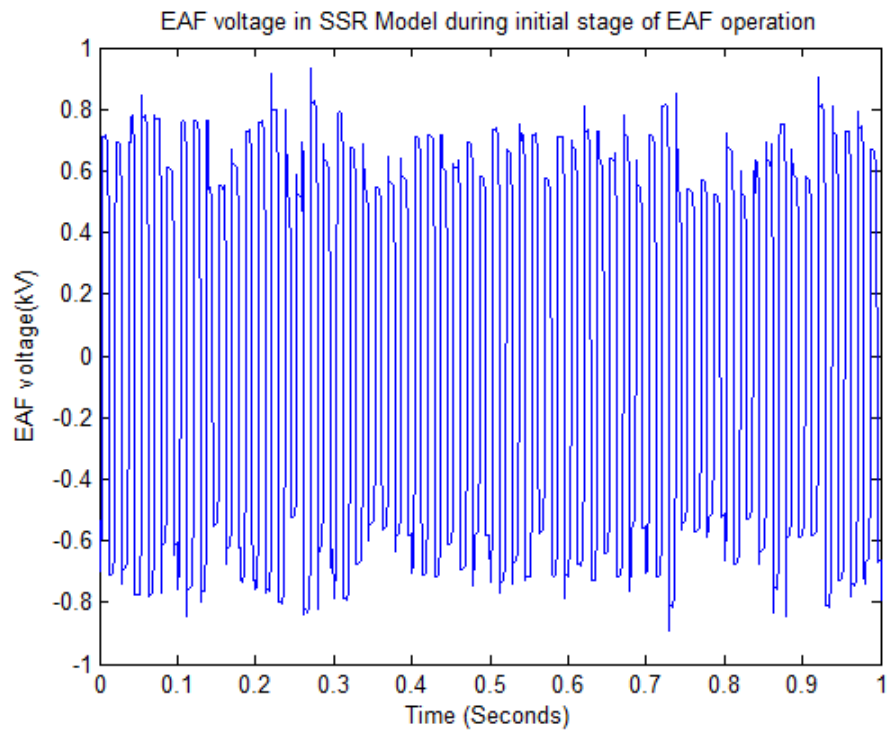


**Figure 5.42 SSR Model EAF voltage during initial stage of EAF operation**

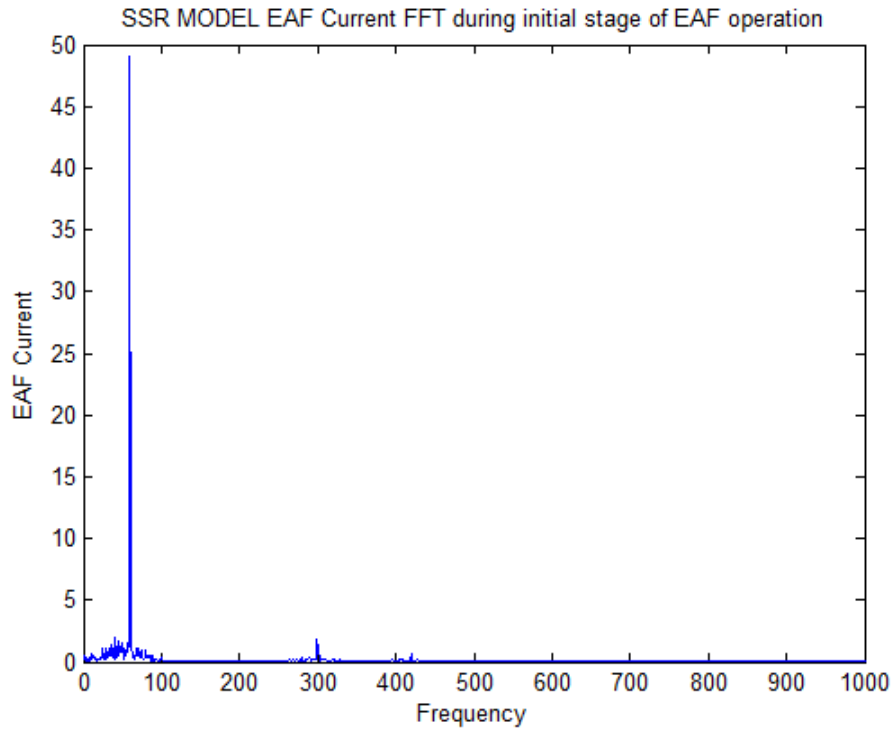


Figure 5.43 EAF current FFT

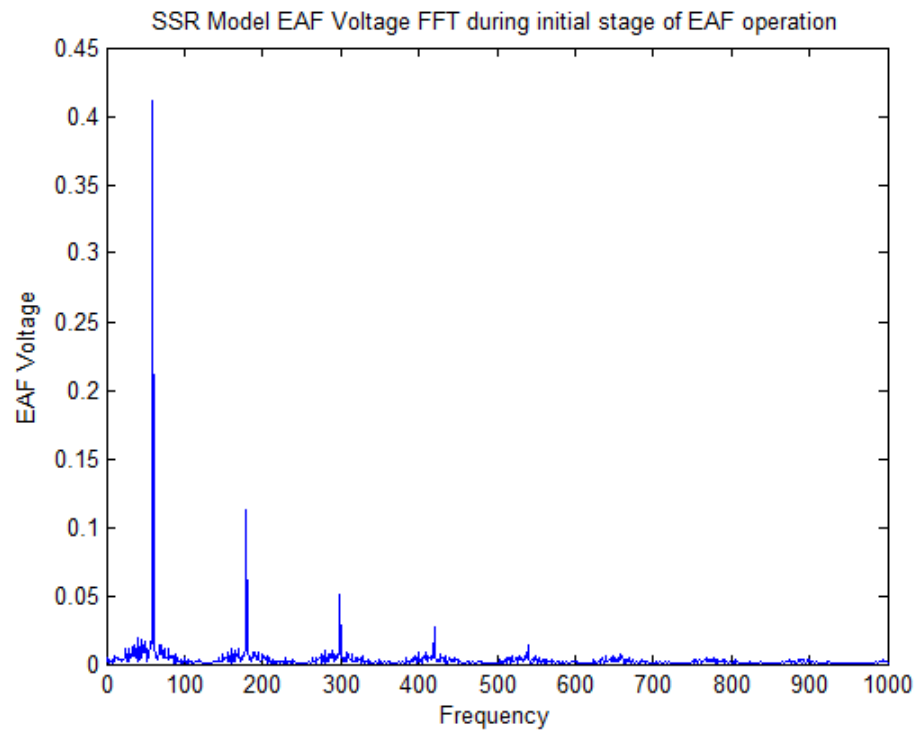
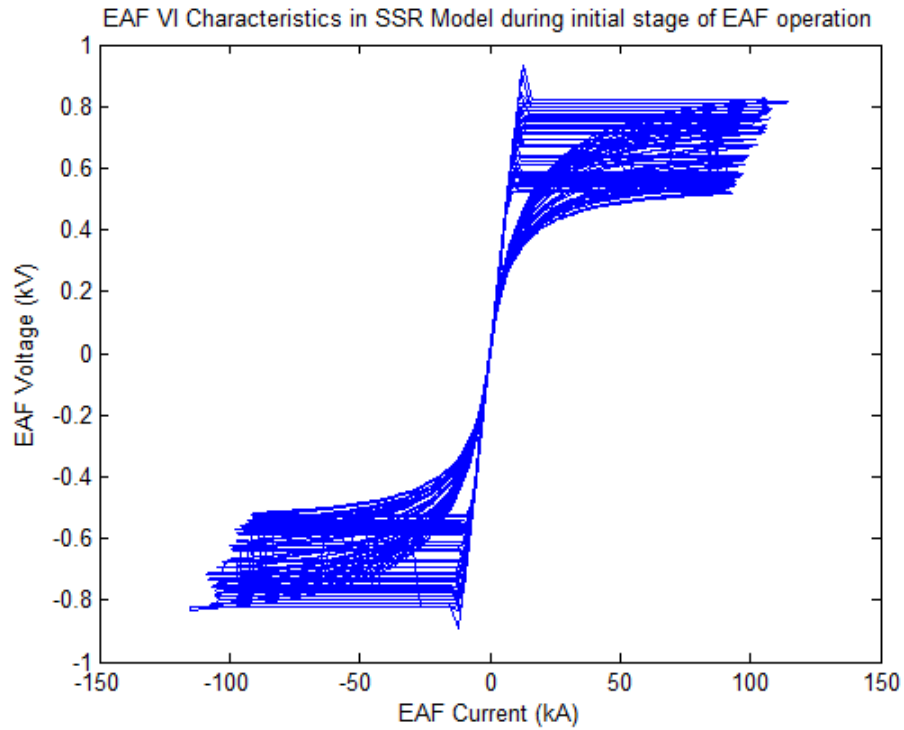


Figure 5.44 EAF voltage FFT



**Figure 5.45 SSR model EAF VI characteristics during initial stage of EAF operation**

Figures 5.41 – 5.45 show the EAF current, EAF voltage, FFT of EAF current, FFT of EAF voltage and the VI characteristics respectively during the first stage of the EAF operation. The low frequency components can be clearly observed in the FFTs of current and voltage.



## 5.5 Simulation results during second stage of the EAF operation

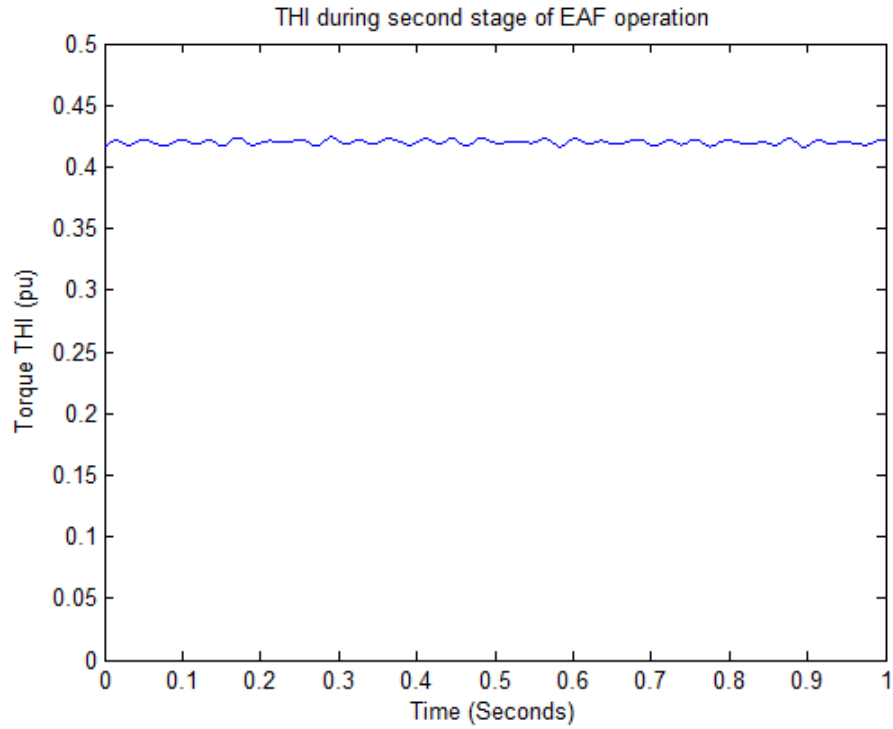


Figure 5.46 THI during second stage of EAF operation

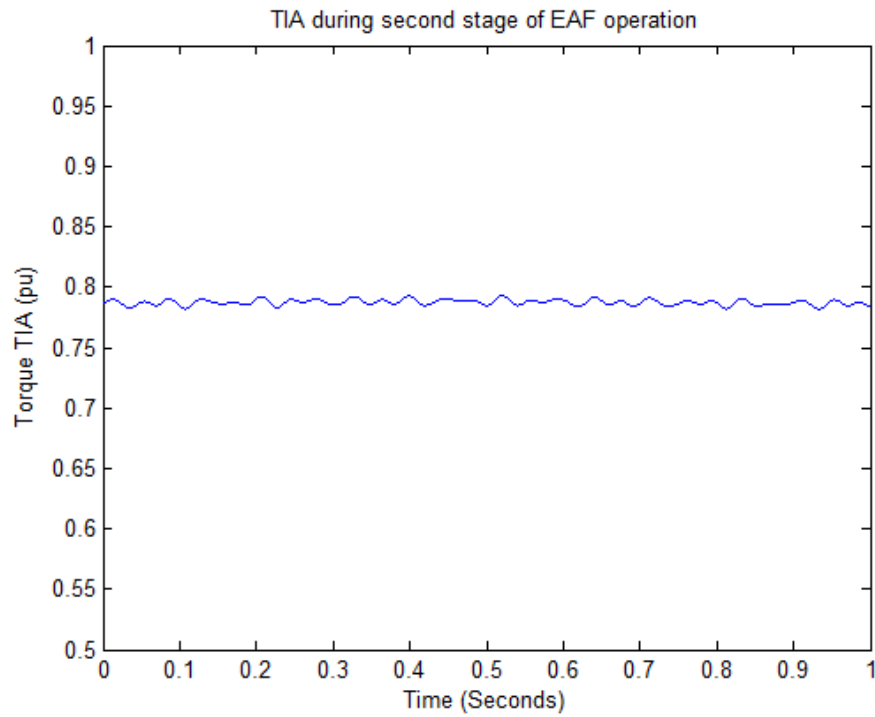
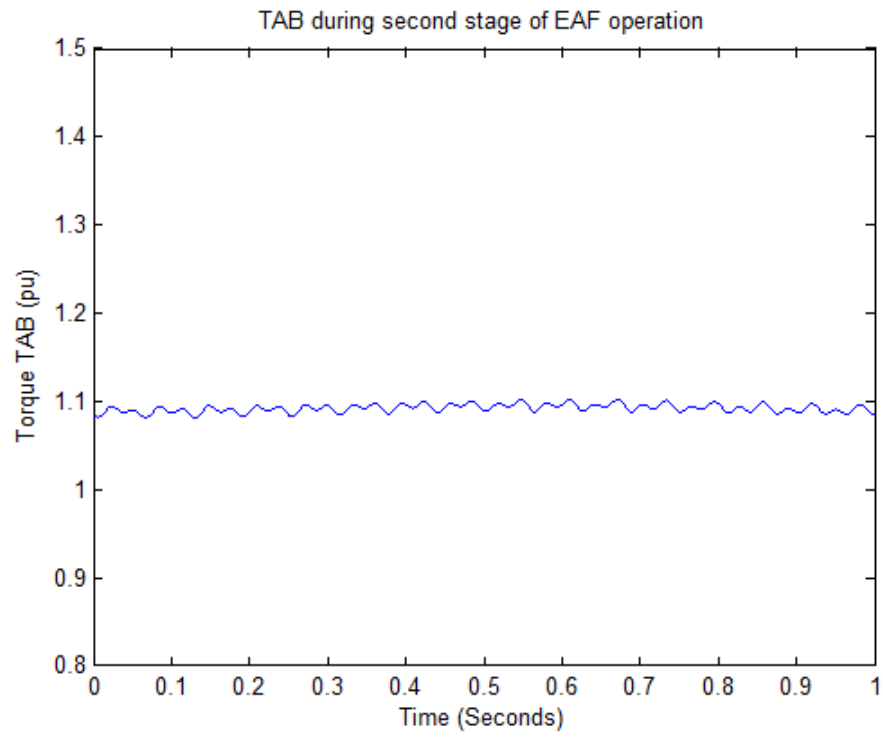
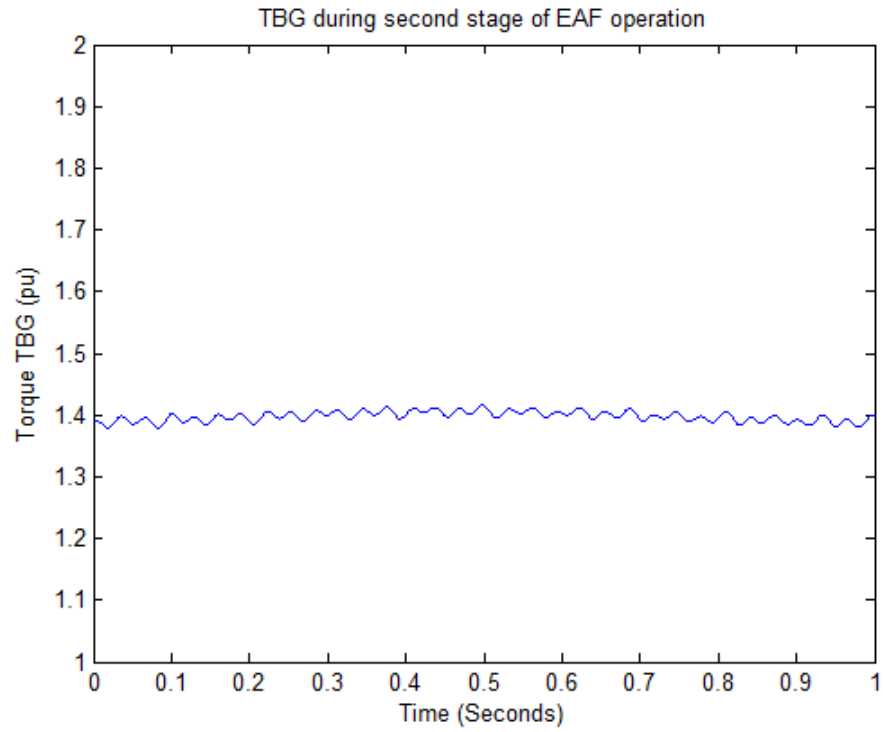


Figure 5.47 TIA during second stage of EAF operation



**Figure 5.48 TAB during second stage of EAF operation**



**Figure 5.49 TBG during second stage of EAF operation**

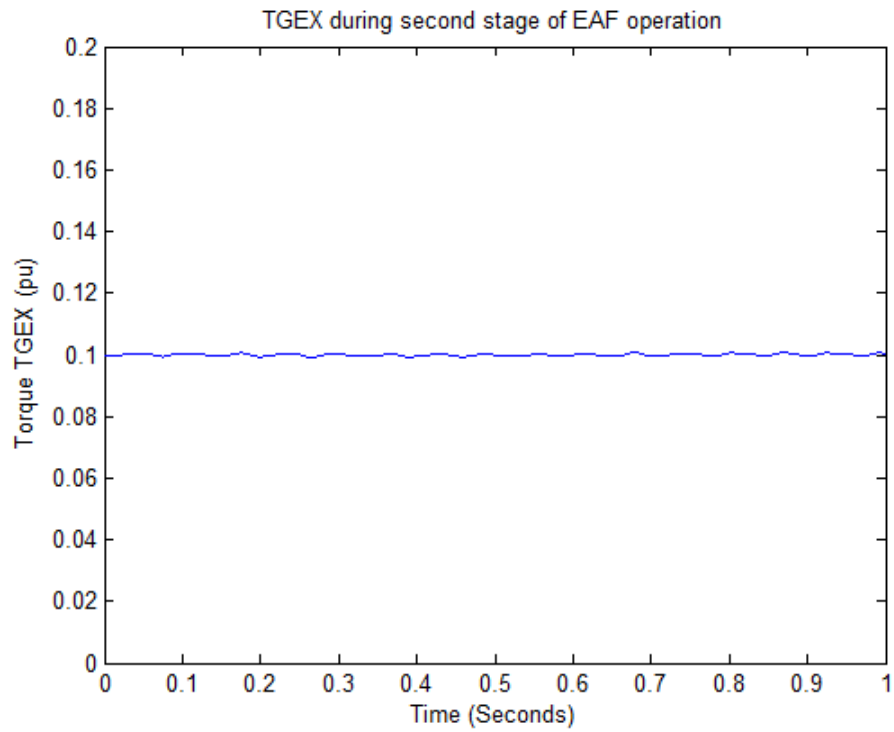


**Figure 5.50 TGEX during second stage of EAF operation**

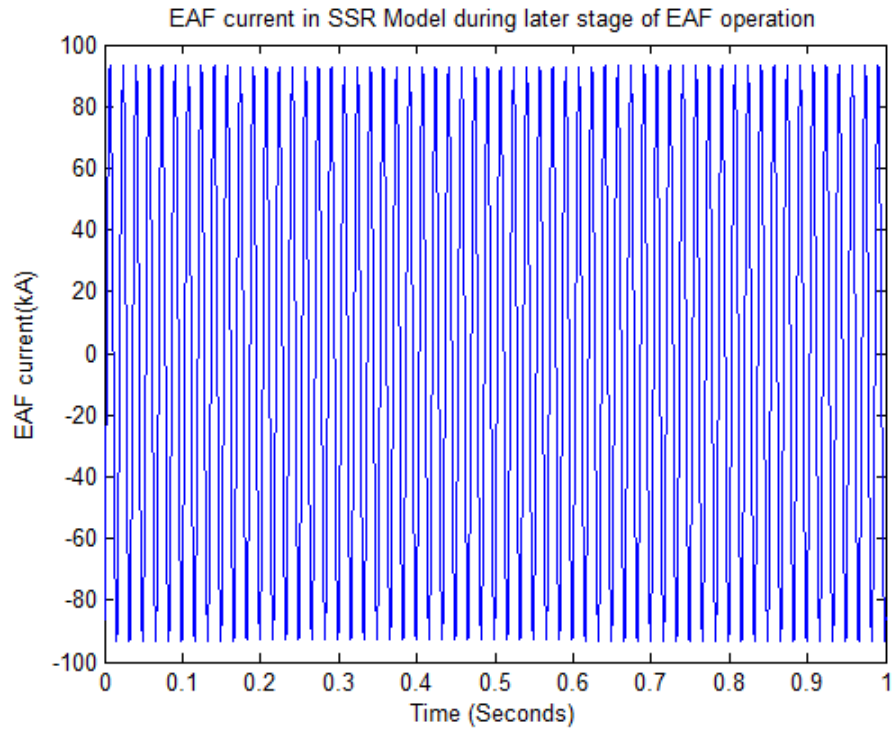


**Figure 5.51 EAF current during second stage of its operation**

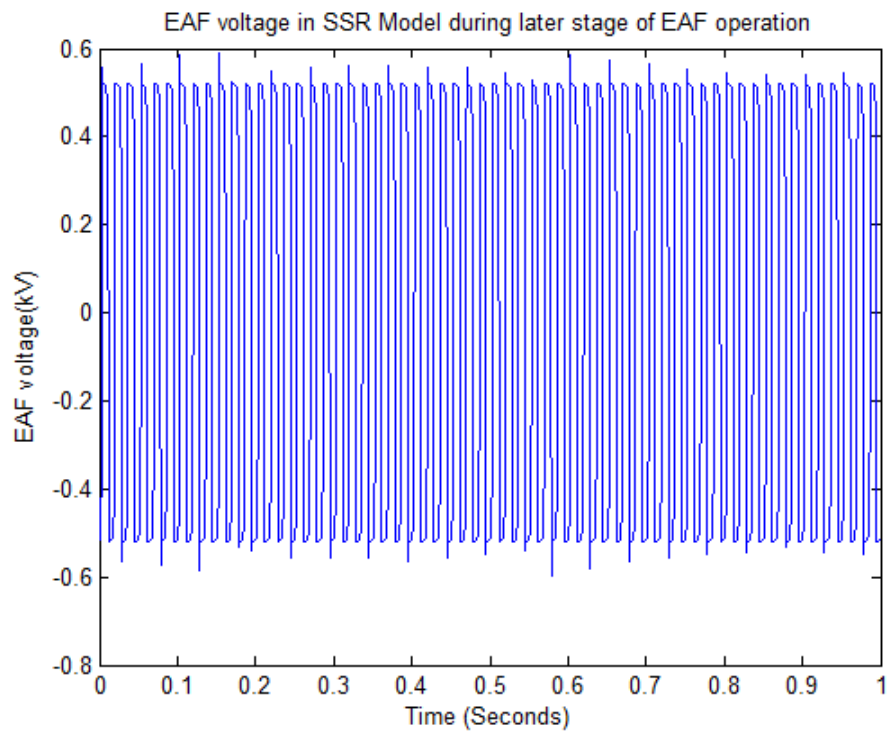


**Figure 5.52 EAF voltage during second stage of its operation**

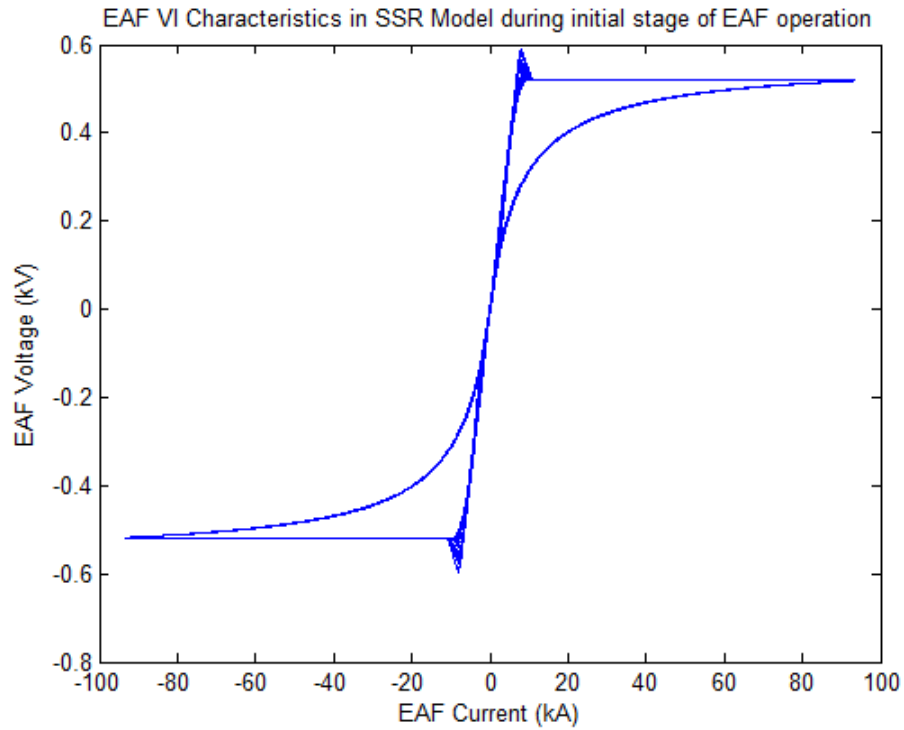


**Figure 5.53 VI characteristics during second stage of EAF operation**

Figures 5.46 - 5.50 show the graphs of THI, TIA, TAB, TBG and TGEX during the second stage of the EAF operation. During this stage high torsional oscillations are not observed as happening in the initial melting stage. Figures 5.51 – 5.53 show the current, voltage and VI characteristics of the EAF respectively during the second stage of its operation.

## **5.6 Analysis of Effects of the EAF Operation on the Shaft of Synchronous Generator**

1. The low frequency components (sub-synchronous) being caused by the EAF during the initial stage of its operation are clearly being seen and noticed in the turbine torques which can damage the shaft of the generator at any instant.
2. The second, third, fourth and fifth torsional modes are found to be the most susceptible.
3. The EAF is not causing SSR instantly but the continuous torsional stresses due to the sub-synchronous frequency components or any sudden change in the power system can severely damage the shaft or any other equipment of the turbo-generator especially during the initial stage of the EAF operation.
4. EAF does not cause any torsional issues during the second stage (quiet melting stage) of its operation.

## CHAPTER 6

### RECOMMENDED MITIGATION TECHNIQUE

The sub-synchronous frequencies appearing in the turbine torques during the first stage of the EAF operation are not equal to the oscillating frequencies of any of the torsional modes of the turbine-generator system. Therefore, the EAF does not cause the SSR during the first stage of its operation. As the EAF does not cause the SSR, no mitigation technique is applied. However, many mitigation techniques are proposed in the literature in order to mitigate the torsional oscillations caused due to the EAF and improve the Power Quality (PQ). Therefore, in this chapter, a mitigation technique to reduce the effects of the EAF operation on the shaft of the synchronous generator is recommended on the basis of critical analysis of the literature. The section 2.4 provides an overview of the mitigation techniques used in the literature to alleviate the impact of the EAF operation on the grid/generator.

It can be clearly noticed from the literature that most of the control techniques used to alleviate the effects of the EAF operation employ FACTS devices such as STATCOM, D-STATCOM and SVC. So, it will be appropriate to discuss the effectiveness and disadvantages of each of these devices and the control techniques based on these devices used in the literature. Based on the facts of a critical analysis of the control techniques used in the literature, a mitigation technique to reduce the effects of the EAF operation on the shaft of the synchronous generator can be recommended.

A STATCOM based controller is proposed in [61]. In this paper, the generator excitation and the STATCOM are synchronized to ameliorate the performance. The authors proposed an effective control law by using a simplified model of the STATCOM and were able to achieve significant damping of the oscillations. However, the STATCOM may be located at a significant distance away from the generator in case of applications like the EAFs and therefore the coordinated generator-STATCOM control may not be realistic [62].

STATCOM based control schemes are used in [41] - [42] and [44] - [46] to mitigate the flicker caused by the EAF. The STATCOM performs as a synchronous voltage source. The STATCOM has a faster response than the SVC. It means that the STATCOM can counteract the varying flicker by compensating the reactive power more rapidly than the SVC. It is an advantage of the STATCOM over the SVC.

The SVC is used in [50] to compensate the reactive power consumed by the EAF. The SVC functions as a controlled reactive admittance. The response time of the SVC is slower than that of the STATCOM. However, the STATCOM is more expensive than the SVC. So, the SVC has an economic advantage over the STATCOM.

Since the SVC is economically more suitable than the STATCOM, many industries employ it. Therefore, if the delay of the SVC is reduced, its performance will enhance. This is done in [53] by forecasting the reactive power consumed by the EAF a half-cycle ahead and the performance of the SVC is improved significantly. Grey-Markov prediction method is used to forecast the reactive power consumption of the EAF. So, it is recommended that the SVC should be used to mitigate the effects of the EAF operation



on the shaft of the synchronous generator because of its economic advantage over the STATCOM. A suitable prediction method such as Grey-Markov prediction method can be used to forecast the reactive power to enhance the performance of the SVC.

## CHAPTER 7

### CONCLUSION AND FUTURE WORK

The electric arc furnace exhibits highly non-linear stochastically varying VI characteristics. The arc length of the arc varies continuously along with the time due to movement of the scrap. Due to this, the electric arc furnace resistance, voltage and current also change with the time dynamically. The electric arc furnace is a high current and low voltage load.

This research work has focused on analyzing the effects of electric arc furnace on the shaft of the synchronous generator especially when the electric arc furnace is located very close to the synchronous generator. The IEEE First Bench Mark Model for SSR is modeled. The electric arc furnace is modeled by its two stages of operation. During the initial stage when the scrap is being melted and the due to very rapid movements of the scrap, the arc length varies continuously. This stage is modeled by using a non-linear time varying resistance model with the arc length varying stochastically. During the second stage, when the scrap has been melted and its movements become very less, the arc length almost becomes constant. This later stage is modeled by a simple non-linear time varying resistance model with constant arc length. The shaft of the generator is modeled by a twelfth order mass-spring system of equations.

The electric arc furnace model is validated by using the real-time data. The parameters of the model are estimated for the real-time data and the measured and simulated values are compared on the basis of Total Harmonic Distortion (THD) and Fast Fourier Transform

(FFT). Then the built-in model is used to analyze the effects of the electric arc furnace operation on the shaft of the synchronous generator. This is done for the evidential purpose so as to validate the electric arc furnace model.

The electric arc furnace is connected at the generator bus in the SSR model. The simulation results clearly show that during the initial stage of the electric arc furnace operation, torsional stresses are very high. Though, the system does not become totally unstable. There are continuous torsional stresses on the shaft of the synchronous generator. Also the FFT of all the turbine torques show the presence of low frequency (sub-synchronous) components in the turbine torque signals. The sub-synchronous frequencies appearing in the turbine torques during the first stage of the EAF operation are not equal to the oscillating frequencies of any of the torsional modes of the turbine-generator system. Therefore, the EAF does not cause the SSR during the first stage of its operation. During the second stage of the EAF operation, no as such torsional stresses on the shaft of the synchronous generator are observed. Since the EAF does not cause the SSR, no mitigation technique is applied. However, based on the critical analysis of the literature, a mitigation technique is recommended to alleviate the torsional oscillations caused by the EAF and improve the power quality.

Concluding all of the above facts, it can be said that during the initial melting stage of the EAF operation, the electric arc furnace will cause high torsional stress on the shaft of the synchronous generator if it is located close to the synchronous generator. It will not cause the SSR instantly but there is a very strong probability that at any instant of time it can cause either the SSR or the damage of the shaft due to any sudden change in the power system or the continuous torsional stresses on the shaft.

The future work will focus on the comparison of actual (measured) and simulated voltage waveforms of the EAF on the basis of short-term flicker severity index. The effect of the EAF operation on the shaft of synchronous generator will be again analyzed but with different parameters of the turbine-generator system.

## References

- [1] G. Carpinelli, F. Iacovone, A. Russo, and P. Varilone, "Chaos-Based Modeling of DC Arc Furnaces for Power Quality Issues," *IEEE Trans. Power Deliv.*, vol. 19, no. 4, pp. 1869–1876, Oct. 2004.
- [2] Sakulin M., "Simulation of electric arcs in melting furnaces," in *Electroheat for Metals Conference*, 1982, p. 1.4.
- [3] I. Vervenne, K. Van Reusel, and R. Belmans, "Electric arc furnace modelling from a 'power quality' point of view," *2007 9th Int. Conf. Electr. Power Qual. Util.*, pp. 1–6, Oct. 2007.
- [4] M. R. Ingram, D. T. Bradshaw, S. Eckroad, and M. L. Crow, "EAF voltage flicker mitigation by FACTS/ESS," in *IEEE PES Power Systems Conference and Exposition, 2004.*, 2004, pp. 898–904.
- [5] T. Y. Andorka, M., "Vibration induced retaining ring failure due to steel mill—Power plant electromechanical interaction," in *IEEE 1996 Summer Power Meeting Panel Session on "Steel-Making, Inter-Harmonics and Generator Torsional Impacts.*, 1996.
- [6] S. Varadan, E. B. Makram, and A. A. Girgis, "A new time domain voltage source model for an arc furnace using EMTP," *IEEE Trans. Power Deliv.*, vol. 11, no. 3, pp. 1685–1691, Jul. 1996.
- [7] T. Zheng, E. B. Makram, and A. A. Girgis, "Effect of different arc furnace models on voltage distortion," in *8th International Conference on Harmonics and Quality of Power. Proceedings (Cat. No.98EX227)*, 1998, vol. 2, pp. 1079–1085.
- [8] E. B. M. Tongxin Zheng, "An adaptive arc furnace model," *IEEE Trans. Power Deliv.*, vol. 15, no. 3, pp. 931–939, Jul. 2000.
- [9] C. Sharmeela and G. Uma, "Voltage flicker analysis and mitigation-case study in ac electric arc furnace using PSCAD/EMTDC," in *... 2004. PowerCon 2004 ...*, 2004, no. November, pp. 21–24.
- [10] G. C. Montanari, M. Loggini, A. Cavallini, L. Pitti, and D. Zaninelli, "Arc-furnace model for the study of flicker compensation in electrical networks," *IEEE Trans. Power Deliv.*, vol. 9, no. 4, pp. 2026–2036, 1994.

- [11] M. A. Golkar, M. T. Bina, and S. Meschi, "A Novel Method of Electrical Arc Furnace Modeling for Flicker Study," in *International Conference on Renewable Energies And Power Quality*, 2007, pp. 1–8.
- [12] W. "36-05: CIGRE, "Harmonics, characteristic parameters, methods of study, estimates of existing values in the network," in *Electra* 77, 1981, pp. 35–54.
- [13] S. Kolluri and M. F. McGranaghan, "Voltage flicker prediction for two simultaneously operated AC arc furnaces," in *Proceedings of 1996 Transmission and Distribution Conference and Exposition*, 1996, pp. 255–262.
- [14] V. Terzija and V. Stanojevic, "Power quality indicators estimation using robust Newton-type algorithm," *IEE Proc. - Gener. Transm. Distrib.*, vol. 151, no. 4, p. 477, 2004.
- [15] D. M. Vilathgamuwa, "An experimentally verified hybrid Cassie-Mayr electric arc model for power electronics simulations," *IEEE Trans. Power Electron.*, vol. 12, no. 3, pp. 429–436, May 1997.
- [16] H. Mokhtari and M. Hejri, "A new three phase time-domain model for electric arc furnaces using MATLAB," in *IEEE/PES Transmission and Distribution Conference and Exhibition*, 2002, vol. 3, no. i, pp. 2078–2083.
- [17] J. G. Mayordomo, R. Asensi, L. F. Beites, J. Bueno, L. Zabala, and J. Amantegui, "A frequency domain arc furnace model for harmonic power flows under balanced conditions," in *Proceedings of the 7th IEEE International Conference on Harmonics and Quality of Power (ICHQP)*, 1996, pp. 419–427.
- [18] O. Ozgun and a. Abur, "Flicker study using a novel arc furnace model," *IEEE Trans. Power Deliv.*, vol. 17, no. 4, pp. 1158–1163, Oct. 2002.
- [19] J. G. Mayordomo, L. F. Beites, R. Asensi, M. Izzeddine, L. Zabala, and J. Amantegui, "A new frequency domain arc furnace model for iterative harmonic analysis," *IEEE Trans. Power Deliv.*, vol. 12, no. 4, pp. 1771–1778, 1997.
- [20] A. M. O. Haruni, K. M. Muttaqi, and M. Negnevitsky, "Analysis of harmonics and voltage fluctuation using different models of Arc furnace," *2007 Australas. Univ. Power Eng. Conf.*, no. 3, pp. 1–6, Dec. 2007.
- [21] H. M. Petersen, R. G. Koch, P. H. Swart, and R. Van Heerden, "Modelling arc furnace flicker and investigating compensation techniques," *IAS '95. Conf. Rec. 1995 IEEE Ind. Appl. Conf. Thirtieth IAS Annu. Meet.*, vol. 2, pp. 1733–1740, 1995.

- [22] A. H. Fahad, P. P. Dutta, and A. H. Chowdhury, "A voltage flicker severity analysis module for multiple electric arc furnace operation," in *8th International Conference on Electrical and Computer Engineering*, 2014, pp. 643–646.
- [23] Y.-J. Liu, G. W. Chang, and R.-C. Hong, "Curve-fitting-based method for modeling voltage–current characteristic of an ac electric arc furnace," *Electr. Power Syst. Res.*, vol. 80, no. 5, pp. 572–581, May 2010.
- [24] G. Chang, C. Chen, and Y. Liu, "A neural-network-based method of modeling electric arc furnace load for power engineering study," *Power Syst. IEEE ...*, vol. 25, no. 1, pp. 138–146, 2010.
- [25] G. W. Chang, M.-F. Shih, Y.-Y. Chen, and Y.-J. Liang, "A Hybrid Wavelet Transform and Neural-Network-Based Approach for Modelling Dynamic Voltage-Current Characteristics of Electric Arc Furnace," *IEEE Trans. Power Deliv.*, vol. 29, no. 2, pp. 815–824, Apr. 2014.
- [26] M. A. P. Alonso and M. Perez Donsion, "An Improved Time Domain Arc Furnace Model for Harmonic Analysis," *IEEE Trans. Power Deliv.*, vol. 19, no. 1, pp. 367–373, Jan. 2004.
- [27] F. Wang, Z. Jin, Z. Zhu, and X. Wang, "Application of Extended Kalman Filter to the Modeling of Electric Arc Furnace for Power Quality Issues," in *2005 International Conference on Neural Networks and Brain*, 2005, vol. 2, pp. 991–996.
- [28] L. Hocine, D. Yacine, B. Kamel, and K. M. Samira, "Improvement of electrical arc furnace operation with an appropriate model," *Energy*, vol. 34, no. 9, pp. 1207–1214, Sep. 2009.
- [29] Y. Wang, Z. Mao, Y. Li, H. Tian, and L. Feng, "Modeling and parameter identification of an electric arc for the arc furnace," in *2008 IEEE International Conference on Automation and Logistics*, 2008, pp. 740–743.
- [30] S. M. Mousavi Agah, S. H. Hosseinian, H. A. Abyaneh, and N. Moaddabi, "Parameter Identification of Arc Furnace Based on Stochastic Nature of Arc Length Using Two-Step Optimization Technique," *IEEE Trans. Power Deliv.*, vol. 25, no. 4, pp. 2859–2867, Oct. 2010.
- [31] F. Janabi-Sharifi and G. Jorjani, "An adaptive system for modelling and simulation of electrical arc furnaces," *Control Eng. Pract.*, vol. 17, no. 10, pp. 1202–1219, Oct. 2009.
- [32] J.-S. R. Jang, "ANFIS: adaptive-network-based fuzzy inference system," *IEEE Trans. Syst. Man. Cybern.*, vol. 23, no. 3, pp. 665–685, 1993.

- [33] M. Torabian Esfahani and B. Vahidi, "A New Stochastic Model of Electric Arc Furnace Based on Hidden Markov Model: A Study of Its Effects on the Power System," *IEEE Trans. Power Deliv.*, vol. 27, no. 4, pp. 1893–1901, Oct. 2012.
- [34] A. Sadeghian and J. D. Lavers, "Dynamic reconstruction of nonlinear v-i characteristic in electric arc furnaces using adaptive neuro-fuzzy rule-based networks," *Appl. Soft Comput.*, vol. 11, no. 1, pp. 1448–1456, Jan. 2011.
- [35] H. Samet, E. Farjah, and Z. Sharifi, "A dynamic, nonlinear and time-varying model for electric arc furnace," *Int. Trans. Electr. Energy Syst.*, vol. 20, no. 2, p. n/a–n/a, 2014.
- [36] A. J. P. Rosentino Junior, I. N. Gondim, J. R. Macedo Junior, and A. C. Delaiba, "A Practical Electric Arc Furnace Model For Flicker Assessment," *J. Control. Autom. Electr. Syst.*, vol. 26, no. 1, pp. 68–79, 2014.
- [37] B. Mirzaeian Dehkordi, A. Parsapoor, and R. Hooshmand, "Effect of different operating conditions of Electric Arc Furnace on synchronous generator shaft," in *2007 International Aegean Conference on Electrical Machines and Power Electronics*, 2007, pp. 824–829.
- [38] M. W. Baldwin, "Electric arc furnace impact on generator torque," in *IEEE PES Power Systems Conference and Exposition, 2004.*, 2004, pp. 1368–1372.
- [39] R. Hooshmand, M. T. Esfahani, and A. Kiyoumars, "Study of electric arc furnace operation effect on the shaft of local power system generators by employing furnace real model," in *2008 18th International Conference on Electrical Machines*, 2008, pp. 1–5.
- [40] M. Baldwin, M. R. Ingram, D. T. Bradshaw, S. Eckroad, and M. L. Crow, "A solution for EAF-induced problems in bulk power systems by FACT/ESS," in *IEEE Power Engineering Society General Meeting, 2005*, 2005, pp. 1831–1838.
- [41] M. L. Crow and A. Yazdani, "An improved nonlinear STATCOM control for electric arc furnace voltage flicker mitigation," in *IEEE PES General Meeting*, 2010, pp. 1–1.
- [42] C. Schauder, "STATCOM for compensation of large electric arc furnace installations," in *199 IEEE Power Engineering Society Summer Meeting. Conference Proceedings (Cat. No.99CH36364)*, 1999, vol. 2, pp. 1109–1112.
- [43] P. Ladoux, G. Postiglione, H. Foch, and J. Nuns, "A Comparative Study of AC/DC Converters for High-Power DC Arc Furnace," *IEEE Trans. Ind. Electron.*, vol. 52, no. 3, pp. 747–757, Jun. 2005.



- [44] Y. F. Wang, J. G. Jiang, L. S. Ge, and X. J. Yang, "Mitigation of Electric Arc Furnace Voltage Flicker Using Static Synchronous Compensator," in *2006 CES/IEEE 5th International Power Electronics and Motion Control Conference*, 2006, pp. 1–5.
- [45] C. Han, Z. Yang, B. Chen, A. Q. Huang, B. Zhang, M. R. Ingram, and A.-A. Edris, "Evaluation of Cascade-Multilevel-Converter-Based STATCOM for Arc Furnace Flicker Mitigation," *IEEE Trans. Ind. Appl.*, vol. 43, no. 2, pp. 378–385, 2007.
- [46] P. Luttamus and H. Tuusa, "Simulated electric arc furnace voltage flicker mitigation with 3-level current-controlled STATCOM," in *2008 Twenty-Third Annual IEEE Applied Power Electronics Conference and Exposition*, 2008, pp. 1697–1703.
- [47] A. K. Jain, A. Behal, X. T. Zhang, D. M. Dawson, and N. Mohan, "Nonlinear Controllers for Fast Voltage Regulation Using STATCOMs," *IEEE Trans. Control Syst. Technol.*, vol. 12, no. 6, pp. 827–842, Nov. 2004.
- [48] Y. Li, Z. Mao, Y. Wang, P. Yuan, and M. Jia, "Model Predictive Control Synthesis Approach of Electrode Regulator System for Electric Arc Furnace," *J. Iron Steel Res. Int.*, vol. 18, no. 11, pp. 20–25, Nov. 2011.
- [49] K. Anuradha, B. P. Muni, and A. D. R. Kumar, "Modeling of Electric Arc Furnace & control algorithms for voltage flicker mitigation using DSTATCOM," in *2009 IEEE 6th International Power Electronics and Motion Control Conference*, 2009, pp. 1123–1129.
- [50] M. D. Cox and A. Mirbod, "A New Static Var Compensator for an Arc Furnace," *IEEE Trans. Power Syst.*, vol. 1, no. 3, pp. 110–119, 1986.
- [51] C. J. Wu, S. S. Yen, W. N. Chang, C. N. Cheng, C. H. Li, and T. Y. Guo, "Enhancement of static excitation system performance for generators near electric arc furnace loads," *IEEE Trans. Energy Convers.*, vol. 14, no. 2, pp. 225–231, Jun. 1999.
- [52] C. J. Wu, Y. S. Chuang, C. P. Huang, and Y. P. Chang, "Tuning of Static Excitation Systems to Improve Dynamic Performance for Generators Serving Electric Arc Furnaces Loads," *IEEE Trans. Energy Convers.*, vol. 22, no. 2, pp. 350–357, Jun. 2007.
- [53] H. Samet and A. Mojallal, "Enhancement of electric arc furnace reactive power compensation using Grey–Markov prediction method," *IET Gener. Transm. Distrib.*, vol. 8, no. 9, pp. 1626–1636, 2014.

- [54] G. W. Chang, H. J. Lu, and C. S. Chuang, “An accurate hybrid intelligent approach for forecasting flicker severity caused by electric arc furnaces,” *Electr. Power Syst. Res.*, vol. 121, pp. 101–108, 2015.
- [55] H. Samet, A. MOJALLAL, and T. GHANBARI, “Employing Grey System Model for Prediction of Electric Arc Furnace Reactive Power to Improve Compensator Performance,” *PRZEGLĄD ELEKTROTECHNICZNY*, vol. 89, no. 12/2013, pp. 110–115, 2013.
- [56] N. F. Jamaludin and a F. Abidin, “Phase-Locked Loop ( PLL ) Controller for Distribution Synchronous Static Compensator ( D-STATCOM ) to Mitigate Voltage Flicker,” no. June, pp. 334–339, 2013.
- [57] Y. Yu, *Electric power system dynamics*. ACADEMIC PRESS, INC., 111 FIFTH AVE., NEW YORK, NY 10003, USA, 1983, 256, 1983.
- [58] J. G. Proakis and D. G. Manolakis, *Digital Signal Processing: Principles, Algorithms, and Applications.*, Third. Prentice-Hall International INC, 1996.
- [59] G. C. Montanari, M. Loggini, L. Pitti, E. Tironi, and D. Zaninelli, “The effects of series inductors for flicker reduction in electric power systems supplying arc furnaces,” in *Conference Record of the 1993 IEEE Industry Applications Conference Twenty-Eighth IAS Annual Meeting*, pp. 1496–1503.
- [60] J. Sousa, M. T. Correia de Barros, M. Covas, and A. Simoes, “Harmonics and flicker analysis in arc furnace power systems,” in *IPST'99-Int. Conf. Power Systems Transients, Budapest, Hungary*, 1999.
- [61] Q. J. Liu, Y. Z. Sun, T. L. Shen, and Y. H. Song, “Adaptive nonlinear co-ordinated excitation and STATCOM controller based on Hamiltonian structure for multimachine-power-system stability enhancement,” *IEE Proceedings - Control Theory and Applications*, vol. 150, no. 3. p. 285, 2003.
- [62] A. Yazdani, M. L. Crow, and J. Guo, “An improved nonlinear STATCOM control for electric arc furnace voltage flicker mitigation,” *IEEE Trans. Power Deliv.*, vol. 24, no. 4, pp. 2284–2290, 2009.

## APPENDIX

### SYSTEM DATA FOR THE FIRST BENCH MARK MODEL OF IEEE [57]

Inertia Constants (Seconds):

$$M_H = 0.185794 \quad M_I = 0.311178 \quad M_A = 1.717340 \quad M_B = 1.768430$$

$$M_G = 1.736990 \quad M_X = 0.068433$$

Stiffness Constants (pu Torque/radian):

$$K_{HI} = 19.303 \quad K_{IA} = 34.929 \quad K_{AB} = 52.038 \quad K_{BG} = 70.858 \quad K_{GX} = 2.822$$

Turbine and Governor Parameters:

$$F_H = 0.3 \quad F_I = 0.26 \quad F_A = 0.22 \quad F_B = 0.22 \quad T_{CH} = 0.3 \text{ sec} \quad T_{RH} = 7.0 \text{ sec}$$

$$T_{CO} = 0.2 \text{ sec} \quad K_G = 25 \quad T_{SR} = 0.2 \text{ sec} \quad T_{SM} = 0.3 \text{ sec}$$

Transformer and Transmission Line:

$$R_T = 0.01 \text{ pu} \quad X_T = 0.14 \text{ pu} \quad R_L = 0.02 \text{ pu} \quad X_L = 0.5 \text{ pu} \quad X_C = 0.2 * X_L$$

$$X_{SYS} = 0.06 \text{ pu}$$

Synchronous Generator (Equivalent circuit parameters in pu):

$$x_{md} = 1.660 \quad x_d = 1.790 \quad x_F = 1.700 \quad x_D = 1.666 \quad x_{mq} = 1.580 \quad x_q = 1.710$$

$$x_Q = 1.695 \quad x_S = 1.825 \quad r_F = 0.001 \quad r_D = 0.0037 \quad r_Q = 0.0053 \quad r_S = 0.0182$$

$$r_a = 0.0015$$

Exciter and Voltage Regulator:

$$K_A = 50 \quad T_E = 0.002 \text{ sec} \quad T_A = 0.01 \text{ sec}$$

Initial Operating Conditions:

$$P_e = 0.9 \text{ pu} \quad v_t = 1.05 \text{ pu} \quad \text{PF} = 0.9 \text{ (lag)}$$

## VITAE

Name: FAZAL ILLAHI

Nationality: Pakistani

Date of Birth: 2/21/1985

Email: fazal\_petarian@hotmail.com

Address: Flat No: B-8, Diplai Memon Avenue, Diplai Memon Housing Society, Behind Rajputana Hospital, Hyderabad, Pakistan.

Academic Background: MS in Electrical Engineering, 2014, King Fahd University of Petroleum & Minerals.

Bachelor of Engineering in Electronic Engineering, 2007, Mehran University of Engineering & Technology, Jamshoro, Pakistan.

Research Papers: Modeling of Electric Arc Furnace by Using Multi-Objective Optimization Technique. (In Progress)

Membership: Registered Engineer with Pakistan Engineering Council.